

NASA
Technical
Paper
2761

February 1988

Description of Data
on the Nimbus 7
LIMS Map Archive Tape

Water Vapor and Nitrogen Dioxide

Kenneth V. Haggard,
B. T. Marshall,
Robert J. Kurzeja,
Ellis E. Remsberg,
and James M. Russell III

NASA

rep.00080

**NASA
Technical
Paper
2761**

1988

**Description of Data
on the Nimbus 7
LIMS Map Archive Tape**

Water Vapor and Nitrogen Dioxide

Kenneth V. Haggard
*Langley Research Center
Hampton, Virginia*

B. T. Marshall
*G and A Technical Software
Hampton, Virginia*

Robert J. Kurzeja
*Savannah River Laboratory
Aiken, South Carolina*

**Ellis E. Remsberg
and James M. Russell III**
*Langley Research Center
Hampton, Virginia*



National Aeronautics
and Space Administration

Scientific and Technical
Information Division

Introduction

The Limb Infrared Monitor of the Stratosphere (LIMS) experiment on the Nimbus 7 spacecraft consisted of a thermal infrared limb scanning radiometer with six channels centered at wavelengths ranging from 6.2 to 15 μm (Gille and Russell 1984). The experiment functioned in orbit from October 24, 1978, until May 28, 1979. Radiance profiles measured by LIMS were later processed at the Langley Research Center to infer middle atmospheric temperature profiles and the concentrations of ozone, nitrogen dioxide, water vapor, and nitric acid. The results of this analysis are available on the LIMS Map Archival Tape (LAMAT), which contains Fourier coefficient representations of these atmospheric variables at selected pressures (100, 70, 50, 30, 16, 10, 7, 5, 3, 2, 1.5, 1.0, 0.7, 0.5, 0.4, 0.2, 0.1, and 0.05 mbar) and every 4° of latitude from 64°S to 83.5°N. Coefficients for temperature and ozone were calculated from 100 to 0.05 mbar, water vapor and nitrogen dioxide from 100 to 1 mbar, and nitric acid from 100 to 2 mbar. Geopotential heights were calculated from 100 to 0.05 mbar. The Fourier coefficients were determined with a Kalman filter technique to estimate synoptic maps from asynoptic satellite data. This approach is discussed in detail in Haggard et al. (1986) and is applied to temperature and geopotential heights in that report. The pertinent LAMAT analysis notation, formats, and terminology are also available there. The LAMAT, as well as the LIMS Inverted Profile Archival Tape (LAIPAT), is archived at the National Space Sciences Data Center (NSSDC), NASA Goddard Space Flight Center, Greenbelt, MD 20771.

This report, which discusses water vapor (H_2O) and nitrogen dioxide (NO_2), is the last in a three-part discussion of the quality of data on the LAMAT. The first two reports describe temperature and geopotential height fields (Haggard et al. 1986) and ozone and nitric acid fields (Remsberg et al. 1986). Results for the water vapor and nitrogen dioxide species are grouped in this report because both channels occur in a similar spectral region (water vapor, 6.9 μm , nitrogen dioxide, 6.2 μm) and have equivalent vertical fields of view (about 4 km). Because of the interference of water vapor in the nitrogen dioxide results, water vapor profiles were retrieved first and then nitrogen dioxide (Russell et al. 1984a, b). On the other hand, both species possess unique characteristics that dictated care in the mapping process. For example, the water vapor fields are often fairly flat, both vertically and horizontally, and any determination of the relatively small zonal wave components is sensitive to the data precision. Conversely, nitrogen dioxide exhibits large gradients, but the existence of

a diurnal variation of a factor of 2 or greater means that maps of the combined mode (ascending, or day, plus descending, or night, modes) data are meaningless. Therefore, nitrogen dioxide coefficients are calculated for only the ascending and descending modes. Interpretation of these derived nitrogen dioxide fields is further complicated near the terminator zones because of these large diurnal variations. This report addresses, in turn, the quality of the LAMAT water vapor and nitrogen dioxide results followed by an overall summary of their potential utility for scientific study.

Symbols

K	vector defined in equation (2)
M	order of Fourier series, less than or equal to 6
p	pressure, mbar
S	error covariance matrix
t	time
W	water vapor, ppmv
X	vector of Fourier coefficients
X_0, X_1, \dots, X_{2M}	elements of X
θ	latitude, deg
λ	longitude, deg
σ^2	variance
$\sigma_{n,m}$	input measurement precision
σ_{obs}	observed standard deviation at noon GMT between synoptic field and asynoptic data
τ	relaxation time, days
Subscripts:	
<i>e</i>	estimate
<i>m</i>	measured
<i>n</i>	index of data points (see eq. (3))
Superscript:	
<i>T</i>	transpose
Abbreviations:	
FOV	field of view
GM	Greenwich meridian
GMT	Greenwich Mean Time
LAIPAT	LIMS Inverted Profile Archive Tape

LAMAT	LIMS Map Archival Tape
LIMS	Limb Infrared Monitor of the Stratosphere
NLTE	nonlocal thermodynamic equilibrium
NO _x	total odd nitrogen
PSC	polar stratospheric cloud
RMSD	root-mean-square difference between LAMAT and LAIPAT data
S/N	signal-to-noise
ZMT	zonal mean trend
Units:	
gpkm	geopotential kilometers
gpm	geopotential meters
ppbv	parts per billion by volume
ppmv	parts per million by volume

The LAMAT Water Vapor Data

Processing of the LIMS water vapor data is discussed in this section with emphasis on the specific characteristics of the water vapor data, the choice of suitable parameters for the mapping, and the presentation of selected results. The generally high quality and overall utility of the individual profile results have been discussed previously by Russell et al. (1984a) and Remsberg et al. (1984). Monthly zonal mean cross sections from the LAMAT data are shown by Russell et al. (1986), along with monthly averaged polar stereographic maps at 10 mbar. Precision estimates are of the order of 5 percent from 3 to 50 mbar. The uncertainty in LIMS zonal mean descending mode water vapor is about 17 percent from 3 to 30 mbar with somewhat higher values above and below. Some of the initial scientific results using the LIMS water vapor are reviewed by Remsberg et al. (1984).

There are several error sources associated with the water vapor channel radiances which can degrade the derived water vapor coefficients over restricted altitudes and/or for specific times. First, the single-profile data exhibit marginal signal-to-noise ratios near 1 mbar and also during colder-than-normal conditions in the lower stratosphere winter polar vortex. Second, a substantial systematic difference between the ascending and descending modes was observed in the upper stratosphere, and there were also instances of a large scan-to-scan variation observed at

pressure levels of the upper stratosphere. Finally, there are problems that are common to all the LIMS channels, such as emission from polar stratospheric clouds in the field of view at winter high latitudes in the mid-to-low stratosphere (Hamill and McMaster 1984; Remsberg et al. 1986) and from cirrus clouds in the lower tropical stratosphere (Remsberg et al. 1984). The effect of these data characteristics on the mapping of water vapor is examined in detail following a brief discussion of the Kalman filter algorithm and a description of how parameters were selected for it. (See Haggard et al. 1986.)

Calculation of Synoptic Fields

The calculation of the synoptic fields will be illustrated using water vapor; however, the following discussion applies equally to all other measured LIMS species. The synoptic water vapor fields have been represented by a set of Fourier coefficients calculated for noon GMT for each of the three modes and at each latitude and pressure level (4° latitude increments and 12 atmospheric pressure levels). The water vapor W at a particular time t (GMT), latitude θ , and pressure p is given in vector form by

$$W_{t,\theta,p}(\lambda) = \mathbf{K}^T(\lambda) \cdot \mathbf{X}_{t,\theta,p} \quad (1)$$

where

$$\mathbf{K}^T(\lambda) = [1, \cos \lambda, \sin \lambda, \cos 2\lambda, \dots \sin M\lambda] \quad (2)$$

λ	longitude
M	order of the Fourier series (less than or equal to 6)
\mathbf{X}	vector of the Fourier coefficients
T	superscript denoting the transpose of a vector

For the rest of this paper the subscripts θ , t , and p will be implicit. Synoptic data (or "snapshots" of global parameters) are required to calculate \mathbf{X} in equation (1) exactly. However, the discrete form of equation (1) is actually used to solve for \mathbf{X} :

$$W_n = \mathbf{K}_n^T \cdot \mathbf{X}_n \quad (3)$$

where W_n is the measured value of the field at time t_n and longitude λ_n .

A Kalman filter technique was used to find \mathbf{X}_n , such that a best fit field for a particular time was obtained. This approach is well-suited to handling the LIMS data, since the instrument was turned off

for whole orbits or even for a whole day. The Kalman filter can be thought of as a sequential estimator. It is assumed that an initial estimate of the field is available, and then that estimate is updated by the assimilation of each measurement in the data time series. Inherent in the use of the Kalman filter is the assumption that certain virtual data are known. These virtual data consist of an estimate of both the uncertainty in the input data and the rate of increase of the uncertainty involved in the field. Since all the measurements W_n that were used to calculate the field X_n involve some error (assumed to be random), there must be an uncertainty associated with X_n , represented by an error covariance matrix S_n . If equation (3) is used to calculate the water vapor field at λ_n and t_n , then the uncertainty, or variance, associated with this estimate is

$$\sigma_{n,e}^2 = K_n^T S_{n,e} K_n \quad (4)$$

When X_n is used to estimate the field at a time other than t_n , the error covariance matrix must be increased by an amount $(dS/dt)\Delta t$. Here, dS/dt and dX/dt are calculated as described in Haggard et al. (1986). The amount by which X_n and S_n are incremented for the next time step is determined by considering the difference between the measured and estimated water vapor values, weighted by the variances of the measured data $\sigma_{n,m}^2$ and the estimated value of the variance at the next data point $\sigma_{n+1,e}^2$.

Mapping Parameters

As discussed in Haggard et al. (1986), subjective input has been reduced to the selection of only one parameter $\sigma_{n,m}^2$. The single-scan precision estimates, as reported in Russell et al. (1984a), were used to estimate lower limits of the variance. These precision estimates were based on up to 75 determinations of standard deviation $\sigma_{n,m}$ about separate six-scan means at selected latitudes. The results of those original variance calculations are shown in figure 4 of Russell et al. (1984a). Data variance inputs utilized here were then selected by modification of those estimates, according to the results of preliminary Kalman filter runs. Table 1 provides an example of $\sigma_{n,m}^2$ used in those final analyses. Relaxation times for the Kalman filter were similar to those for temperature for each wave number (see Haggard et al. 1986), and they range from 5.0 to 3.5 days for the zonal mean and wave 1 and from 4.5 to 1.5 days for higher wave numbers.

Normally, Fourier coefficients were calculated through wave 4 for both the ascending and descending mode data and through wave 6 for the combined data. Occasionally, however, it was not possible to

obtain the nominal number of coefficients. For example, because of data rejection due to cloud contamination in the lower stratosphere tropics, the determination of even a zonal mean was not possible at times. Also, in winter high latitudes, data rejection due to low signal-to-noise levels and polar stratospheric cloud effects (Austin et al. 1986) often prohibited the determination of the nominal number of coefficients. The number of wave coefficients calculated was determined in the same manner as that for temperature (Haggard et al. 1986). The average number of data points per day for each latitude for each Kalman filter processing run was calculated, and the number of waves to be calculated was determined from the relation

$$M = 0.5 \times (\text{Number of points per day} - 1)$$

In no case was M greater than 6 for the combined mode (mode 3) or greater than 4 for the ascending and descending modes (modes 1 and 2, respectively). This procedure can produce changes in the wave resolution on the LAMAT in both latitude, pressure, and time. (The typical temporal length of a filter run was about 30 days.) An example of the spatial distribution of those waves is given for January 2, 1979, in table 2. Generally, only the longest waves appeared to have amplitudes substantially above the precision estimates given in table 1. As stated in the temperature discussion (Haggard et al. 1986), even though there can be difficulties with interpreting synoptic fits to asynoptic data, such a diagnostic was relied upon to determine the validity of the mapped product. The latitude, altitude, and time consistency of the coefficients have also been considered as a means of gauging the usefulness of the LAMAT product.

Characteristics and Limitations of the LAMAT Water Vapor

Russell et al. (1984a) and Remsberg et al. (1984) emphasize the fact that the zonal mean water vapor results are considered more reliable than the wave amplitudes and phases because of the relative flatness of the water vapor fields and the sensitivity of the waves to any noise in the retrieved profiles. Both the zonal mean and low wave number results are presented here in more detail.

Figure 1 shows the behavior of the zonal mean versus latitude for the ascending, descending, and combined orbit modes for 50, 10, and 3 mbar on January 2, 1979. (With the exception of the contour plots, all figures in this paper use solid lines for representing the combined mode results, dotted lines for the ascending mode results, and dashed lines for

the descending mode results.) The large differences in the three modes for the 3-mbar level clearly show a consistent ascending/descending mode bias in the data. The ascending mode result is of the order of 1 ppmv higher than the descending mode value at that level. Interestingly, even though the 10-mbar zonal means show much smaller modal differences at most latitudes, the high northern latitudes can exhibit substantial differences. The 50-mbar-level results present no significant modal differences even at high latitudes. Figure 2 shows similar results for February 26, 1979, at 10 mbar. However, for these data, there are no large modal differences at northern high latitudes as there were for the January 2 situation. Examination of many such plots revealed that the anomalous modal behavior at 10 mbar at high latitude occurred only for periods corresponding to the observations of a strong winter polar vortex during the Northern Hemisphere midwinter, from late December to mid-January. Many of the high-latitude LAIPAT water vapor profiles exhibited lower precision as well as larger systematic errors in temperature during that period.

Figure 3 presents the average ascending-minus-descending mode differences as a function of latitude and pressure. A more complete picture of the seasonal variation of the mode differences appears in figures 3(a) and 3(c) (January and May, respectively), and the January combined mode zonal mean cross section is shown in figure 3(b) for estimates of percentage differences using figure 3(a). Generally one sees that there are substantial mode differences in the upper stratosphere for both the January and May time periods, particularly in the Southern Hemisphere and tropics. The differences are seen to be as high as 2.0 ppmv at 1 mbar and decrease to about 0.2 ppmv at 10 mbar. Such large mode differences are suspect and are probably caused by apparent positive radiance measurement biases of the ascending mode, perhaps (as suggested by Russell et al. 1984a) because of either backscattered solar radiation or solar-induced nonlocal thermodynamic equilibrium (NLTE) effects compounded by a nonlinearity in the water vapor absorption band at these altitudes. (That is, small differences in the measured radiance can lead to quite large differences in retrieved water vapor mixing ratio (Gordley et al. 1985).)

For example, Manuilova and Shved (1985) calculated vibrational temperatures T_v at 70 km for the 6.3- μ m band that were 10 K higher for day than for night. The nighttime temperature should be an excellent approximation for the kinetic temperature T_k . This means that use of T_k rather than T_v in the forward radiance calculation during the retrieval

process will lead to an inferred water vapor mixing ratio that is too high at the top of profiles during the day. The highly nonlinear character of the water vapor lines that contribute to the emission can result in overestimates of daytime water vapor at lower altitudes as well. However, present indications are that those overestimates would not be sufficient to explain the magnitude of the observed day/night H₂O differences from 3 to 10 mbar. Recent work indicates that emission from higher vibrational states of NO₂ is responsible for the daytime enhancement in retrieved H₂O in the upper stratosphere (Kerridge and Remsberg 1987).

In addition to the orbital mode differences, the upper stratosphere also exhibits a substantial data variance due largely to low signal-to-noise levels at the top of profiles compounded by the nonlinearity problem mentioned above. Figure 4, which illustrates both the mode difference and the data variance behavior, confirms the difficulty of fitting the LIMS water vapor data in the upper stratosphere. Throughout this paper the square symbols are used to denote the ascending mode data and the diamond symbols are used to denote the descending mode data. The solid symbols mark the first data point of the day for each mode, and the temporal sequence of data is from east to west (i.e., right to left on the figure) for each mode. Figure 4 indicates that the coefficient fit of the three modes to the observed 3-mbar data at the Equator on January 26, 1979, is quite different for each mode in both zonal mean and wave characteristics. It is also apparent that the data have large variances, particularly in the descending mode. Indeed, such a high data variance is larger than the precision measurements used as a basis for the actual variance inputs to the filter. One must remember, however, that the precision measurements were based on a series of six consecutive scans taken within 10 min of each other, whereas the data presented in figure 4 were taken over a 24-hr period. Thus, the precisions shown in table 1 do not account for temporal and spatial variations induced by atmospheric motions or by, perhaps, instrumental effects which exhibit an oscillatory behavior with a period of more than 10 min (Remsberg et al. 1984).

Two other effects can explain some reduction in the longitudinal variation in the water vapor from the LAIPAT to the LAMAT in figure 4. Profile data on the LAIPAT were sampled every 1.5 km in altitude, and those profiles were interpolated to the LAMAT pressure levels that have a vertical separation from 2 to 4.3 km. The effective vertical resolution of the LAIPAT water vapor data is also reduced somewhat in the LAMAT, even for the water vapor (and NO₂) channel with its relatively coarse FOV of 3.8 km.

(The effective LAIPAT resolution is such that a vertical wave with a half-wavelength of 5.3 km can be determined.) Because of the larger separation of pressure levels, the effective vertical resolution that can be obtained using the LAMAT H₂O coefficients ranges from 3.5 to 6.5 km. Of more significance is the rather long relaxation time (about 2 days) prescribed for the Kalman filter for waves 2 through 6. If the observed apparent longitudinal variations in the data of figure 4 are due to systematic radiance bias errors at the top of profiles that occur somewhat randomly for adjacent orbits (as suspected), then such features will be smoothed by the time constant in the Kalman filter algorithm.

Based upon the preceding discussions of observed mode differences, it is concluded that one should be cautious when using the combined mode coefficients in the upper stratosphere. If these mode differences are due, in fact, to a positive bias in the ascending mode data due to NLTE effects, then one should expect the descending mode coefficients to be more accurate. In most cases, however, the descending mode data in the upper stratosphere also exhibit high variances that limit the confidence in the coefficient fit to those data as well. It is suggested that researchers should consider the descending mode zonal mean to be the most reliable water vapor LAMAT product at altitudes above the 7-mbar level (Russell et al. 1986).

The middle and lower stratosphere data allow a confident picture of the water vapor distribution at those levels. Systematic mode differences are of the order of or smaller than the data precision at these levels, and the standard deviation of the coefficient fit to the observed data is usually small. Figure 5 shows the coefficient fit to the combined mode data at 10 mbar and 60°S on November 2, 1978. The orbital mode difference is quite small and the standard deviation of the fit is 0.27 ppmv, or about twice as large as the precision estimate (0.17 ppmv) calculated from the variance in table 1. Figure 5 presents data for late spring when wave activity is reduced in the Southern Hemisphere midstratosphere and the fit to the data is very good.

Occasionally, the ascending and descending mode data exhibited marked differences in a limited longitude sector, yet agreed closely at other longitudes. One of the most pronounced examples of this variation occurred during a period of large transient waves in high northern latitudes at 10 mbar at the beginning of February. Figure 6 defines a data sequence for February 3 to 6 at 76°N and 10 mbar. Significant mode differences much larger than the estimated precision of 0.22 ppmv (calculated from table 1) occur from 300°E to 120°E on all 4 days. The peak in the ascending mode data at 60°E to 120°E appears

consistent for February 3 to 5, ranging from 7.5 to 10 ppmv, whereas there is only a slight indication in the descending mode of such a peak. A peak in the descending mode at 300°E to 360°E longitude is apparent for all 4 days, but there is no such feature in the ascending mode. Simulations suggest that this behavior is most likely associated with the very large temporal and spatial temperature gradients observed at those locations during the early February stratospheric warming. Since horizontal temperature gradients were represented on a daily basis using a Fourier series with four waves in the reduction of the LAIPAT data, it was difficult to account accurately for gradients under rapidly changing conditions. In regions of large local temperature gradients, it is estimated that temperature retrievals can be off by up to 5 K. Temperature uncertainties, compounded by the fact that the LIMS instrument view path was very different for the ascending and descending modes, contribute to substantial mode differences in water vapor in such instances.

For example, figure 7 displays temperature data at 10 mbar and 76°N on February 5; a substantial mode difference in temperature occurs from 60°E to 120°E where the ascending mode water vapor data of figure 6(c) reached 10 ppmv. On the other hand, there appears to be much less modal difference in temperature in the region of the descending mode water vapor data of 7.5 ppmv near 315°E. Table 1 in Russell et al. (1984a) presents accuracy estimates for temperature-sensitivity studies of the LIMS water vapor retrieval. A constant 2-K temperature profile bias can result in a 15-percent change in the water vapor mixing ratio. Thus, it is very likely that the mode differences in figure 6 are largely due to consistent temperature mode biases resulting from a combination of temperature retrieval problems in regions of large temperature gradients (both horizontal and vertical) of the different view paths of the two modes and the effects of the temperature transient. Such situations are expected primarily at high latitudes during winter for highly disturbed situations.

The high-latitude winter data have additional characteristics that must be addressed. As already mentioned, cold temperatures in the region of the winter polar vortex extended the altitude range for low signal-to-noise levels for the water vapor channel radiance. This extension resulted in the rejection of data in the polar vortex at most pressure levels in the lower stratosphere, which in turn created a bias in the longitudinal sampling distribution of the water vapor data at high northern latitudes during those situations.

Figure 8 illustrates the Kalman filter fit to the combined mode data at 76°N and 10 mbar on

January 2, 1979, and emphasizes the extent of the missing data from 180°E to 360°E. Such a sampling bias degrades the coefficient fit and indicates that even the zonal mean term may be somewhat misleading. Although this is an extreme example, this characteristic was present to some extent for latitudes between 64°N and the North Pole and from mid-November through mid-January. Water vapor radiance values during the stratospheric warming periods after mid-January were larger and signal-to-noise levels were correspondingly higher, thus leading to very little loss of data for the LAMAT. One must be cautious in interpreting the LAMAT product for the prewarming periods in polar regions.

A rejection of data also occurred because of the presence of interfering emission from polar stratospheric clouds (PSC's) and from clouds in the tropical lower stratosphere. In the case of the PSC's, which occurred in the polar vortex region, the affected scan segments, as determined from signatures observed in the LAIPAT ozone data, were deleted before the Kalman filter algorithm was applied to the processing of the LAMAT water vapor. The occurrence and distribution of the PSC's are described in Remsberg et al. (1986) and Austin et al. (1986).

Water Vapor Fields Processed From LAMAT Data

Examples of water vapor plots obtained from the LAMAT include time series plots at a given latitude and surface contour plots at a constant pressure. Because water vapor in the upper stratosphere is believed to be more correct for the descending mode, the latitude-pressure plots are presented for that mode only.

Figure 9(a), which presents a time series of the zonal mean water vapor at 48°N of the descending mode, illustrates the consistency of the zonal mean trends as well as the seasonal variations in the data. To obtain this plot, the LAMAT data were smoothed in latitude (1-2-1 weighted average at 4° latitude intervals) and the means for 5-day periods were calculated. The field appears fairly uniform at all levels, an effect which points out the importance of high data precision in the detection of trends for this species.

Figure 9(b) is similar to figure 9(a) except that trends in the wave 1 amplitude are presented in figure 9(b). In the midstratosphere (near 7 mbar), where the water vapor accuracy and precision are high, a maximum amplitude exists in mid-December, but from February through May the amplitude is small. Plots of amplitudes of the other wave numbers possess time and space coherency through wave 4. The variation of wave number coefficients with time

and/or latitude suggests that generally the combined mode water vapor data do not warrant a six wave number analysis (referred to as a "6-wave fit"). The four wave number analysis (4-wave fit) of the ascending and descending mode data appears to be valid under most cases, and the four wave representation may be the effective limit for the combined mode field.

It has been noted by Remsberg et al. (1984) that the precision estimates for water vapor may be unduly optimistic because they were based on sets of six consecutive scans, rather than on sets whose scans were spaced farther apart. This feeling becomes more apparent in figure 10, which shows wave amplitude versus latitude at 10 mbar for January 26, 1979. The somewhat noisy behavior is present at all latitudes and for other time periods as well. It is, therefore, suggested that some latitudinal smoothing of the coefficients may be useful as a means of clarifying small persistent features of the water vapor field.

Figure 11 further illustrates the possible advantages of smoothing. Figure 11(a) is a contour plot at 10 mbar of the six wave number analysis of the January 26 combined mode data. Figure 11(b) displays the latitudinally smoothed (1-2-1) analysis to the same data, and the difference from figure 11(a) is dramatic. Finally, figure 11(c) displays the same smoothed analysis but truncated at four wave numbers; the high wave number features that were present in figure 11(b), which may or may not be real, are missing in figure 11(c). Figure 11(c) suggests a meteorological picture that is very similar to that observed in the calculated geopotential height field in figure 12, which is a six wave number, combined mode height analysis. Thus, when the water vapor wave numbers 5 and 6 have amplitudes that are within the standard deviation of the Kalman filter fits to the data, truncation to wave number 4 may be justified.

Individual water vapor profiles on the LAIPAT also display a somewhat "noisy" character (Russell et al. 1984a). To examine the effects of such "noise" on a plot, the water vapor data on January 26 were interpolated to a surface of constant potential temperature, that is, $\Theta = 850$ K (near 10 mbar). Results are given in figure 13, where no latitudinal smoothing or wave number truncations were performed. The improvement over the field in figure 11(a) is pronounced, although it is apparent that some latitudinal smoothing would still be desirable. Because geopotential is a vertically integrated quantity, there is most likely less structure in figure 12 than would be expected for a quantity like potential vorticity (see fig. 9(b) of Grose (1984)), where the comparison with figure 11(c) is striking. In summary, if one develops

plots like figure 11(a) from the LAMAT data, the fields may appear disorganized, but by taking advantage of estimates of the noise with height and latitude, one can smooth the fields slightly and obtain what appears to be very realistic results.

Generally, the water vapor fields do not show any high wave number character that would be considered significant. One exception is the recurrence of propagating medium-scale waves in the lower stratosphere of the Southern Hemisphere (Miles and Grose 1986). These waves have been observed in all the LIMS constituents and derived heights in which a combined mode, six wave number analysis was performed, and their amplitude oscillated with a period of a week or two in a sporadic fashion during the Southern Hemisphere summer. A time series plot of the 100-, 70-, 50-, 30-, and 16-mbar amplitudes of wave 5 from 40°S to 64°S (fig. 14) reveals this behavior. Even though these wave amplitudes do not exceed the precision estimates of the measurements (0.24 ppmv), their persistence permits the resolution of the wave (Miles et al. 1987). The cross correlation of each curve to the 100-mbar level shows significant correlations for the 70- and 50-mbar levels, but little correlation at 30 mbar and none at 16 mbar. Figure 15 is a different view of the propagating medium-scale waves at 70 mbar on February 26. This same structure was apparent at other adjacent levels with no significant change in phase with altitude. Remsberg et al. (1984) showed a similar plot at 30 mbar for January 7, and a wave number 5 feature is still apparent there. Theory indicates that such a wave should damp out quickly with height in the summer hemisphere and not be noticeable at 30 mbar (Salby 1982; Miles and Grose 1986). Because of the relatively large (about 4 km) FOV for the LIMS water vapor channel, it is probable that atmospheric wave signatures that are several kilometers below the tangent altitude are affecting radiances being registered according to the midpoint altitude of the LIMS vertical FOV. Thus, waves would appear to dampen out more slowly with height in the H₂O coefficients than in the ozone or temperature fields derived with more narrow FOV's.

The LAMAT Nitrogen Dioxide Data

Data Characteristics

The LAIPAT NO₂ data have been shown to be of excellent quality (Russell et al. 1984b), and a summary of the LIMS NO₂ results is given by Russell et al. (1986). Monthly zonal mean cross sections of the ascending (near 1 p.m.) and descending (near 11 p.m.) modes of NO₂ from the LAMAT are presented by Russell et al. (1986). At higher latitudes

the local times depart from these nominal values (fig. 16). Monthly mean polar plots of NO₂ at 3 mbar were also prepared from the descending mode LAMAT coefficients (Russell et al. 1986). At that level the descending mode NO₂ approximates the total odd nitrogen (NO_x) except near the terminator region at high latitudes. The uncertainty in the zonal mean nighttime NO₂ is about 16 percent from 10 to 3 mbar, and it increases to 43 percent at 30 mbar and to 26 percent at 1 mbar. Errors for daytime NO₂ are similar except from 1 to 2 mbar, where mixing ratios are very low and systematic effects are more important. The vertical resolution of the daily NO₂ coefficients from the LAMAT ranges from 3.5 to 6.5 km. The mapping of LIMS NO₂ data presents several special characteristics when compared with the other LIMS parameters. Synoptic mapping difficulties occur primarily because of the large diurnal variation of NO₂ and the sampling pattern which makes measurements at only two local solar times at each latitude. For these reasons, this section contains not only a discussion of the empirical fit to the data but also some thoughts about the overall significance of any derived maps.

The character of the LIMS NO₂ data is discussed in terms of the LAMAT generation. The vertical spatial extent of the LIMS NO₂ maps ranges from the mid to upper stratosphere because of the low NO₂ signal-to-noise ratio for mixing ratios at levels above and below this region. For the ascending mode, Fourier coefficients for the entire latitude range (64°S to 84°N) were obtained between 30 and 2 mbar. For the descending mode, the corresponding range was 30 to 1 mbar. Since the signal-to-noise ratio for the NO₂ channel radiance decreases with temperature, significant data gaps occur in the lower stratosphere near the winter pole where the temperatures are coldest. This is also the location where the absolute NO₂ levels are very low (Russell et al. 1984c). The data gaps tend to reoccur in the same longitudinal bands because the longitudinal temperature variations are controlled by quasi-stationary planetary waves. High-latitude data gaps were seen in early January when the temperatures were coldest, but by February the temperatures near the winter pole were sufficiently warm to permit much better data coverage.

An indication of the wave number resolution in the LAMAT is given in table 3, which shows wave number as a function of latitude and pressure in early January. In some places, no coefficients were calculated; in others, only a zonal mean was calculated; whereas in still others, all four waves were calculated. As noted above, the data coverage at high latitudes was the least for January, and thus table 3

is somewhat atypical of the whole data set. The paper of Russell et al. (1986) contains monthly mean polar stereographic maps of NO₂ at 3 mbar. However, because many coefficients were not calculated north of 68°N for the first half of January, a January mean map is appropriate for only the latter part of that month.

Because NO₂ varies diurnally, it is especially important to keep in mind the sampling characteristics of the LIMS instrument, as discussed by Haggard et al. (1986). On each day at a given latitude, data were obtained at 26 longitudes (13 for the ascending mode and 13 for the descending mode). Except near the North Pole and poleward of about 40°S, all the ascending mode data were taken at nearly the same local (solar) time (about 1 p.m.), and the descending mode data were taken at about 11 p.m. (See fig. 16.) Near the winter pole, the LIMS tangent point was in darkness on both modes, whereas near the summer pole, it was in daylight on both modes. (See fig. 16.) Since the nighttime NO₂ mixing ratio exceeds the daytime value, winter and summer LIMS NO₂ maps show a sharp meridional gradient at high latitudes as the LIMS tangent point track crosses the terminator. (See fig. 1 of Haggard et al. 1986.)

When interpreting the NO₂ coefficients in the LAMAT, it is best to think of the ascending and descending modes of NO₂ as two separate species. For example, the ascending mode "zonal mean coefficient" at a latitude and pressure is not a zonal mean coefficient but rather an estimate of the average NO₂ value for the local solar time for that latitude (fig. 16). In a similar way, the coefficients of the sine and cosine terms in equation (2) are not estimates of zonal waves, but they do contain effects of wave transport on the NO₂ field. By considering the "zonal variations" of the NO₂ in the Kalman filter analysis, it is possible to calculate a more accurate estimate of the "zonal mean" NO₂ coefficient for that local time. For the following NO₂ discussion, the terms "wave" and "zonal mean" are subject to these qualifying interpretations and the quotation marks will be understood.

Kalman Filter Analysis Procedure for NO₂

The method used to obtain the virtual data set for the NO₂ analysis was similar to that used for ozone (see Remsberg et al. 1986). The amplitude variances and zonal mean trends were obtained from preliminary Kalman filter runs. Only descending mode data were considered in these preliminary runs because of their better signal-to-noise ratio in the upper stratosphere. Table 4 lists the amplitude variances in dS/dt and the zonal mean trend dX_0/dt for

a 31-day Kalman filter run in midwinter. The relaxation times τ calculated from those runs were found to be rather variable with latitude and pressure, and thus their reliability was questioned. Instead of using those times, the relaxation times obtained from the temperature analyses were applied to the NO₂ estimates. The physical justification for this substitution is that NO₂ is coupled photochemically and dynamically to temperature (and ozone) and, therefore, should vary with a similar relaxation time. The relaxation times used in the January Kalman filter runs are shown in table 5.

The data precision $\sigma_{n,m}$ applied to the Kalman filter was determined in the following way. Initial estimates of the measurement standard deviations were obtained from a series of measurements. (See figs. 3 and 4 of Russell et al. 1984b). Those standard deviations were then averaged over latitude to obtain a set of values for each pressure level, and they are listed in table 6. Standard deviations from 50 to 100 mbar are small because the retrieved results at those levels were weighted toward a climatological profile according to the radiance signal-to-noise.

An approximate measure of the closeness of the empirical fit to the data is given in the noon GMT (12Z) root-mean-square deviation (RMSD). This quantity is called σ_{obs} and represents the comparison of the noon GMT fit with all data for the day for a given mode. Since there is not a diurnal variation in the LAMAT data, there is no special significance to the selection of noon GMT as the reference time other than it provides a regular interval for producing the output product. In general, σ_{obs} will exceed the actual RMSD except for slowly changing fields. Thus, σ_{obs} will equal the input measurement precision $\sigma_{n,m}$ only for ideal conditions. The behavior of the 12Z σ_{obs} for the ascending mode for January is shown in figure 17. The σ_{obs} for the daytime measurements reached a maximum of 0.7 ppbv at 7 mbar and decreased to 0.4 ppbv at 30 and 3 mbar. These values are one to two times those input to the Kalman filter. (See table 6.) It is also interesting that they tend to be proportional to the zonal mean NO₂ mixing ratio (fig. 18). The large standard deviations seen in the polar night region (poleward of 68°N) can also be explained on this basis since nighttime rather than daytime NO₂ is being measured.

There are two likely explanations for σ_{obs} being proportional to the zonal mean. The first is related to the nature of the measurement errors. As noted by Russell et al. (1984b), some of the measurement errors are proportional to the NO₂ concentration. When these errors dominate, a pattern of σ_{obs} values will occur like those in figure 4 of Russell et al. (1984b). The σ_{obs} may also be due to unresolved

spatial and temporal scale transport acting on zonal mean gradients. Since the gradients in this case are roughly proportional to the zonal mean, they also vary with the zonal mean.

An overview of the descending mode results for January is given in figures 19 and 20, where the σ_{obs} and the zonal mean are two to four times as large as those for the ascending mode (figs. 17 and 18). This approximate proportionality is consistent with the conclusion drawn above, i.e., that the σ_{obs} is proportional to the zonal mean NO_2 . It is also of interest that the largest σ_{obs} in January is found near the region of largest mixing ratio (16°S and 3 mbar) and not in the region of largest gradient. This result implies that a large σ_{obs} is due more to inadequate observational precision rather than to natural variability.

The σ_{obs} and zonal mean for the ascending mode for May are shown in figures 21 and 22. The May σ_{obs} value is similar to the January value except that the maximum occurs near the summer pole rather than at low latitudes. As was found for January, the σ_{obs} is roughly proportional to the zonal mean value.

An analysis of one mode of NO_2 contains the longitudinal variations of that mode at only one local solar time. When no atmospheric waves are present (other than the diurnal wave), the longitudinal variations described by the coefficients should be smaller than the σ_{obs} . It is possible for the effects of the diurnal waves to appear in the LAMAT results when the terminator is moving through the local solar time of the measurement. When this happens, the Kalman filter will interpret the sudden change seen across the terminator as the onset of wave activity; but after the transition through the terminator region is finished, the waves, as seen by the filter, will die out and the zonal term will again be dominant. When waves are present, the longitudinal distribution of NO_2 will vary in phase just as total odd nitrogen (NO_x) and ozone (O_3) vary. Such variations occur because dynamical activity directly affects NO_x and O_3 . If σ_{obs} is small, suggesting that the Kalman filter approximation to the data is very good, then even moderate wave amplitudes will appear significant. The relatively large wave standard deviation (standard deviation of the nonzonal coefficients about the zonal mean in the LAMAT) at 50°N and 5 mbar in figure 23 is an excellent example of that circumstance. (Compare with fig. 19.)

Kalman Filter Results for NO_2

The fidelity of the LAMAT coefficients is described for 3 selected days, January 2, January 25, and February 26. Discussion is generally limited to the 10-mbar fields, although the fields are considered

reliable from 1 to 30 mbar. (From 50 to 100 mbar, the NO_2 profiles were constrained to the shape of a climatological first-guess profile at the retrieval stage, and any real variations in atmospheric NO_2 were severely damped at those levels.) The significance of any derived coefficients can be appreciated best in regions of active dynamics and large signal-to-noise ratio. These conditions are most likely to be encountered at high latitudes in late winter near 3 to 10 mbar, and more attention is focused on those findings in the next subsection.

The agreement between the LAMAT and the LAIPAT data for 3 mbar at 40°N for January 26, 1979, is shown in figure 24. The descending mode has a standard deviation of 1.4 ppbv from the LAMAT curve; and the ascending mode, a standard deviation of 0.38 ppbv. This figure illustrates the importance of calculating the wave coefficients. If only the mean term (eq. (2)) had been calculated, the result would have been a slowly varying fit to a mean value of the data averaged over the relaxation time of the Kalman filter and would not have shown any longitudinal detail.

Figures 25 and 26 describe a difficult mapping situation at high northern latitudes in early January where temperatures are cold and sunlight is limited. This situation leads to both low NO_2 and low S/N in the NO_2 radiances. However, the Kalman filter still attempts to follow the retrieved LAIPAT data because its input precision is still 0.45 ppbv. There are also missing data between 180°E and 360°E , and, as a result, even the zonal mean coefficient can be misleading. Russell et al. (1984c) have obtained more reliable results there by averaging NO_2 radiance profiles over 60° longitude sectors and over periods of 5 days before retrieval, thereby alleviating some of the problems of missing data in the LAIPAT. That procedure yields six profiles per latitude and, at most, a two wave number analysis. Furthermore, because of the 5-day averages, the Kalman filter mapping procedure cannot be applied to those data as described in this report.

It is emphasized that there are rapid transient features in the LAIPAT data that are not resolvable by the filter, and the fact that these features are not resolvable in no way indicates that they are not real. Since the Kalman filter can resolve only slowly changing (1 day or more) long waves, the best criteria for the success of the estimate, at least for the nighttime NO_2 , should include the degree of continuity with time and latitude as well as the fit of the field to the data.

Characteristics of NO₂ During Disturbed Periods

The period between late January and March produced perhaps the most interesting NO₂ results of the LIMS mission for three reasons. First, the warmer, late-winter temperatures resulted in better signal-to-noise ratios and fewer data gaps than in early January; second, the planetary wave amplitudes were sufficiently large to cause spatial variations in NO₂ that were large compared with the measurement precision; and third, the terminator was close enough to the pole that only daytime data were gathered with the ascending mode. For these reasons, 2 days in this period, January 25 and February 26, are considered in some detail.

The ascending and descending mode data and the fits to the data at 10 mbar and at 56°N for January 24, 25, and 26 (fig. 27) display excellent time continuity, few data gaps, and small σ_{obs} . The wave pattern is quasi-stationary, at least for the 3-day sequence, and both modes display excellent continuity with time and latitude (not shown).

The data coverage for February 26 is better than that for the 3 January days, and the ascending mode contains only daytime data. The data and the fits for 56°N, 60°N, and 64°N on February 25, 26, and 27 are shown in figure 28, and the comparisons are generally excellent. The one exception would be the poor response of the filter to high NO₂ values near 290°E on February 26 at all three latitudes. This apparent, highly transient situation is difficult to follow and would be smoothed by the filter.

A prominent, slowly changing, wave 2 pattern exists in figure 28 and is somewhat out of phase with the location of the two geopotential lows shown in figure 29. As shown in figure 11 of Russell et al. (1984c), a negative correlation for NO₂ and a geopotential at high latitudes in the mesosphere were observed during early January, and the high NO₂ levels (11 ppbv in the zonal mean) were transported downward to at least 2.3 mbar by mid-February. It is altogether likely that relatively high levels of total NO_x were transported down to 10 mbar by the diabatic circulation in January, that they remained in the remnants of the polar vortex after it was split in mid-February, and that the fraction of NO_x present in the form of NO₂ decreased markedly from 2.3 to 10 mbar. Such a change in the chemical partitioning would cause the NO₂ to be nonconservative during that downward transport, especially if the air parcels were being subjected to sunlight during parts of their trajectories. A detailed study is needed to understand such changes more fully.

Studies of the diurnal changes in NO₂ were con-

ducted by Solomon et al. (1986) using the orbital LAIPAT data at high northern latitudes during May. An appropriate selection of latitudes and days during May yielded NO₂ observations obtained during the afternoon and evening at solar zenith angles ranging from about 35° to 110°. The observations were compared with diurnal model calculations, and there was clear evidence to support the night decay of NO₂ to form N₂O₅ (Solomon et al. 1986). In the foregoing analysis, the most important criteria for judging the significance of the LAMAT empirical fit have been agreement with the LAIPAT and continuity with latitude, time, and mode. The fit to the data is even better at 7 to 3 mbar for the larger nighttime NO₂ levels. The foregoing criteria can be evaluated more objectively by plotting the wave amplitude and phase as functions of time and latitude. In figures 30 through 32 the zonal mean and the amplitudes and phases of waves 1 and 2 at 60°N are plotted for January at 10 mbar. Figure 30 shows that the zonal mean for each mode varies considerably (15 percent) from day-to-day despite the time smoothing inherent in the Kalman filter analysis. A comparison of figure 30 with the corresponding results for ozone reveals that the apparent day-to-day variations in NO₂ are larger than those for ozone, a result which may, in part, be a reflection of the rather large gradients in NO₂ as opposed to those for ozone. This result may also be due to the effects of missing data at some longitudes (figs. 25 through 28). The amplitudes and phases of waves 1 and 2 vary considerably with time (figs. 31 and 32). In addition, the results for the two modes are quite similar, except for the wave 2 amplitude. The agreement between modes and smooth changes with time are further evidence of the significance of the empirical estimates.

Since the fit to the data was performed independently of latitude, the extent of latitudinal continuity in the derived coefficients is a more important indicator of the significance of the results than the continuity with time. Plots of the 10-mbar zonal mean and waves 1 and 2 as functions of latitude are shown in figures 33 through 35 for January 26. Figure 33 shows that the zonal mean for both modes varies smoothly with latitude. The sharp dip in the zonal mean descending mode NO₂ at 60°S is due to a terminator crossing shown in figure 16. The amplitudes and phases of waves 1 and 2 (figs. 34 and 35) are reasonably continuous with latitude and mode except at high latitudes in the Southern Hemisphere. This finding is similar to that obtained before—namely, that the dynamics of the Summer Hemisphere are weak and the resultant wave amplitudes are comparable to the precision of the measurement and, therefore, are of questionable significance. The role

of photochemistry in the relationships between the modes in figures 34 and 35 cannot be neglected.

Concluding Remarks

Water vapor distributions derived from the LIMS Map Archival Tape (LAMAT) coefficients should be excellent, especially when some minimal smoothing is performed prior to generation of the maps. The descending mode data are considered more reliable in the upper stratosphere. The occurrence of mode differences in water vapor (H_2O) in the upper stratosphere means that maps created using combined mode data can be more "noisy" than maps created from just the descending mode data. Sampling biases are present in the LAMAT data for the winter polar vortex region and between 40 and 100 mbar at tropical latitudes. Preliminary comparisons with geopotential height maps indicate that water vapor should be a reliable tracer for transport processes in the lower stratosphere where the Equator-to-Pole gradients are more pronounced.

The nitrogen dioxide (NO_2) data are also of excellent quality in the middle stratosphere although they may be more difficult to interpret than the water vapor data because of their diurnal variations. The descending and ascending mode coefficients are not combined because of this large natural diurnal variability of NO_2 . This occurrence means that the ascending mode zonal mean coefficient is not a zonal mean NO_2 value, but is just the average "near-noon" NO_2 mixing ratio for a particular latitude and pressure. Higher order Fourier coefficients exhibit wave-like variations that contain effects of transport on the NO_2 distribution, but again they cannot represent true zonal wave numbers at a given synoptic time. There is no question, however, that many of the features appearing in the derived fields are due to real atmospheric effects and that the coefficients should provide an approximate picture of NO_2 morphology for much of the observation period of the Limb Infrared Monitor of the Stratosphere (LIMS). Calculation of the coefficients for waves 1 through 4 certainly improves the estimates of the "near-noon" or "near-midnight" zonal mean coefficient. It is recommended that detailed studies of the role of chemistry and dynamics on the NO_2 distributions be conducted using the orbital data on the LIMS Inverted Profile Archive Tape (LAIPAT).

NASA Langley Research Center
Hampton, VA 23665-5225
November 20, 1987

References

- Austin, J.; Remsberg, E. E.; Jones, R. L.; and Tuck, A. F.: Polar Stratospheric Clouds Inferred From Satellite Data. *Geophys. Res. Lett.*, vol. 13, no. 12, Nov. Suppl., 1986, pp. 1256-1259.
- Gille, John C.; and Russell, James M., III: The Limb Infrared Monitor of the Stratosphere: Experiment Description, Performance and Results. *J. Geophys. Res.*, vol. 89, no. D4, June 30, 1984, pp. 5125-5140.
- Gordley, L. L.; Russell, J. M., III; and Remsberg, E. E.: Global Lower Mesospheric Water Vapor Revealed by LIMS Observations. *Atmospheric Ozone*, C. S. Zerefos and A. Ghazi, eds., D. Reidel Publ. Co., c.1985, pp. 139-143.
- Grose, William L.: Recent Advances in Understanding Stratospheric Dynamics and Transport Processes: Application of Satellite Data to Their Interpretation. *Adv. Space Res.*, vol. 4, no. 4, 1984, pp. 19-28.
- Haggard, Kenneth V.; Remsberg, Ellis E.; Grose, William L.; Russell, James M., III; Marshall, B. T.; and Lingenfelter, G.: *Description of Data on the Nimbus 7 LIMS Map Archive Tape—Temperature and Geopotential Height*. NASA TP-2553, 1986.
- Hamill, Patrick; and McMaster, Leonard R., eds.: *Polar Stratospheric Clouds—Their Role in Atmospheric Processes*. NASA CP-2318, 1984.
- Kerridge, B.; and Remsberg, E. E.: Evidence for Non-Local Thermodynamic Equilibrium in the ν_2 Mode of Mesospheric H_2O and ν_3 Mode of Stratospheric NO_2 . *Trans. American Geophys. Union*, vol. 68, no. 16, Apr. 21, 1987, p. 372.
- Manuilova, R. O.; and Shved, G. M.: The 2.7 and 6.3 μm H_2O Band Emissions in the Middle Atmosphere. *J. Atmos. & Terr. Phys.*, vol. 47, no. 5, May 1985, pp. 413-422.
- Miles, T.; and Grose, W. L.: Transient Medium-Scale Wave Activity in the Summer Stratosphere. *Bull. American Meteorol. Soc.*, vol. 67, no. 6, June 1986, pp. 674-686.
- Miles, T.; Grose, W. L.; Russell, J. M., III; and Remsberg, E. E.: Comparison of Southern Hemisphere Radiosonde and LIMS Temperatures at 100 mb. *Q. J. Royal Meteorol. Soc.*, vol. 113, Oct. 1987, pp. 1382-1386.
- Remsberg, Ellis E.; Russell, James M., III; Gordley, Larry L.; Gille, John C.; and Bailey, Paul L.: Implications of the Stratospheric Water Vapor Distribution as Determined From the Nimbus 7 LIMS Experiment. *J. Atmos. Sci.*, vol. 41, no. 19, Oct. 1, 1984, pp. 2934-2945.
- Remsberg, Ellis E.; Kurzeja, Robert J.; Haggard, Kenneth V.; Russell, James M., III; and Gordley, Larry L.: *Description of Data on the Nimbus 7 LIMS Map Archive Tape—Ozone and Nitric Acid*. NASA TP-2625, 1986.
- Russell, James M.; Gille, John C.; Remsberg, Ellis E.; Gordley, Larry L.; Bailey, Paul L.; Fischer, Herbert; Girard, Andre; Drayson, S. Roland; Evans, Wayne F. J.; and Harries, John E.: Validation of Water Vapor Results Measured by the Limb Infrared Monitor of the Stratosphere Experiment on Nimbus 7. *J. Geophys. Res.*, vol. 89, no. D4, June 30, 1984a, pp. 5115-5124.

- Russell, James M., III; Gille, John C.; Remsberg, Ellis E.; Gordley, Larry L.; Bailey, Paul L.; Drayson, S. Roland; Fischer, Herbert; Girard, Andre; Harries, John E.; and Evans, Wayne F. J.: Validation of Nitrogen Dioxide Results Measured by the Limb Infrared Monitor of the Stratosphere (LIMS) Experiment on Nimbus 7. *J. Geophys. Res.*, vol. 89, no. D4, June 30, 1984b, pp. 5099-5107.
- Russell, James M., III; Solomon, Susan; Gordley, Larry L.; Remsberg, Ellis E.; and Callis, Linwood B.: The Variability of Stratospheric and Mesospheric NO₂ in the Polar Winter Night Observed by LIMS. *J. Geophys. Res.*, vol. 89, no. D5, Aug. 20, 1984c, pp. 7267-7275.
- Russell, James M., III; Solomon, Susan; McCormick, M. P.; Miller, A. J.; Barnett, J. J.; Jones, R. L.; and Rusch, D. W.: Middle Atmosphere Composition Revealed by Satellite Observations. *Middle Atmosphere Program--Handbook for MAP, Volume 22*, James M. Russell, III, ed., Univ. of Illinois, Sept. 1986. (Available as NASA CR-180128.)
- Salby, Murry L.: A Ubiquitous Wavenumber-5 Anomaly in the Southern Hemisphere During FGGE. *Mon. Weather Rev.*, vol. 110, no. 11, Nov. 1982, pp. 1712-1720.
- Solomon, S.; Russell, J. M., III; and Gordley, L. L.: Observations of the Diurnal Variation of Nitrogen Dioxide in the Stratosphere. *J. Geophys. Res.*, vol. 91, no. D5, Apr. 30, 1986, pp. 5455-5464.

Table 1. Data Variance of H₂O for Late December Through Mid-January

Pressure, mbar	(Latitude band, deg) σ^2 , ppmv ²			
1.0	(-64 to -44) 0.30	(-40 to 72) 0.40	(76 to 84) 0.50	
1.5	(-64 to 64) .15	(68 to 84) .25		
2	(-64 to 64) .10	(68 to 84) .17		
3	(-64 to 64) .07	(68 to 84) .14		
5	(-64 to 56) .05	(60 to 84) .09		
7	(-64 to 56) .04	(60 to 84) .07		
10	(-64 to 52) .03	(56 to 84) .05		
16	(-64 to 44) .03	(48 to 84) .04		
30	(-64 to 44) .03	(48 to 84) .04		
50	(-64 to 44) .04	(48 to 84) .06		
70	(-64 to 44) .06	(48 to 84) .08		
100	(-64 to -24) .20	(-20 to 20) .30	(24 to 84) .20	

Table 2. Highest Wave Number for Which H₂O Coefficients Are Available on the LAMAT
for Combined Mode on January 2, 1979^a

Latitude, deg	Highest wave number for combined mode at pressure, mbar, of —											
	100	70	50	30	16	10	7	5	3	2	1.5	1.0
64S	6	6	6	6	6	6	6	6	6	6	6	6
56	6	6	6	6	6	6	6	6	6	6	6	6
48	6	6	6	6	6	6	6	6	6	6	6	6
40	6	6	6	6	6	6	6	6	6	6	6	6
32	4	6	6	6	6	6	6	6	6	6	6	6
24	1	5	6	6	6	6	6	6	6	6	6	6
16	0	2	6	6	6	6	6	6	6	6	6	6
8		1	4	6	6	6	6	6	6	6	6	6
0		1	4	6	6	6	6	6	6	6	6	6
8		1	5	6	6	6	6	6	6	6	6	6
16	0	4	6	6	6	6	6	6	6	6	6	6
24	2	6	6	6	6	6	6	6	6	6	6	6
32	6	6	6	6	6	6	6	6	6	6	6	6
40	6	6	6	6	6	6	6	6	6	6	6	6
48	6	6	6	6	6	6	6	6	6	6	6	6
56	6	6	6	6	6	6	6	6	6	6	6	6
64	6	6	6	6	6	6	6	6	6	6	6	5
72	5	6	6	6	6	6	6	6	5	5	4	3
80	4	5	6	6	6	6	5	5	4	3	3	2
84N	4	5	6	6	6	6	5	4	3	2	2	1

^a Blank spaces indicate inability to obtain data.

Table 3. Highest Wave Number for Which NO₂ Coefficients Are Available on the LAMAT
for Ascending, Descending Mode on January 13, 1979^a

Latitude, deg	Highest wave number for ascending, descending mode at pressure, mbar, of —											
	100	70	50	30	16	10	7	5	3	2	1.5	1.0
64S	4,4	4,4	4,4	4,4	4,4	4,4	4,4	4,4	4,4	3,3	0,1	
56	3,2	4,4	4,4	4,4	4,4	4,4	4,4	4,4	4,4	2,4	,2	
48	1,1	4,3	4,4	4,4	4,4	4,4	4,4	4,4	4,4	1,4	,4	,4
40		2,2	2,3	4,4	4,4	4,4	4,4	4,4	4,4	0,4	,4	,4
32		,0	0,1	4,4	4,4	4,4	4,4	4,4	3,4	,4	,4	,3
24				2,3	4,4	4,4	4,4	4,4	3,4	0,4	,4	,3
16				1,2	4,4	4,4	4,4	4,4	3,4	0,4	,4	,3
8				0,1	4,4	4,4	4,4	4,4	4,4	1,4	,4	,3
0				0,1	4,4	4,4	4,4	4,4	4,4	1,4	,4	,3
8				0,1	4,4	4,4	4,4	4,4	3,4	,4	,4	,3
16				1,1	4,4	4,4	4,4	4,4	2,4	,4	,4	,3
24				2,2	4,4	4,4	4,4	4,4	2,3	,3	,3	,2
32	0,0	1,1	1,2	3,4	4,4	4,4	4,4	4,4	2,4	,4	,4	,2
40	1,2	3,3	3,3	3,4	4,4	4,4	4,4	4,4	2,4	,4	,4	,2
48	2,2	3,3	3,3	3,3	3,4	4,4	4,4	3,4	1,3	,3	,3	,2
56	1,1	1,2	2,2	2,2	2,2	2,3	2,3	2,3	1,2	,2	,2	,1
64	0,0	0,1	1,1	1,1	1,1	1,1	1,1	1,1	0,1	,1	,1	,1
72					0,0	1,0	1,0	1,0	1,0	1,0	1,0	
80												
84N												

^a Blank spaces indicate inability to obtain data.

Table 4. Amplitude Variances and Zonal Mean Trend for
NO₂ Analysis for December to January^a

Pressure, mbar	Latitude, deg	Variance, ppbv ² , for wave number—					ZMT
		0	1	2	3	4	
1	52S	0.0291	0.0161	0.0248	0.0202	0.0140	0.006
	0	.5058	.1767	.3350	.3194		.032
	60N	.7721	.5796				.070
10	60S	0.0625	0.0218	0.0248	0.0205	0.0456	0.031
	0	.1080	.0648	.0652	.0587	.0937	-.006
	60N	1.3267	.7700	.6517	.1007		-.040
100	60S	0.0024	0.0016	0.0016	0.0013	0.0002	-0.001
	0						
	60N	.1535	.0089				-.005

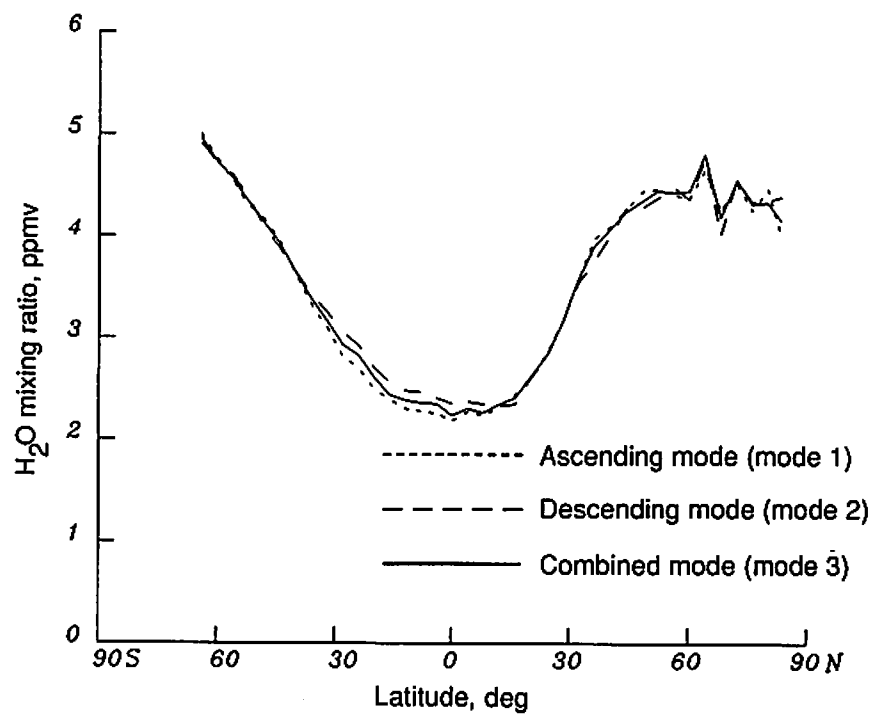
^a Blank spaces indicate inability to obtain data.

Table 5. Relaxation Times for NO₂ Analysis for January

Pressure, mbar	Relaxation time, days, for wave number—				
	0	1	2	3	4
1.0	2.7	2.3	1.7	1.6	1.4
1.5	3.0	2.8	2.2	1.7	1.4
2	3.0	2.8	2.2	1.7	1.4
3	3.0	2.8	2.2	1.7	1.4
5	3.0	2.8	2.2	1.7	1.4
7	3.6	3.6	2.7	2.3	2.2
10	3.6	3.6	2.7	2.3	2.2
16	3.6	3.6	2.7	2.3	2.2
30	4.5	3.7	2.7	2.4	2.3
50	4.5	3.7	2.7	2.4	2.3
70	4.5	3.7	2.7	2.4	2.3
100	3.4	3.8	2.5	2.6	2.1

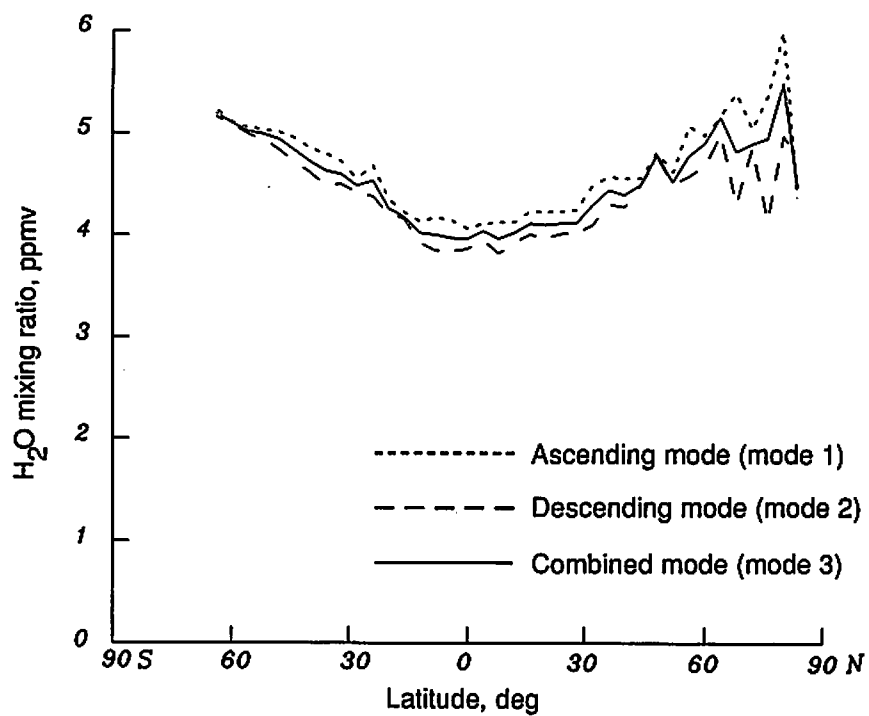
Table 6. Measurement Precision for Final NO₂
Kalman Filter Run

Pressure, mbar	Standard deviation, ppbv
1.0	1.00
1.5	.71
2	.55
3	.50
5	.50
7	.55
10	.45
16	.32
30	.22
50	.07
70	.06
100	.09



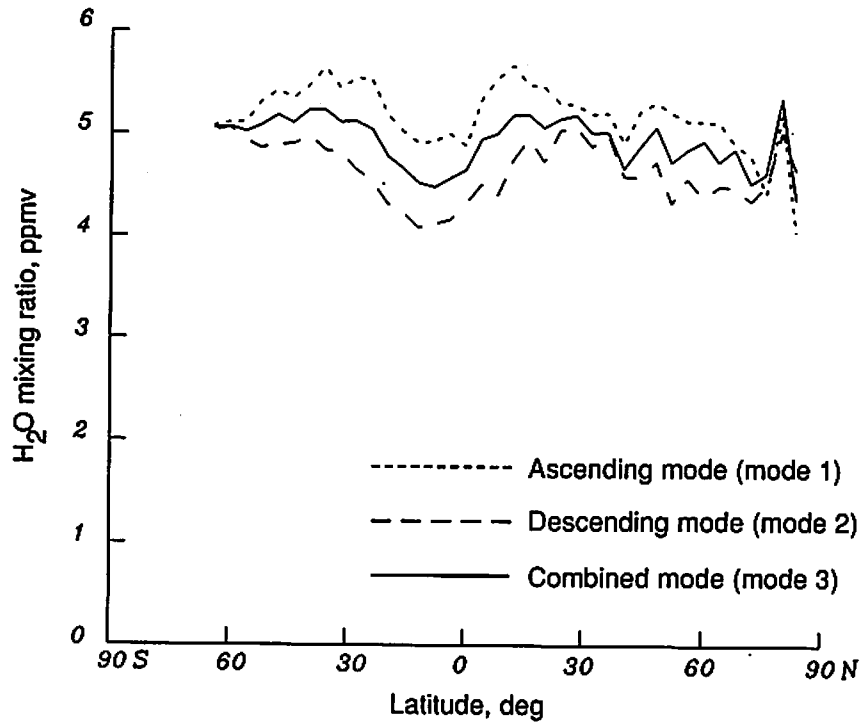
(a) 50 mbar.

Figure 1. Zonal mean H₂O for each mode on January 2, 1979.



(b) 10 mbar.

Figure 1. Continued.



(c) 3 mbar.

Figure 1. Concluded.

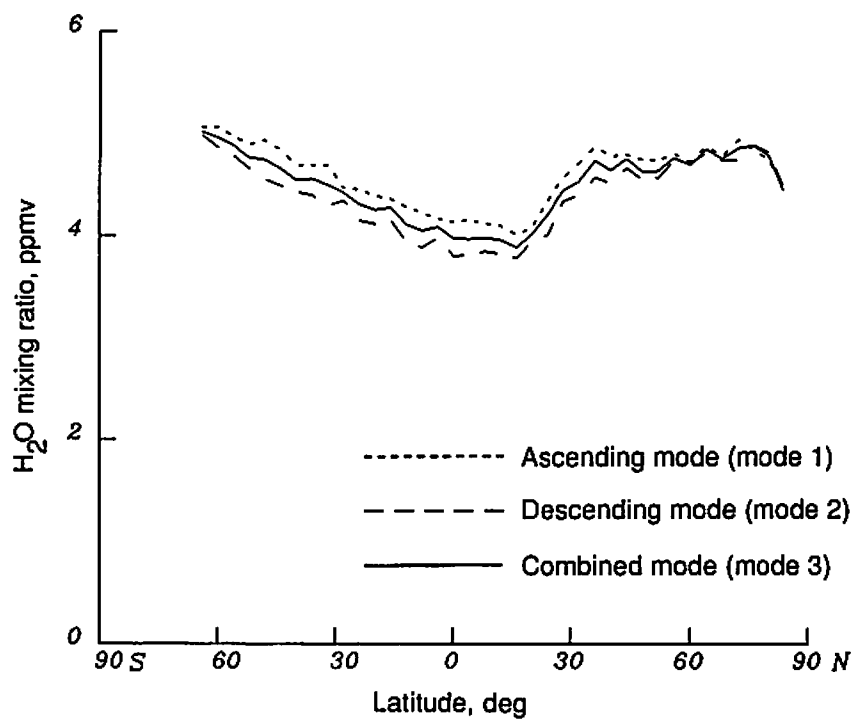
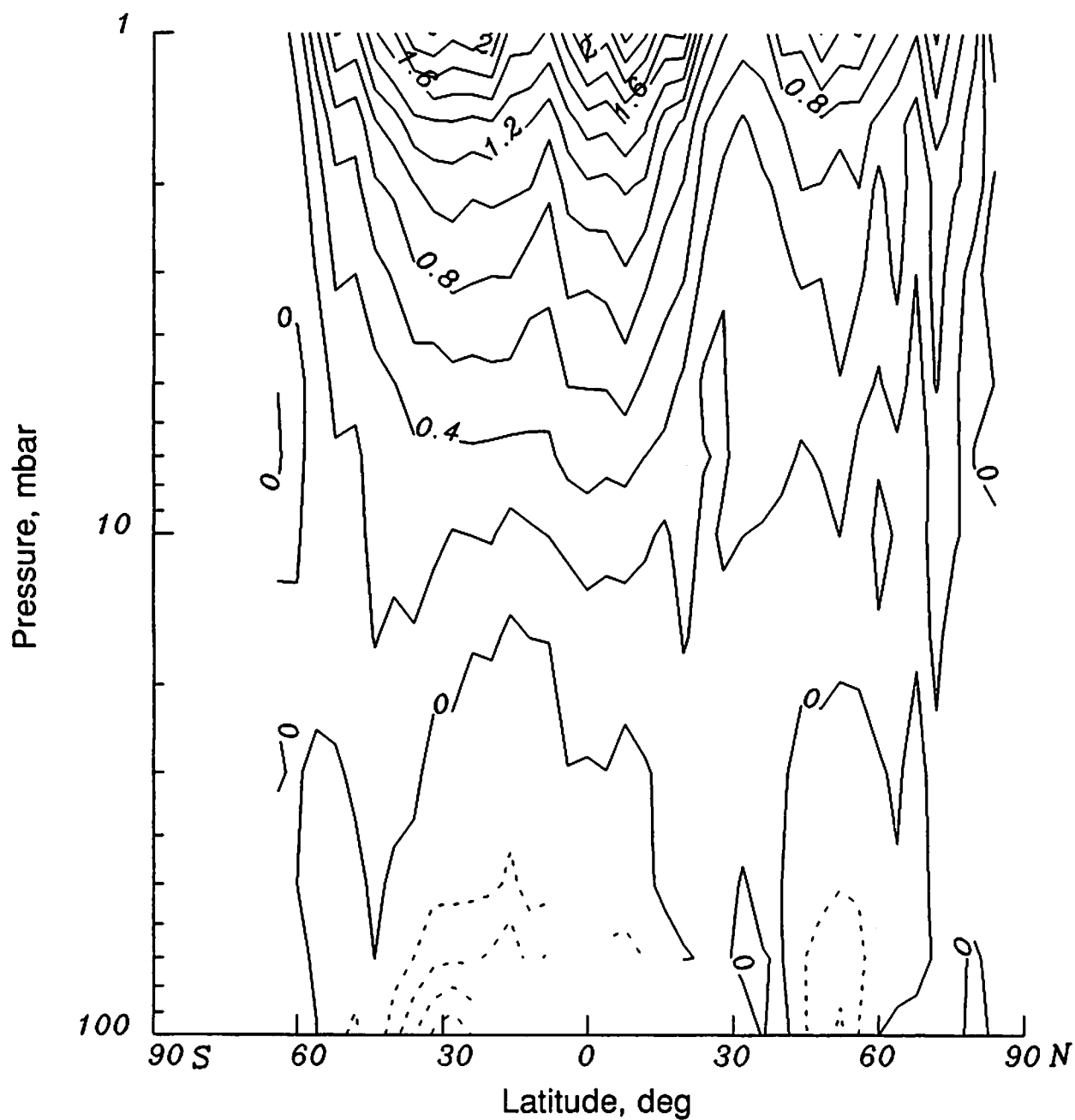
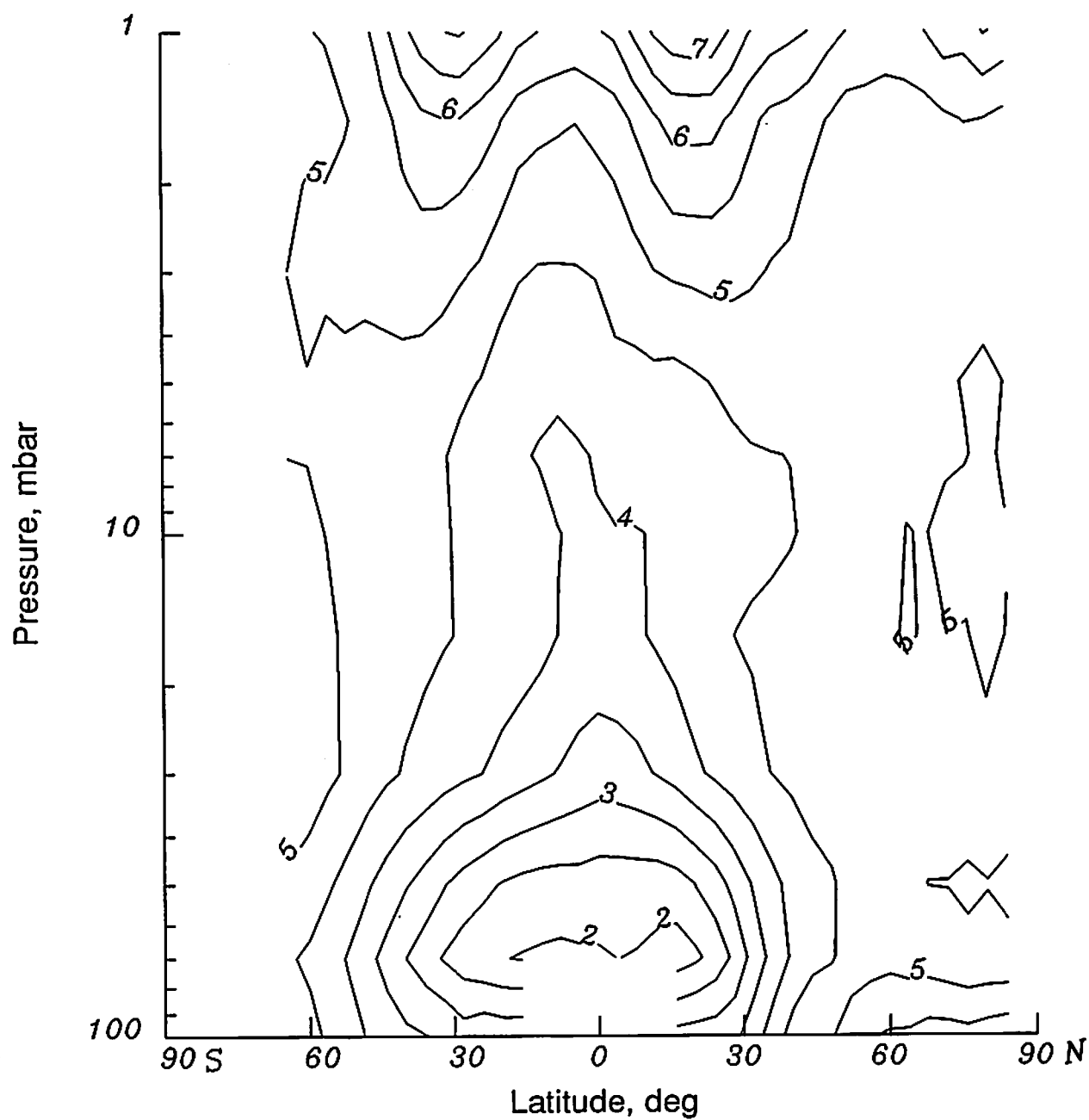


Figure 2. Zonal mean H_2O at 10 mbar on February 26, 1979.



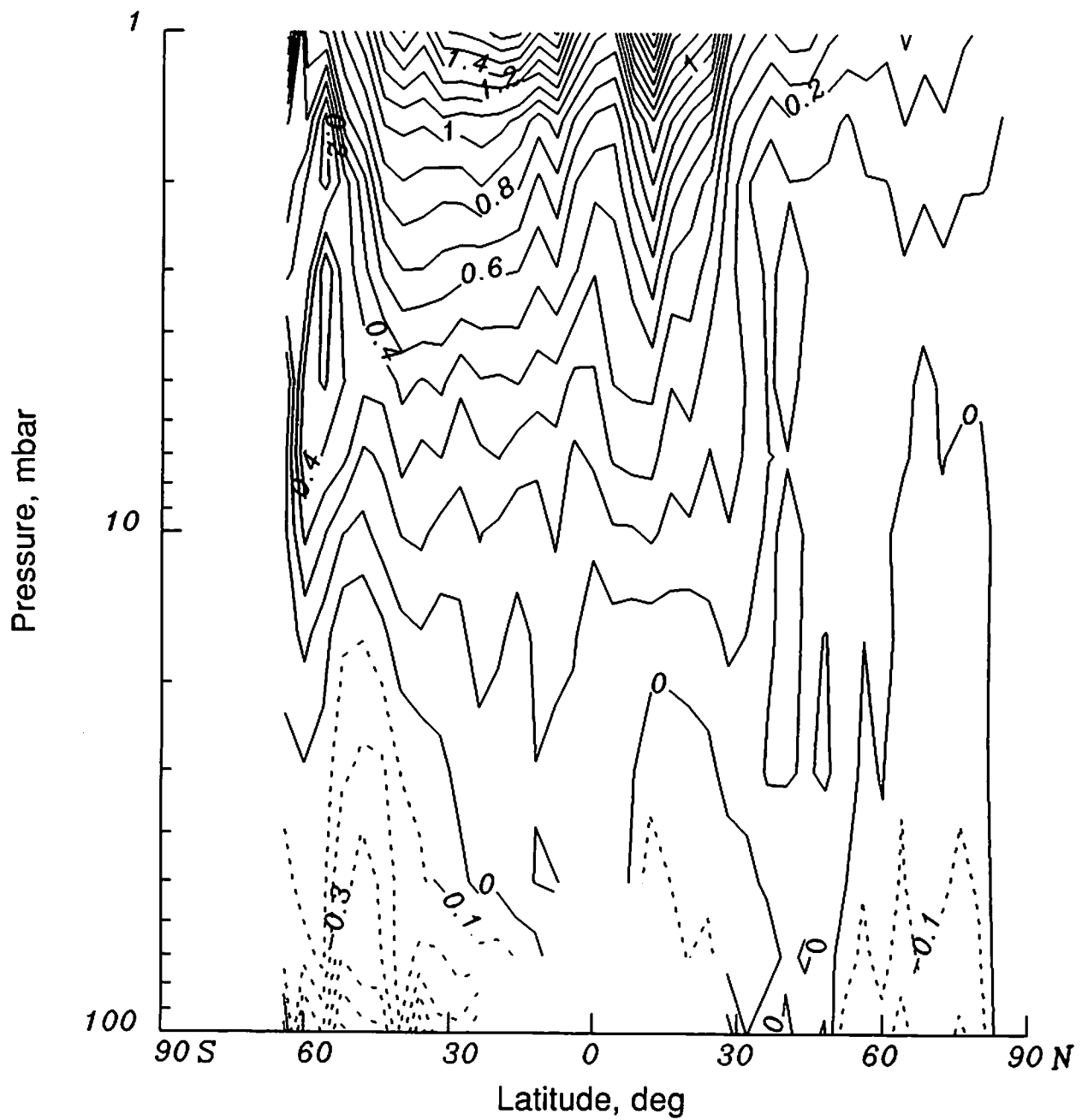
(a) Zonal mean for ascending-minus-descending mode for January 1979. Contour interval, 0.2 ppmv.

Figure 3. Average monthly zonal mean H_2O .



(b) Cross section of zonal mean combined mode for January 1979. Contour interval, 0.5 ppmv.

Figure 3. Continued.



(c) Zonal mean for ascending-minus-descending mode for May 1979. Contour interval, 0.1 ppmv.

Figure 3. Concluded.

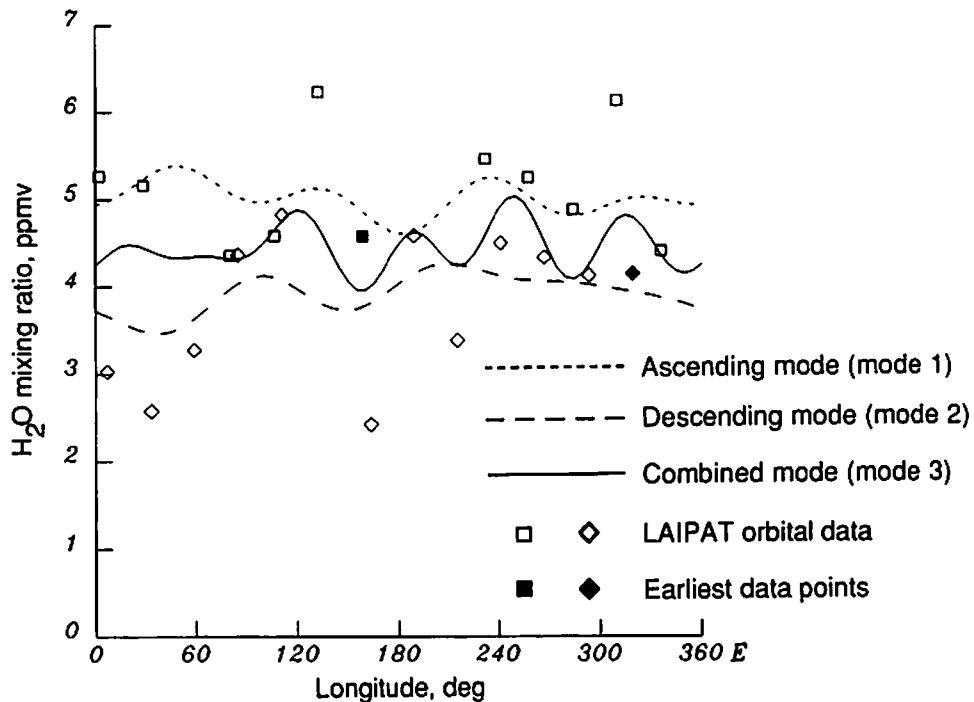


Figure 4. Comparison of the Fourier coefficient estimates of the H_2O data for each mode at the Equator and 3 mbar on January 26, 1979. Square symbols indicate ascending data; diamond symbols, descending data.

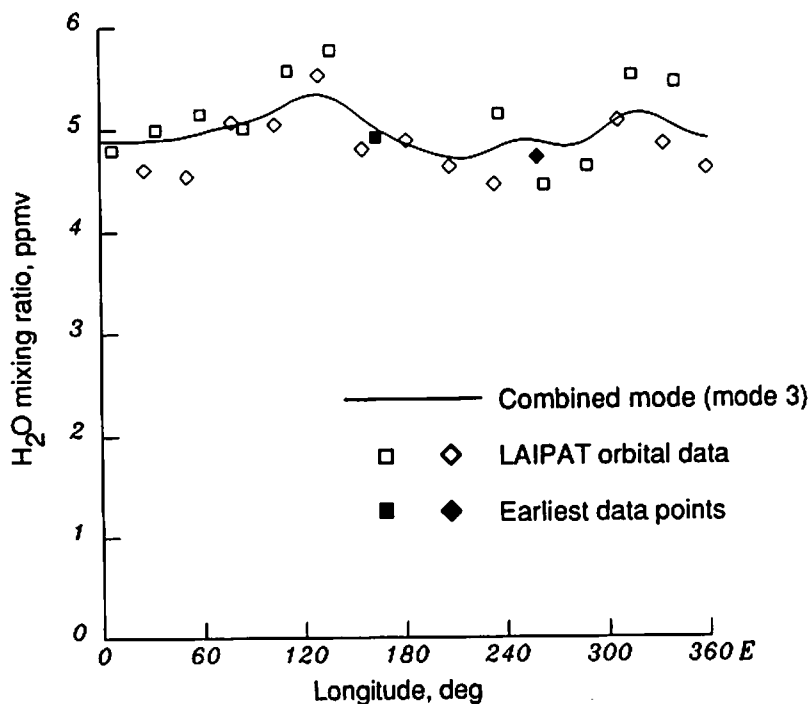
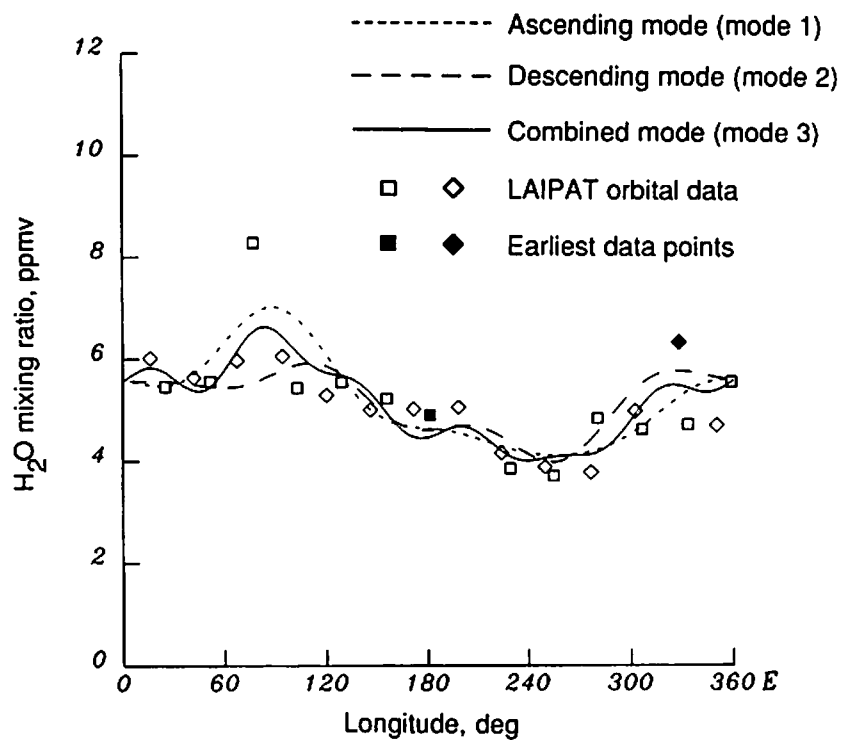
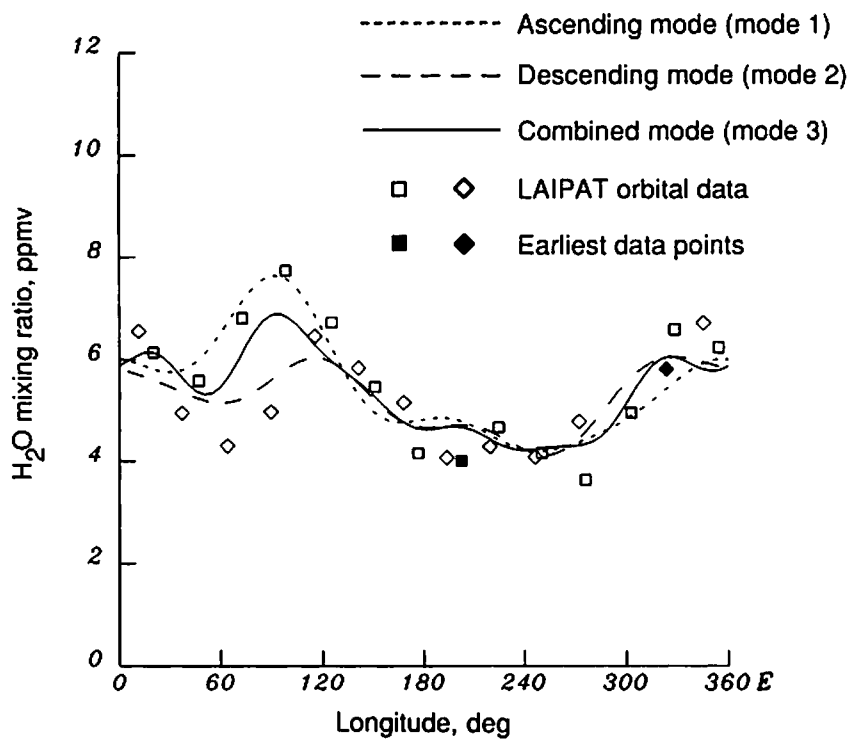


Figure 5. Fourier coefficient fit for combined mode H_2O data at 10 mbar and 60°S on November 2, 1978. Square symbols indicate ascending data; diamond symbols, descending data.

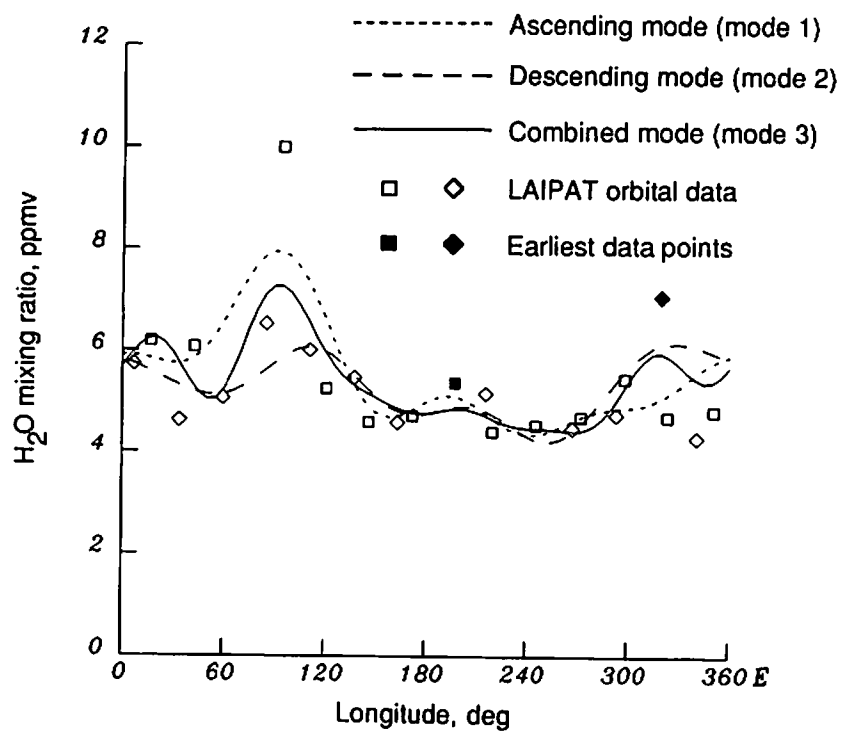


(a) February 3, 1979.

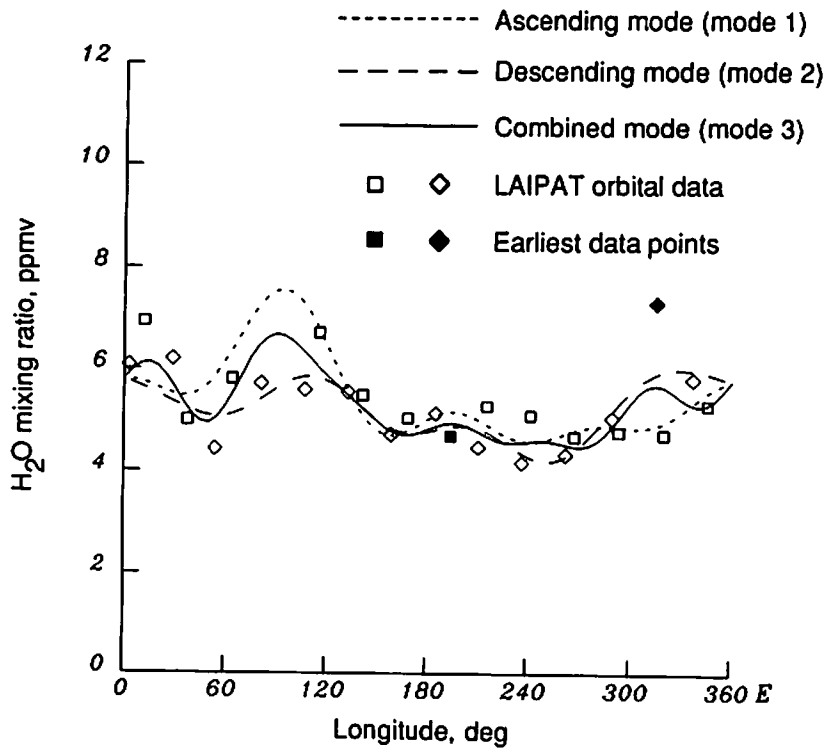


(b) February 4, 1979.

Figure 6. Fourier coefficient fit for each mode of H_2O data at 10 mbar and 76°N on February 3 to 6, 1979. Square symbols indicate ascending data; diamond symbols, descending data.



(c) February 5, 1979.



(d) February 6, 1979.

Figure 6. Concluded.

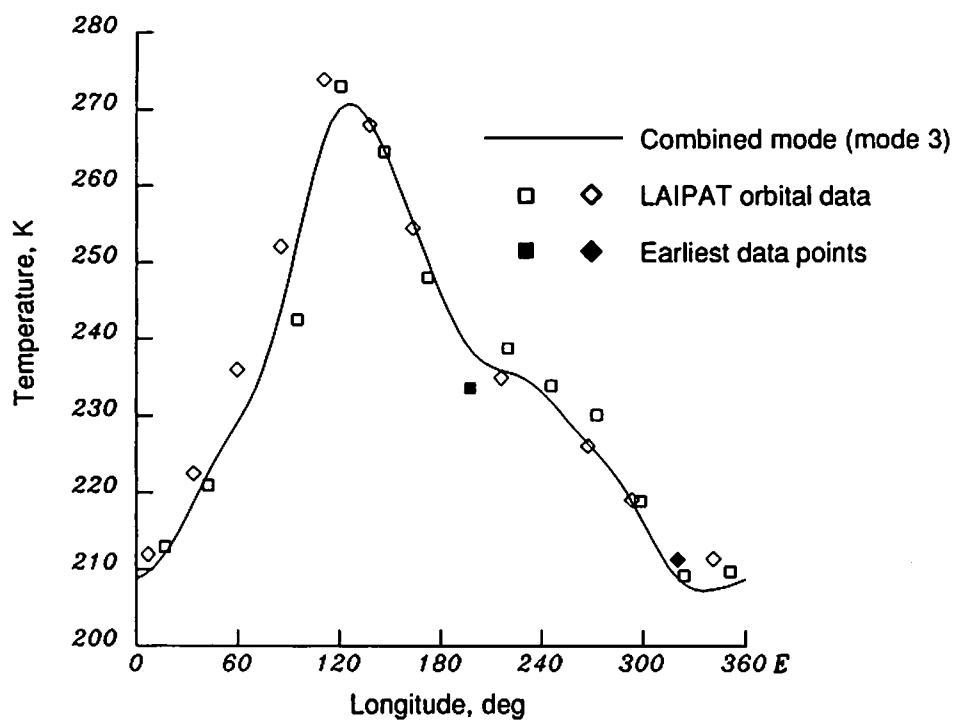


Figure 7. Fourier coefficient estimate of combined mode temperature at 10 mbar and 76°N on February 5, 1979. Square symbols indicate ascending data; diamond symbols, descending data.

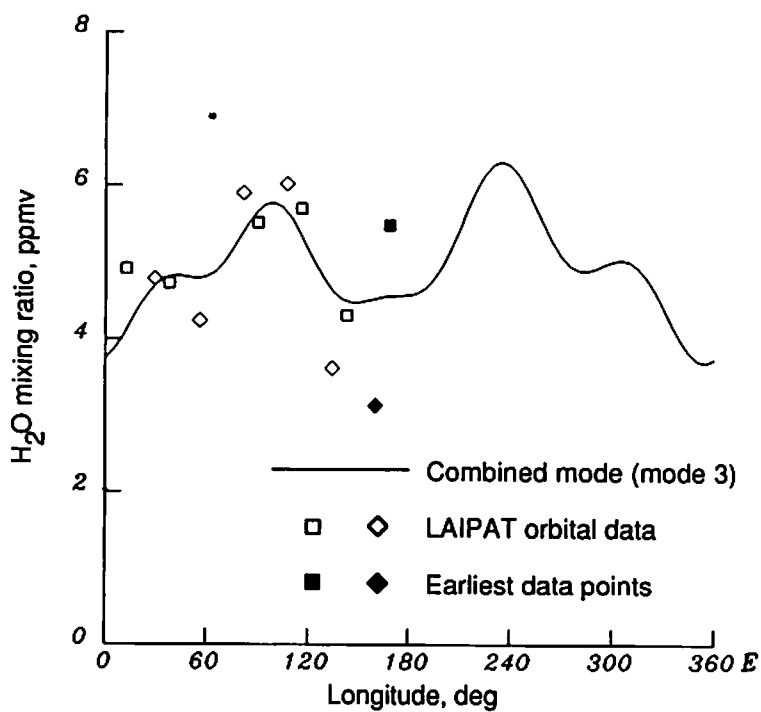
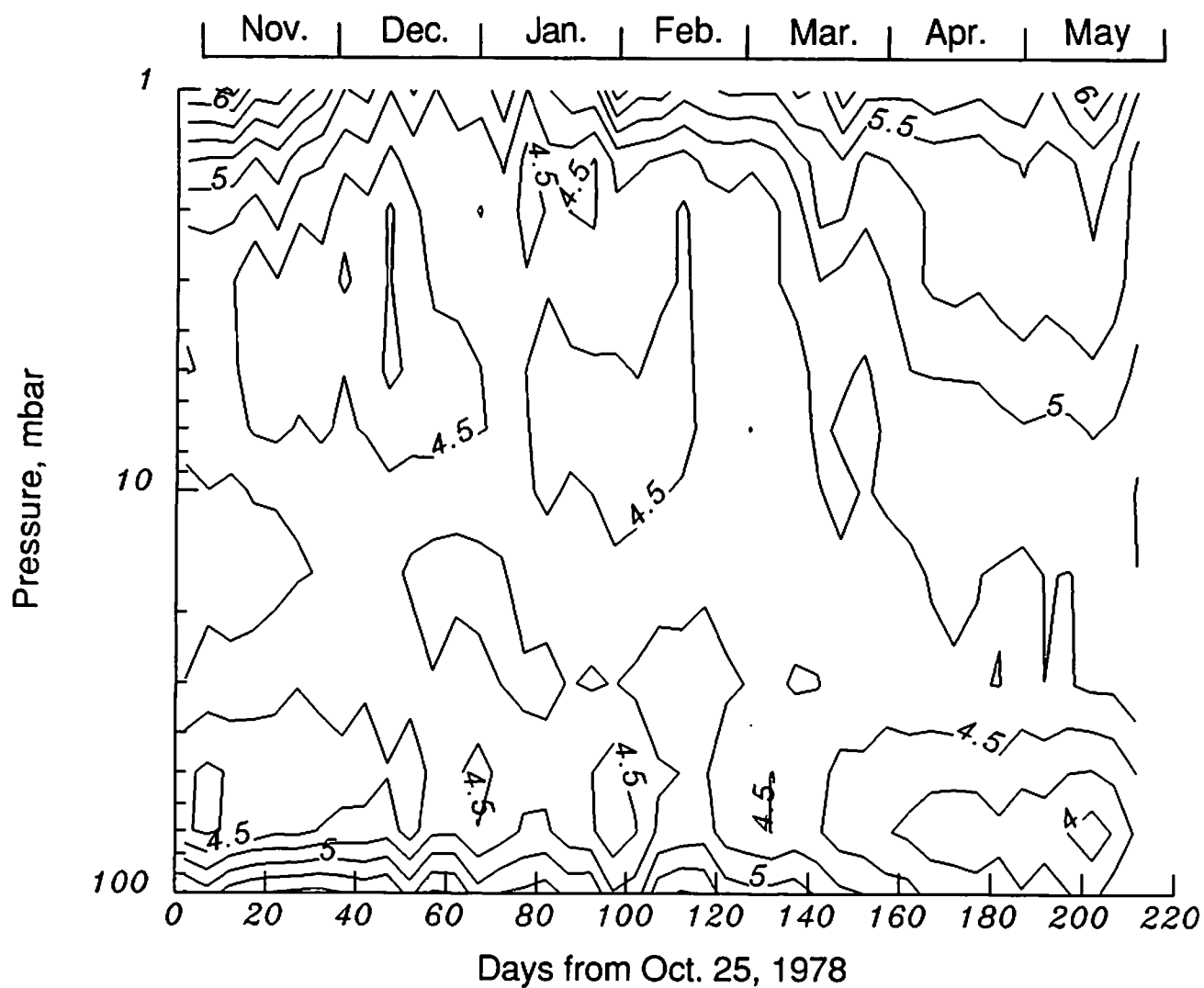
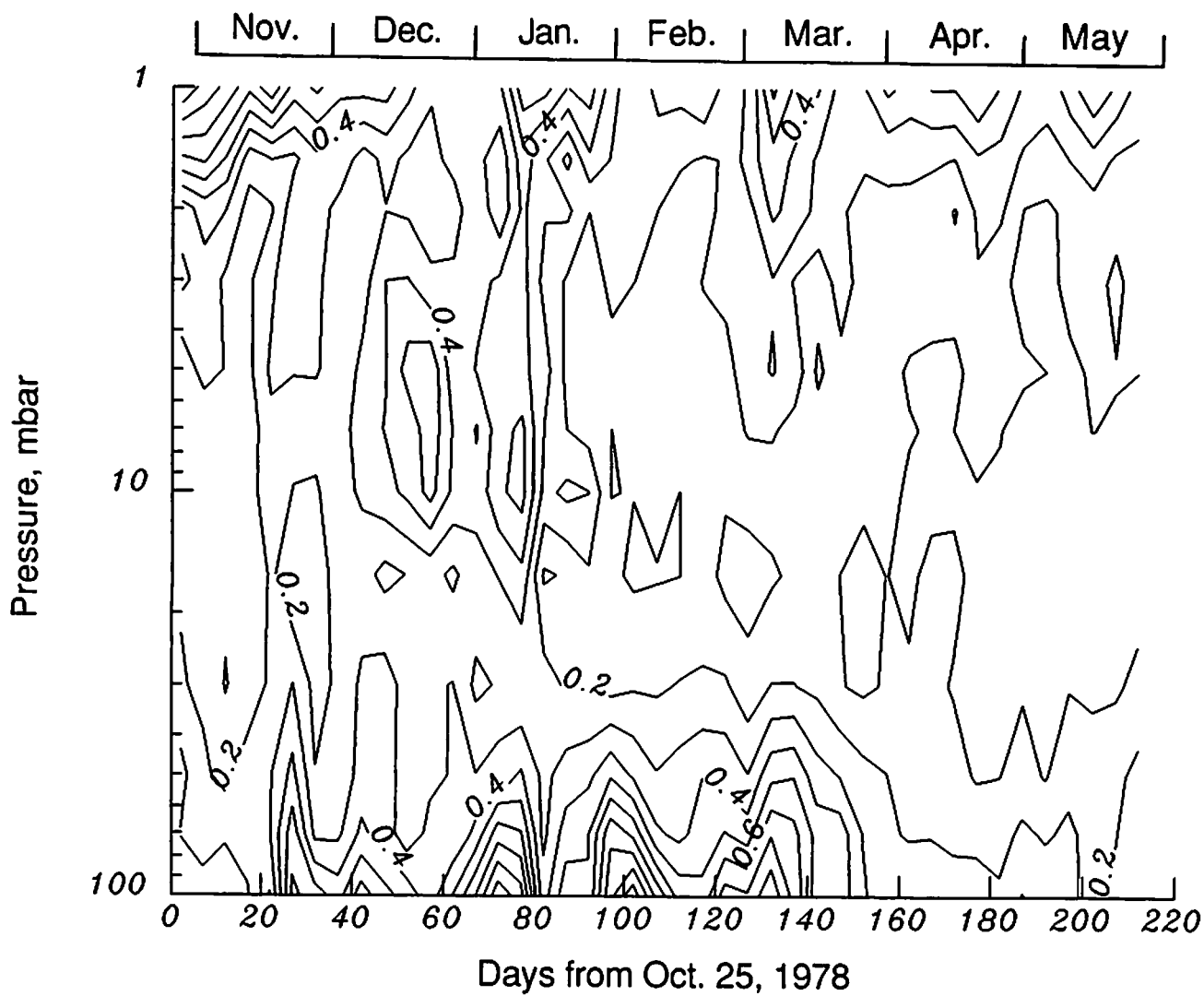


Figure 8. Kalman filter estimate of combined mode H₂O data at 10 mbar and 76°N on January 2, 1979. Square symbols indicate ascending data; diamond symbols, descending data.



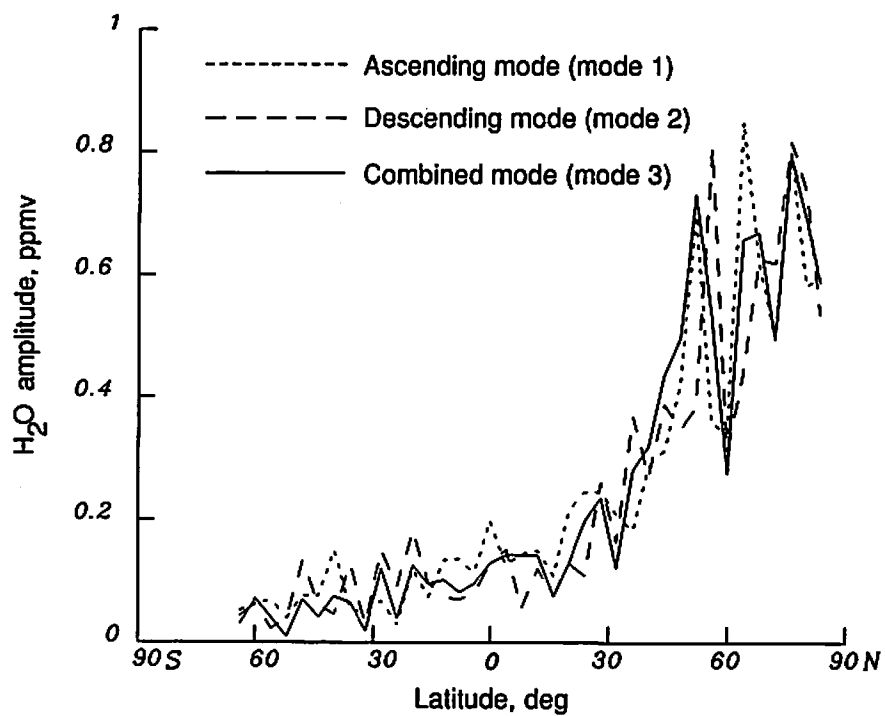
(a) Zonal mean coefficient. Contour interval, 0.25 ppmv.

Figure 9. Time series of descending mode zonal mean coefficient and wave 1 amplitude for H_2O at 48°N . The time series consists of 5-day averages; a 1-2-1 smoother is applied to the LAMAT latitude scale.



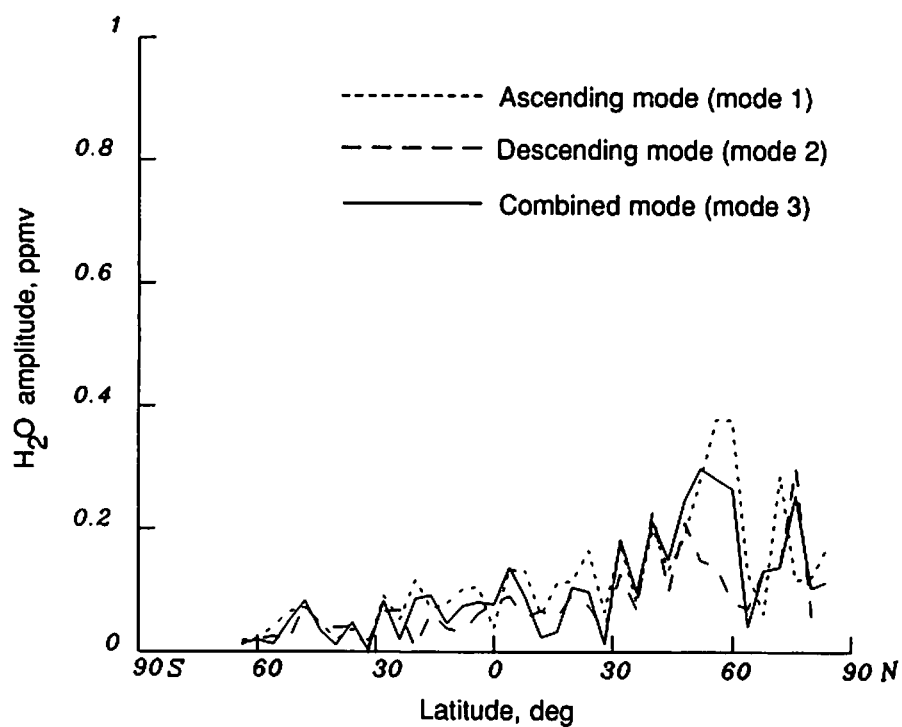
(b) Wave 1 amplitude. Contour interval, 0.1 ppmv.

Figure 9. Concluded.

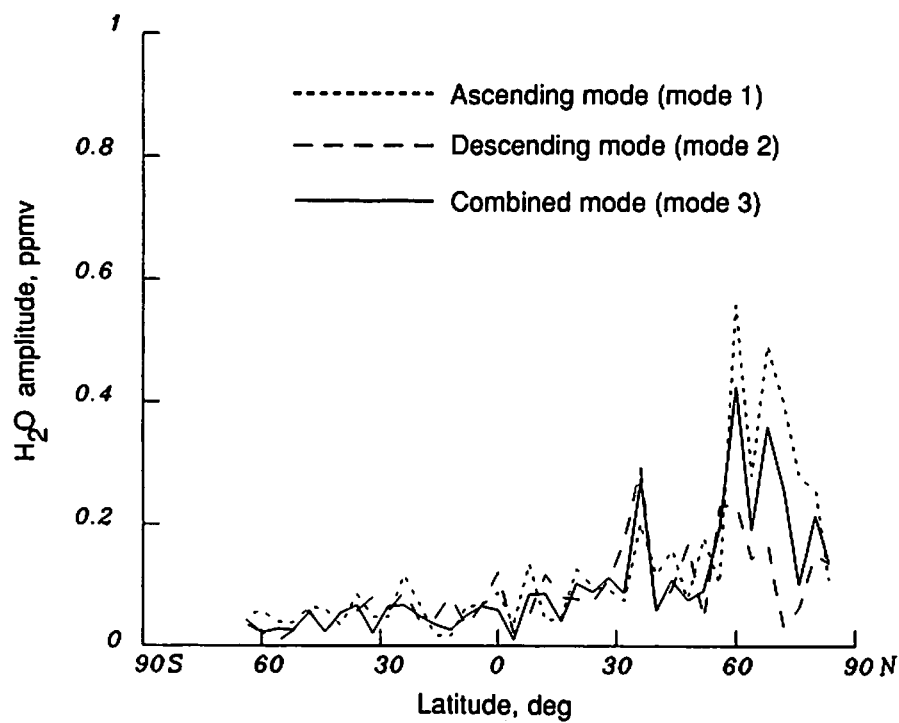


(a) Wave 1.

Figure 10. Wave amplitude versus latitude for H₂O at 10 mbar on January 26, 1979. No smoothing with latitude was conducted.

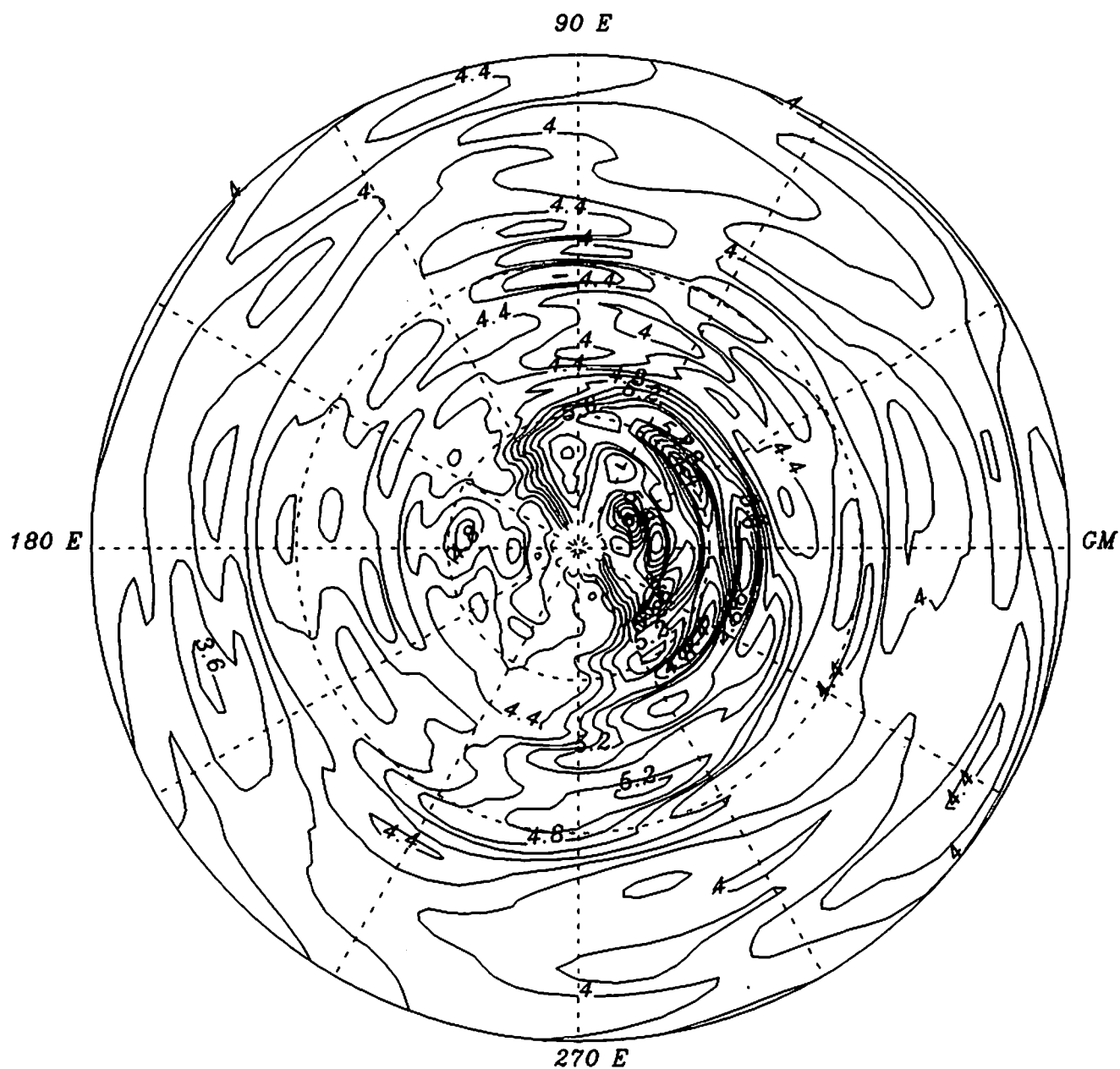


(b) Wave 2.



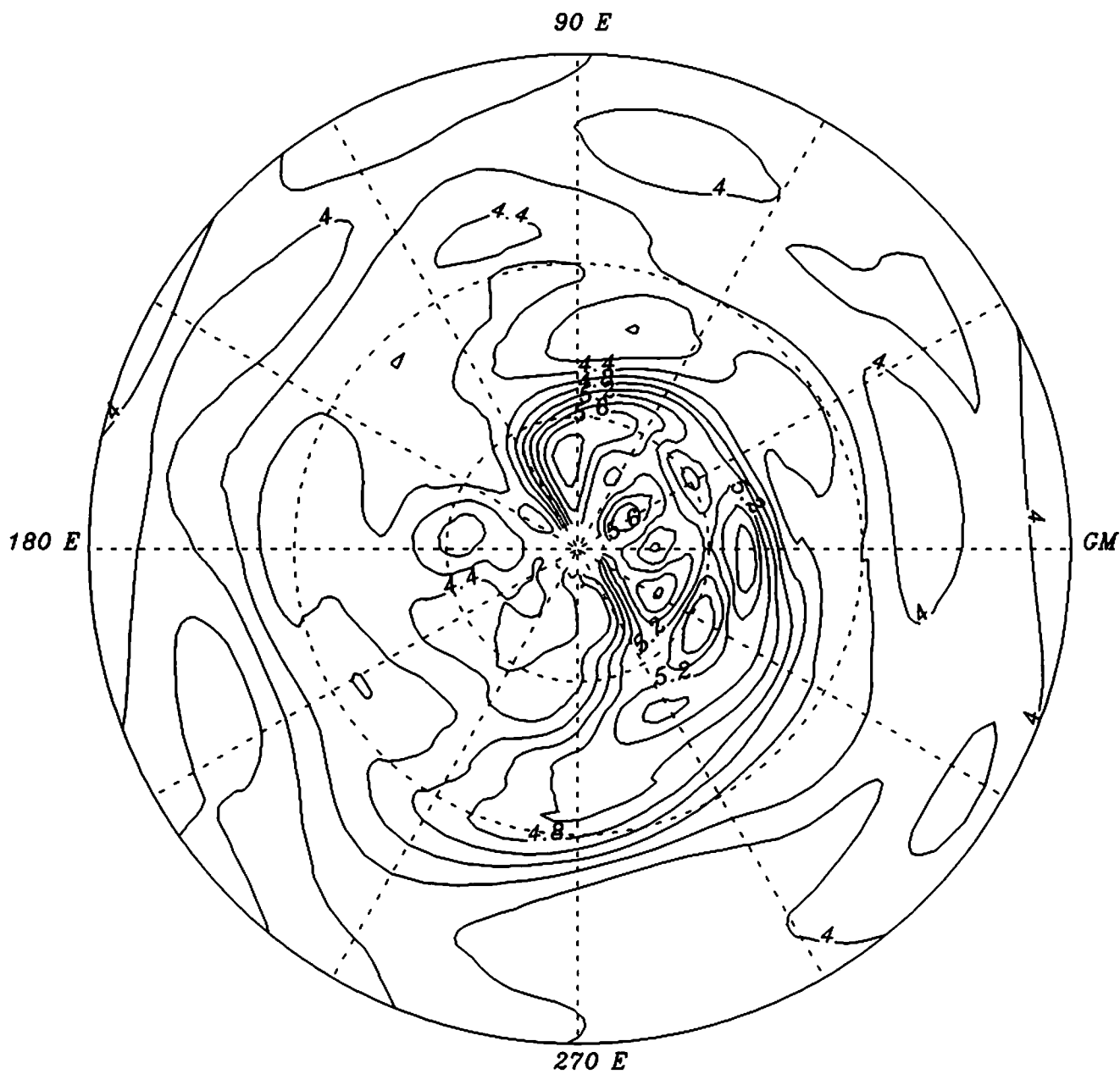
(c) Wave 3.

Figure 10. Concluded.



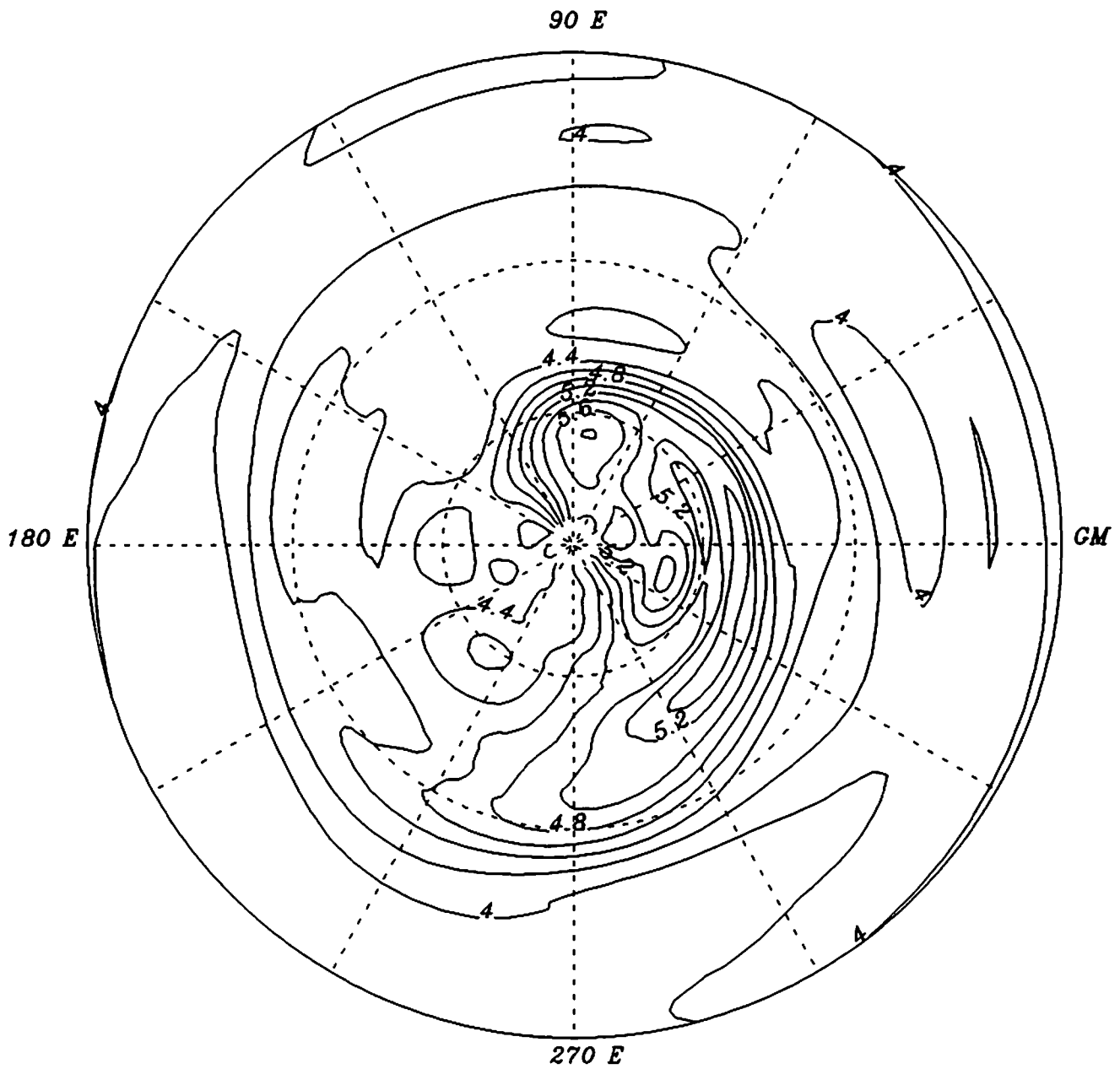
(a) Unsmoothed 6-wave fit.

Figure 11. Polar contour plots of unsmoothed 6-wave fit and both the 1-2-1 smoothed 6-wave fit and the 4-wave fit to the Northern Hemisphere combined mode H₂O data at 10 mbar on January 26, 1979. Dashed circles represent 30°N and 60°N latitudes. Contour interval, 0.2 ppmv.



(b) 6-wave fit using 1-2-1 weighted average in latitude.

Figure 11. Continued.



(c) 4-wave fit using 1-2-1 smoothing in latitude.

Figure 11. Concluded.

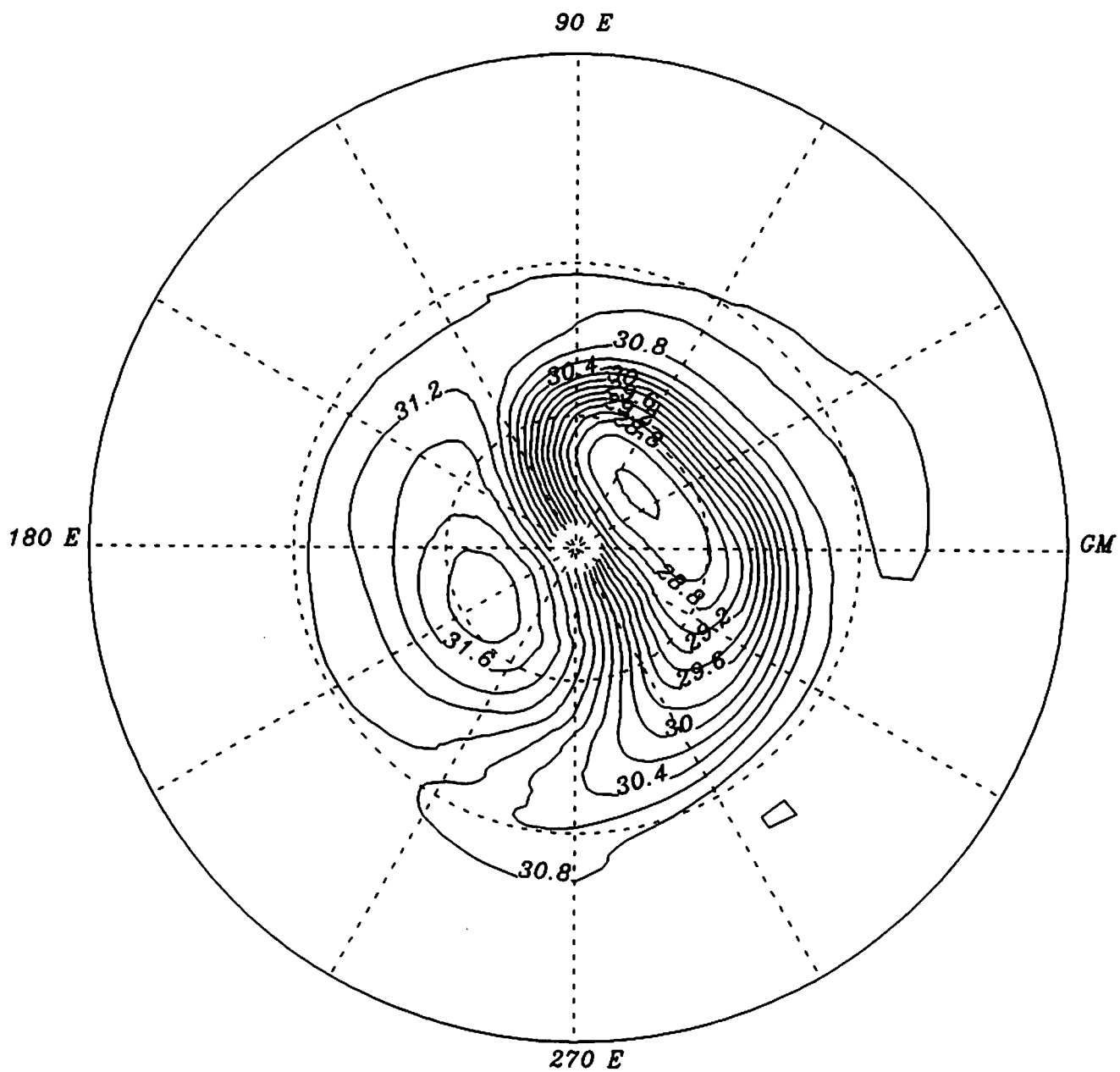


Figure 12. LIMS geopotential height field (in gpm) at 10 mbar on January 26, 1979. Dashed circles represent 30°N and 60°N latitudes. Contour interval, 200 gpm.

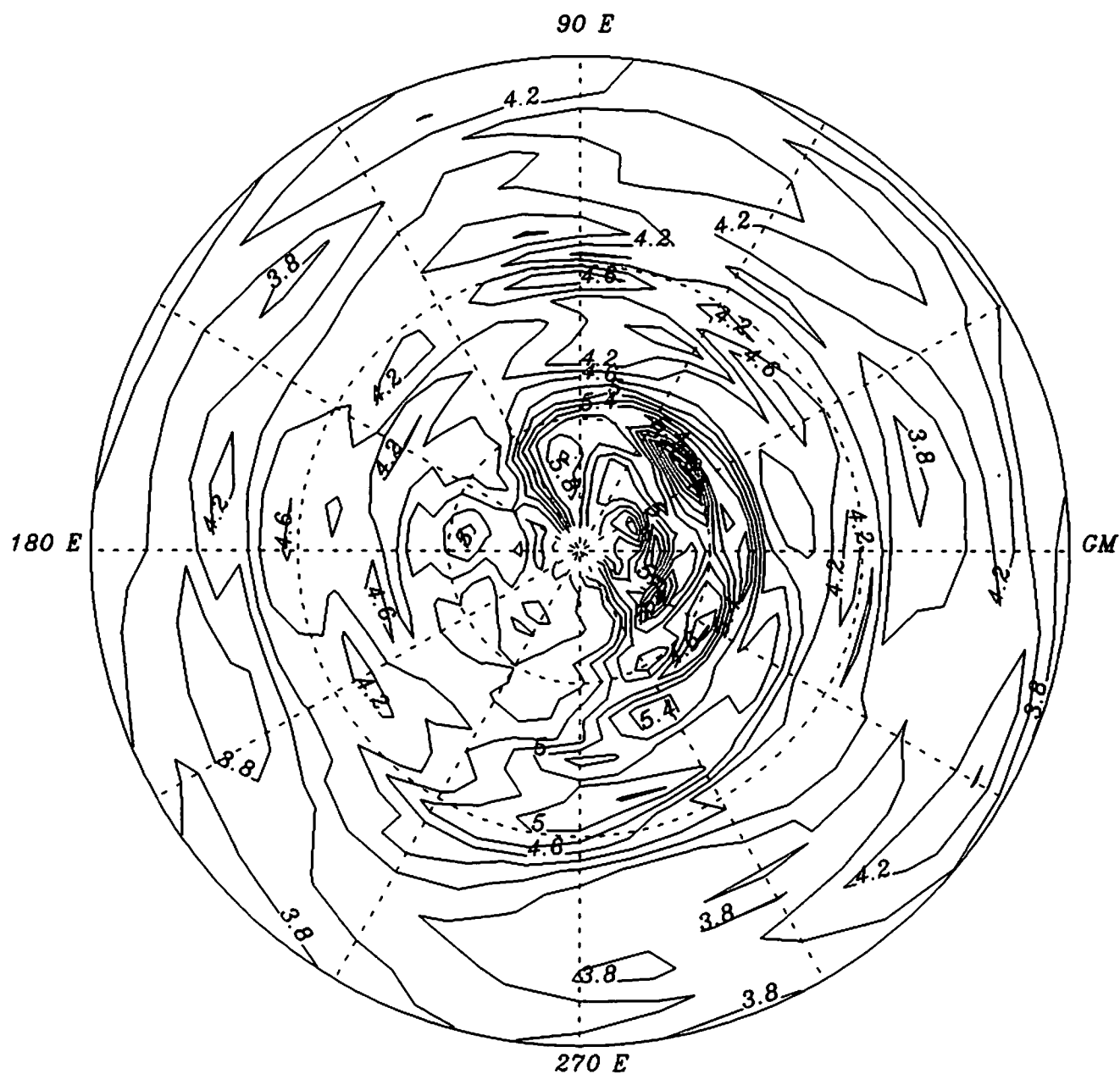


Figure 13. LIMS H₂O (in ppmv) on the 850-K potential temperature surface on January 26, 1979. Dashed circles represent 30°N and 60°N latitudes. Contour interval, 0.2 ppmv.

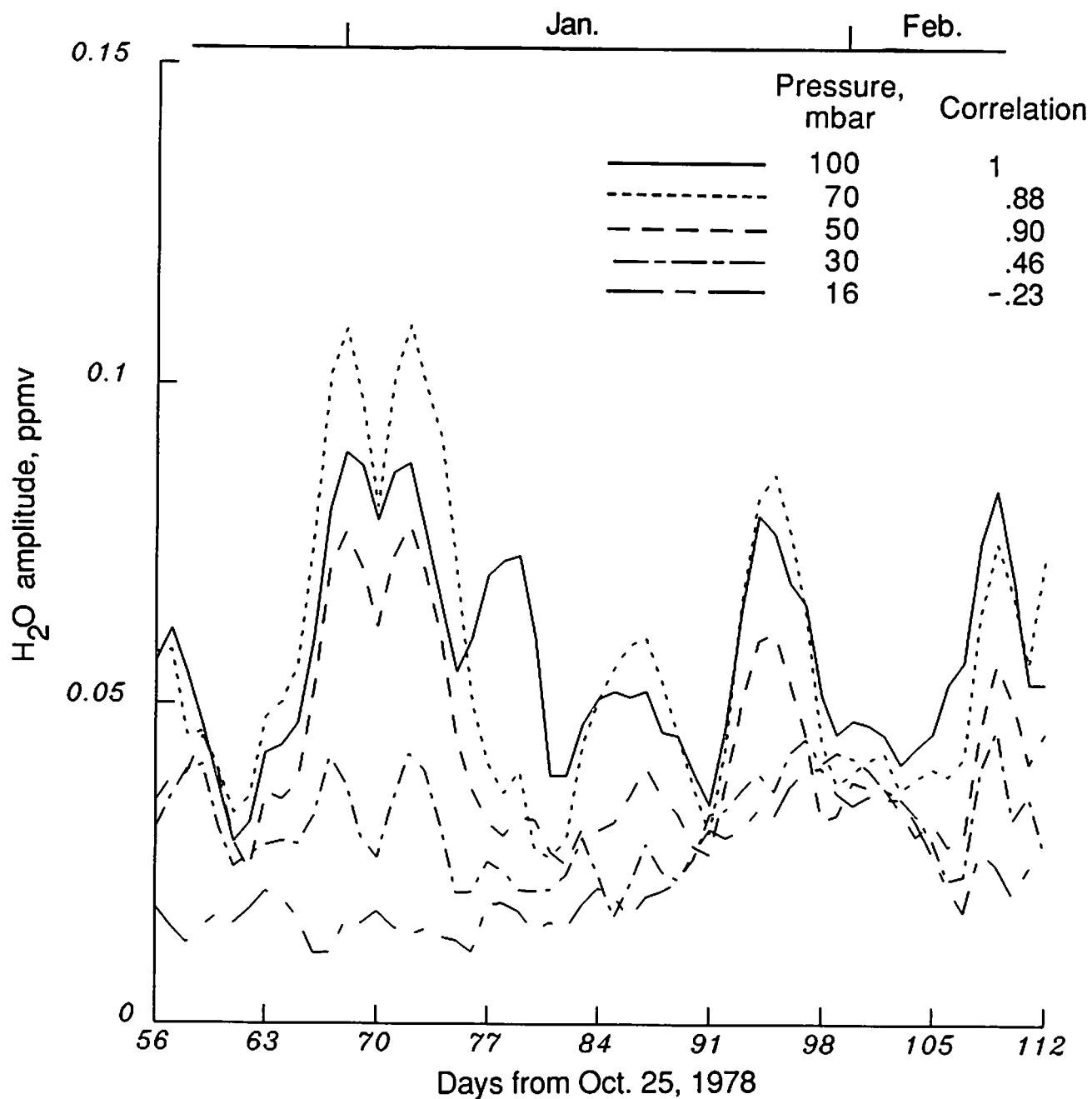
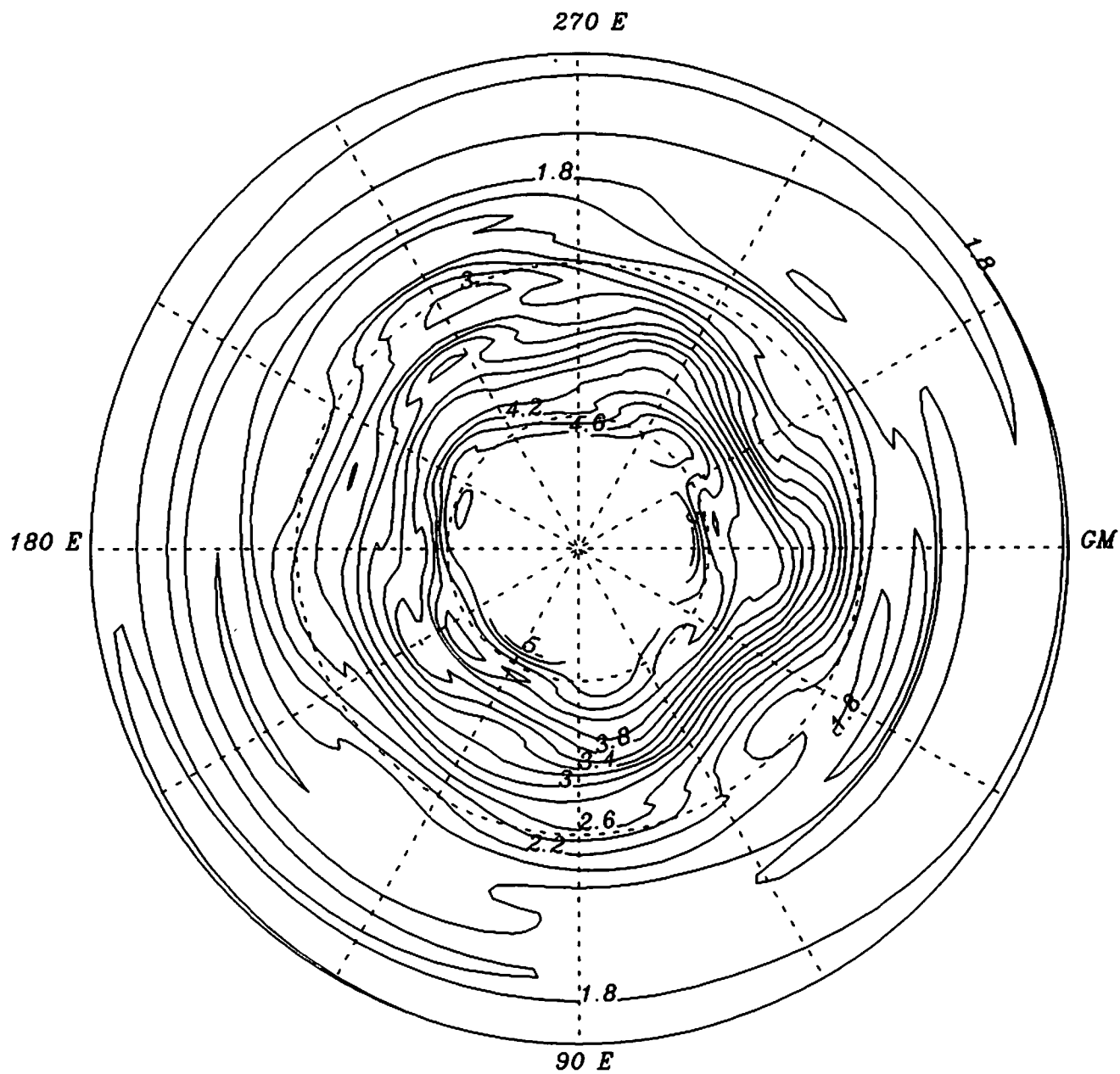


Figure 14. Time series of mean wave 5 amplitude for H₂O from 40°S to 64°S for 100-, 70-, 50-, 30-, and 16-mbar pressure levels.



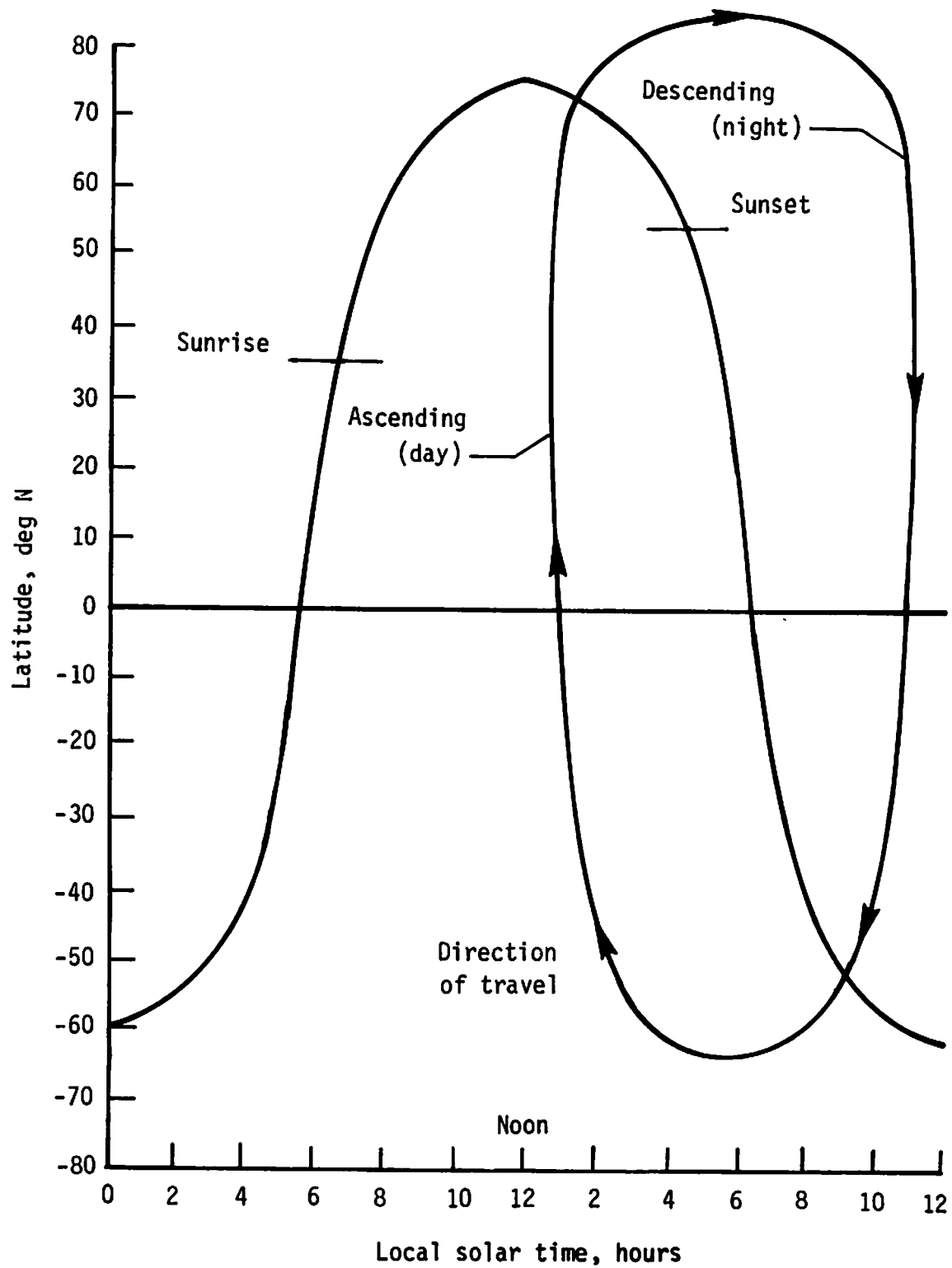


Figure 16. Terminator location on December 21 and tangent point track at 30-km altitude on a latitude local solar time grid.

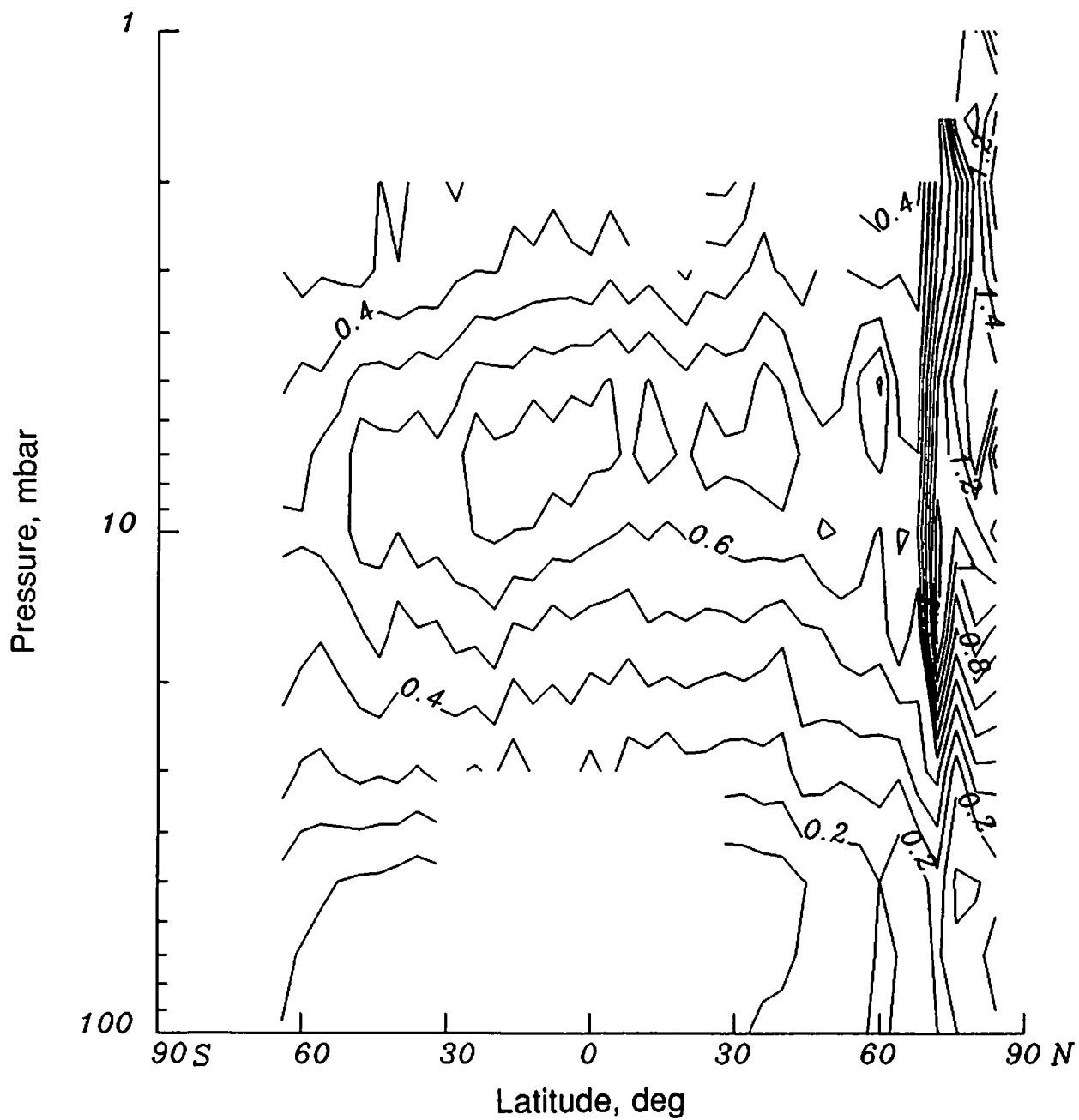


Figure 17. Standard deviations σ_{obs} between ascending mode LAMAT NO₂ (in ppbv) and LAIPAT observations for January 1979. Note the terminator region near 68°N. Contour interval, 0.1 ppbv.

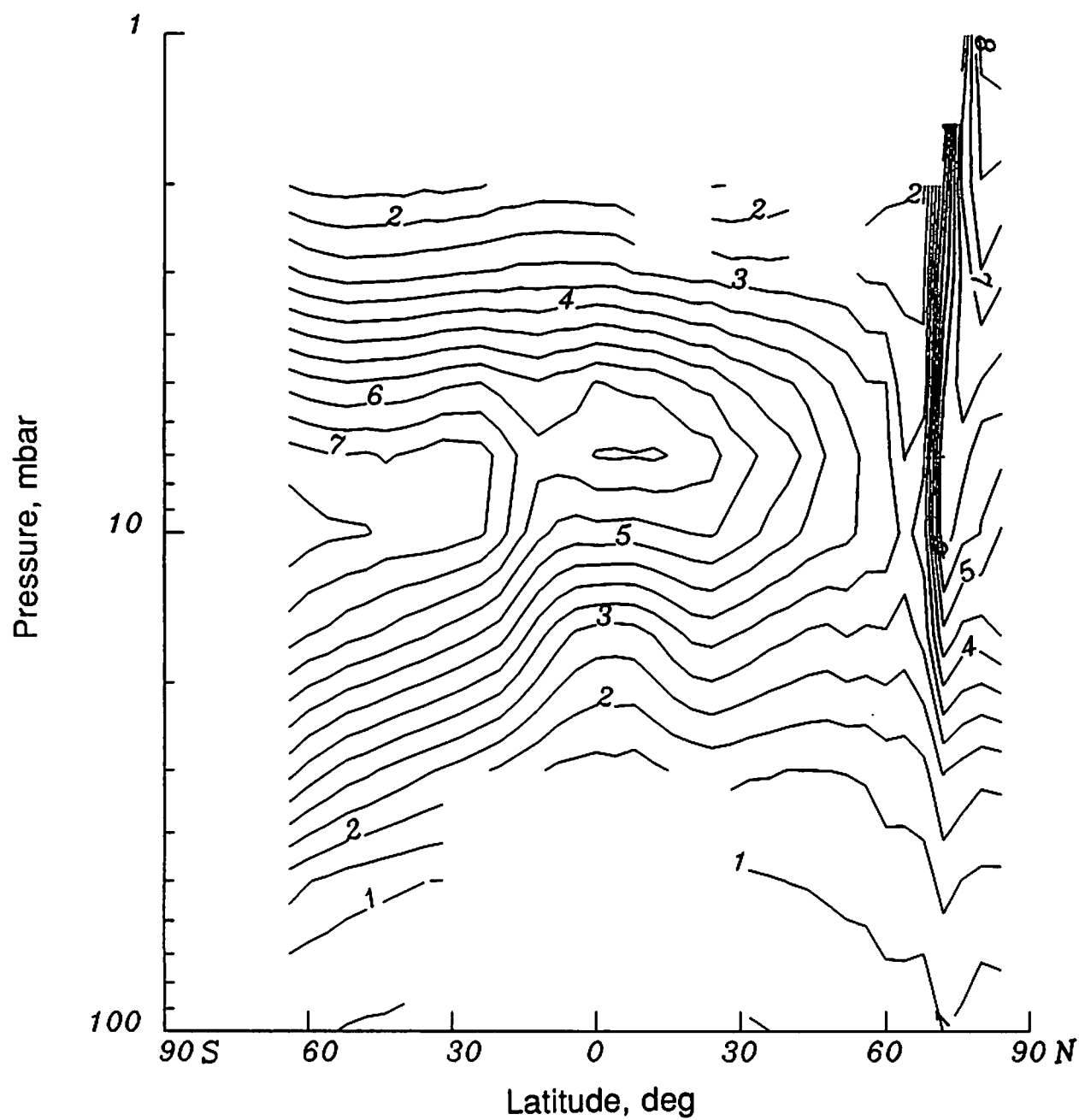


Figure 18. Zonal mean coefficient of ascending mode NO₂ mixing ratio (in ppbv) for January 1979. Contour interval, 0.5 ppbv.

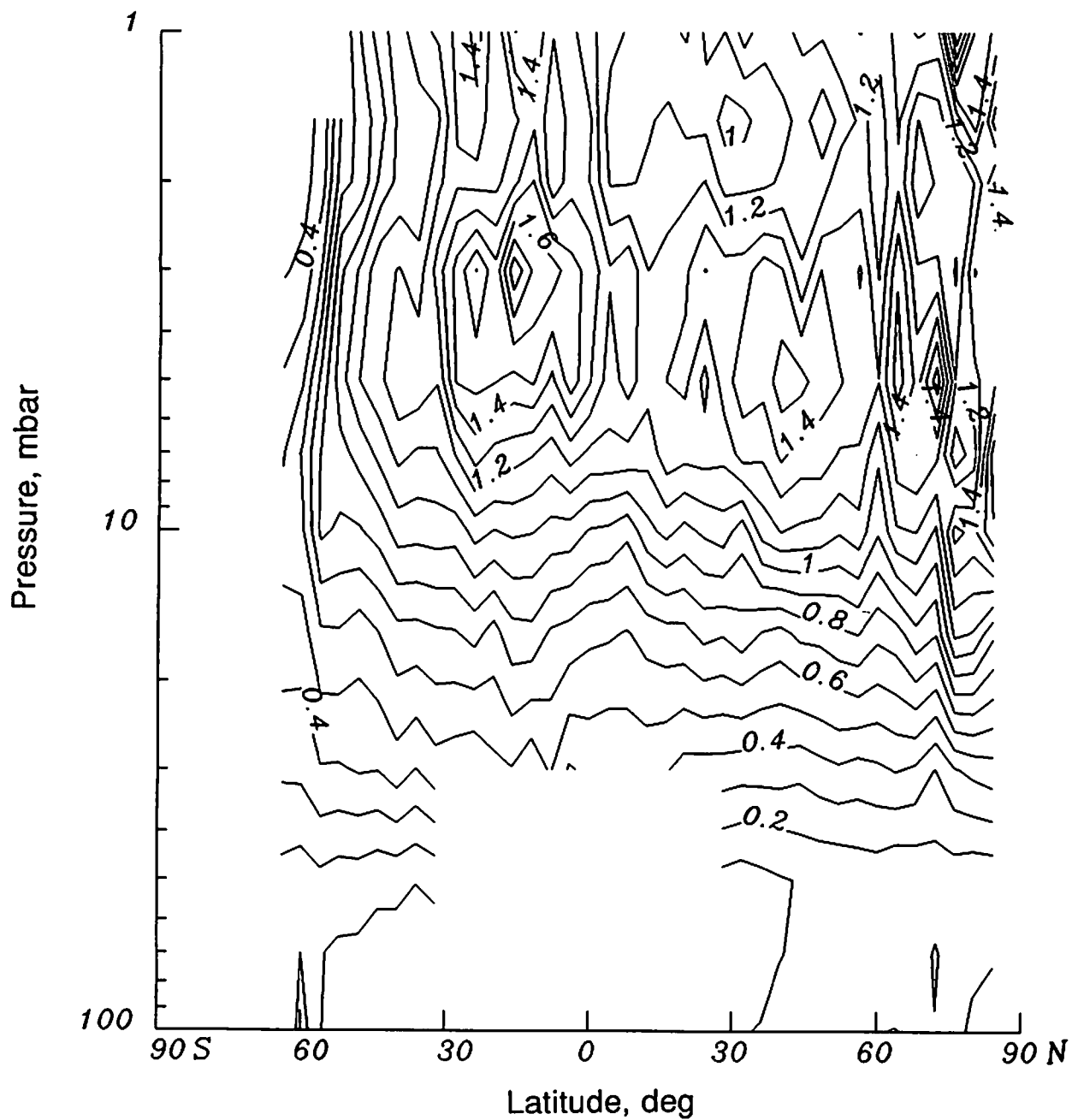


Figure 19. Standard deviations σ_{obs} between descending mode LAMAT NO₂ (in ppbv) and LAIPAT observations for January 1979. Contour interval, 0.1 ppbv.

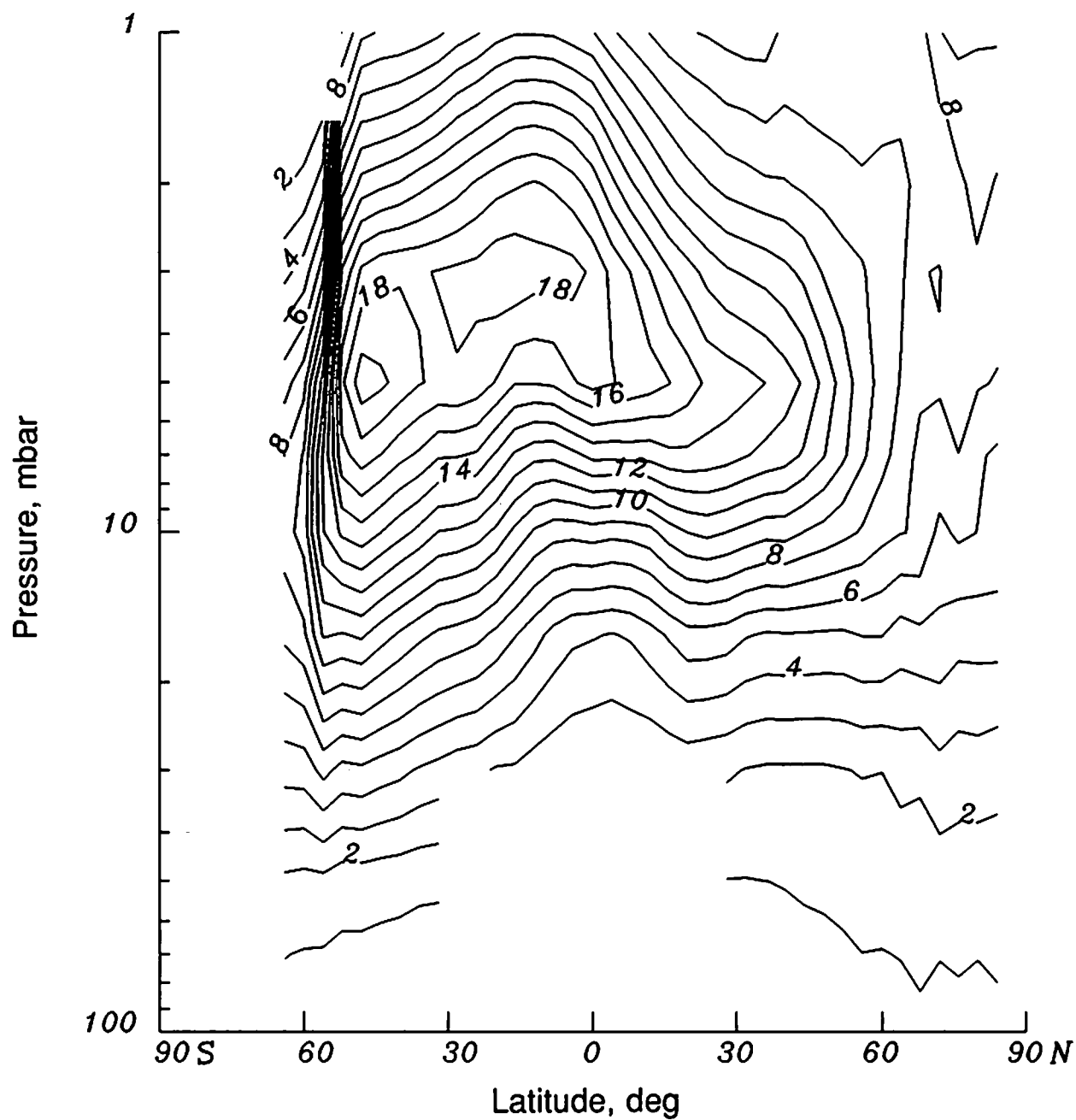


Figure 20. Zonal mean coefficient of descending mode NO₂ mixing ratio (in ppbv) for January 1979. Note the terminator region near 60°S. Contour interval, 1 ppbv.

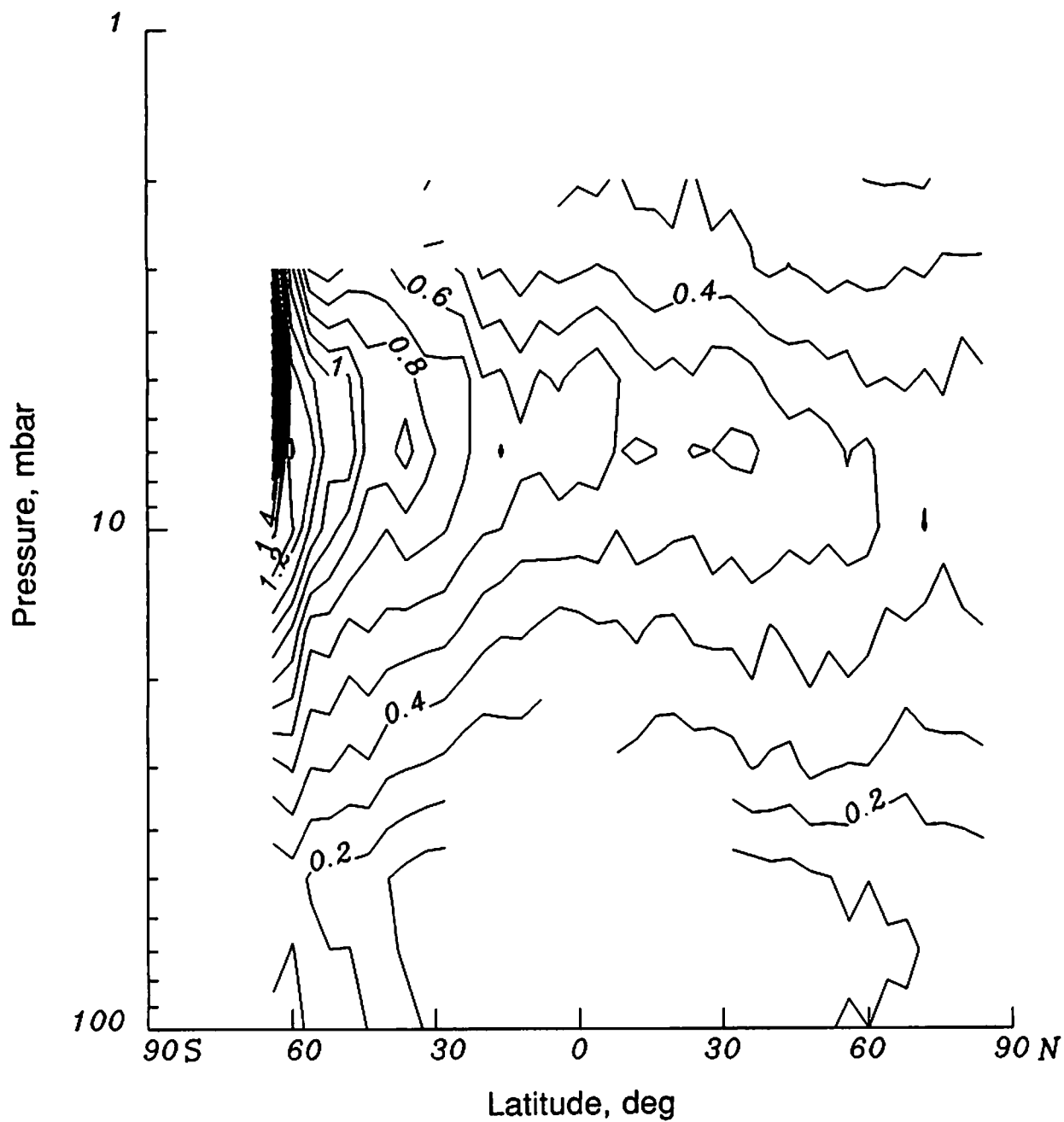


Figure 21. Standard deviations σ_{obs} between ascending mode LAMAT NO₂ (in ppbv) and LAIPAT observations for May 1979. Note the terminator region near 60°S. Contour interval, 0.1 ppbv.

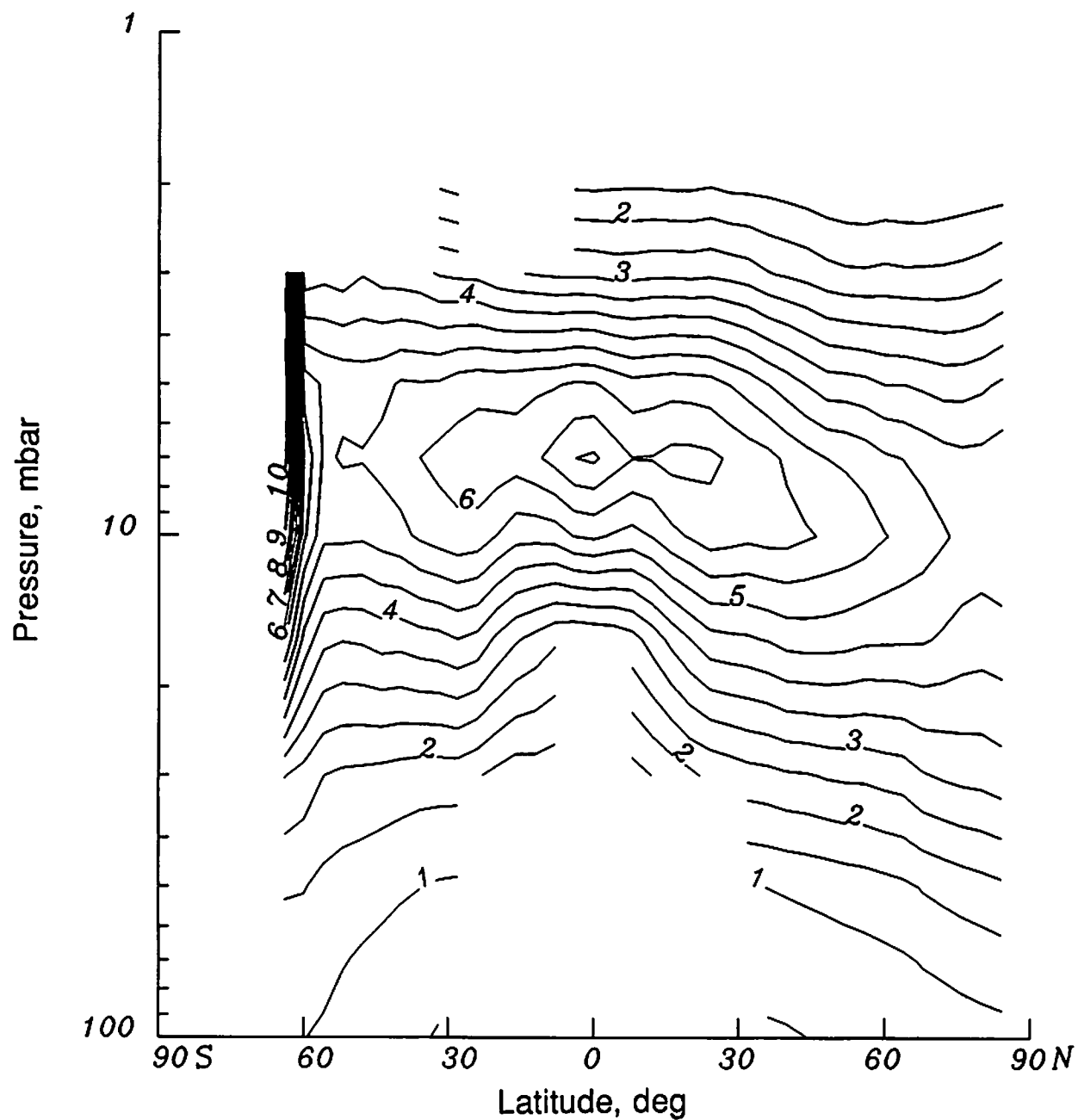


Figure 22. Zonal mean coefficient of ascending mode NO₂ mixing ratio (in ppbv) for May 1979. Contour interval, 0.5 ppbv.

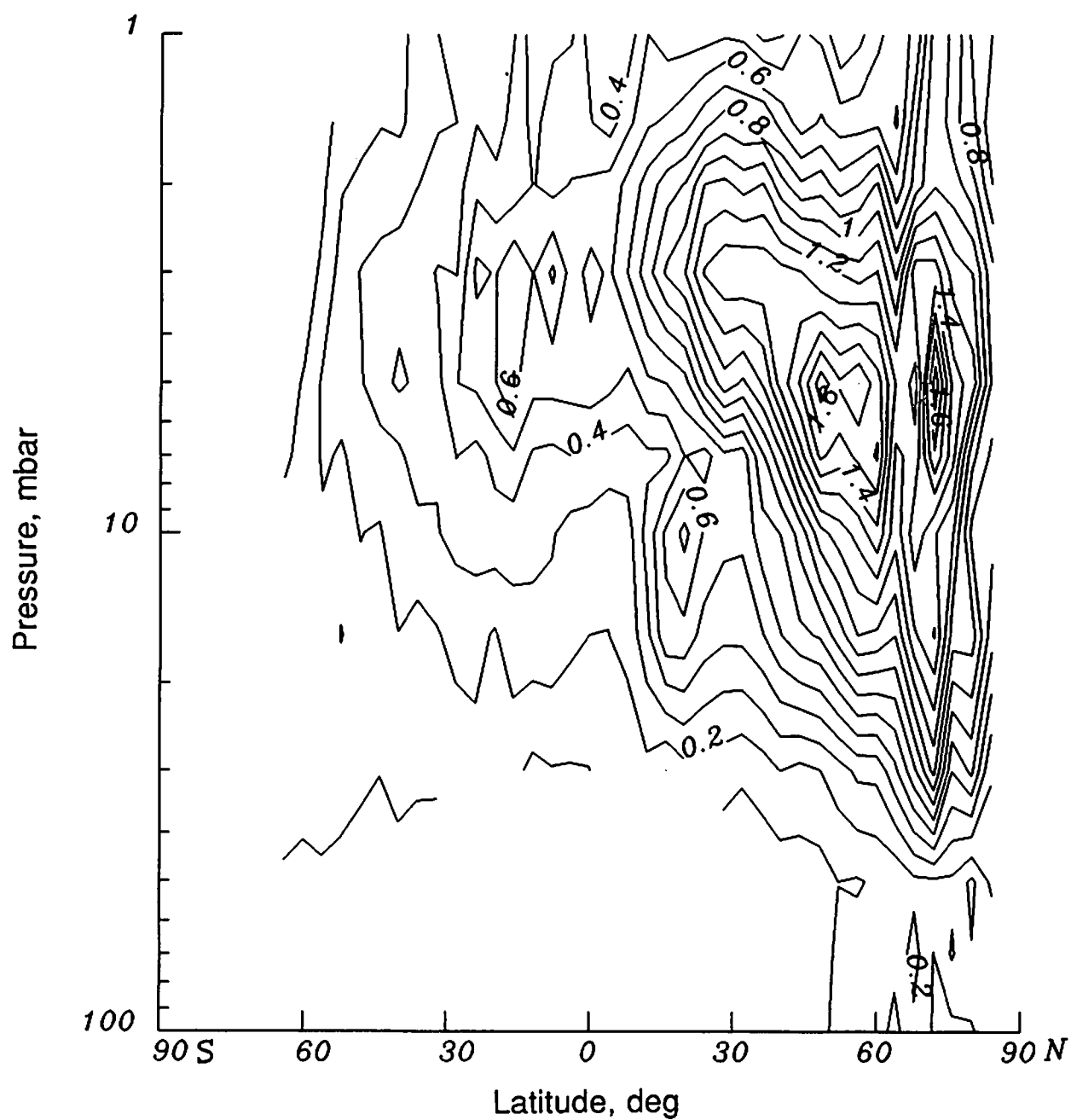


Figure 23. Average wave standard deviation (square root of wave variance) (in ppbv) for descending mode NO₂ for January 1979. Contour interval, 0.1 ppbv.

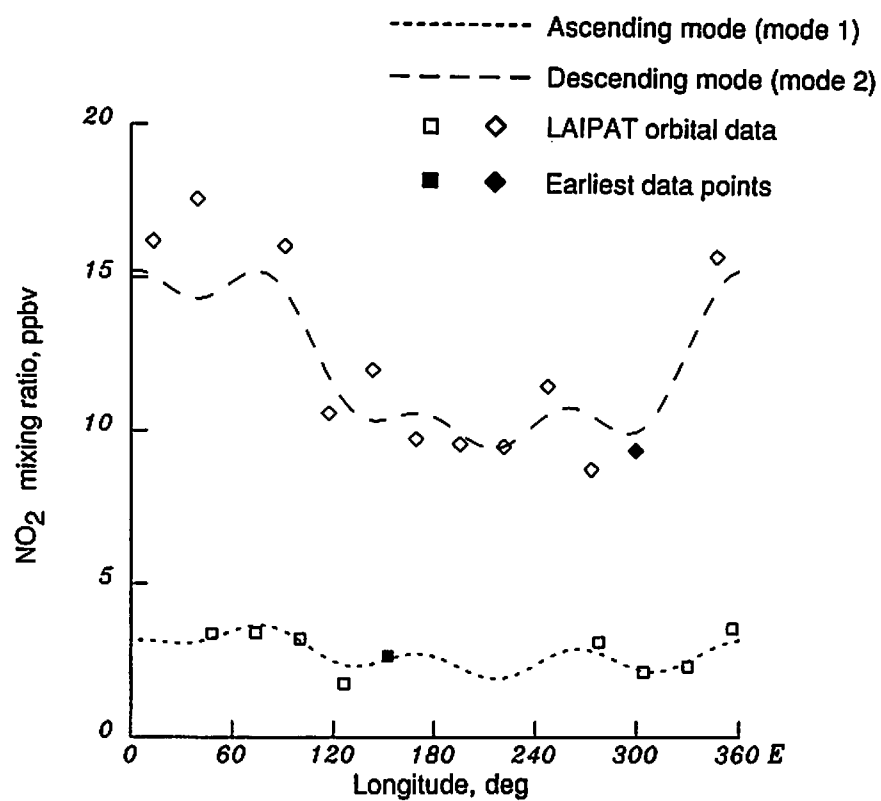
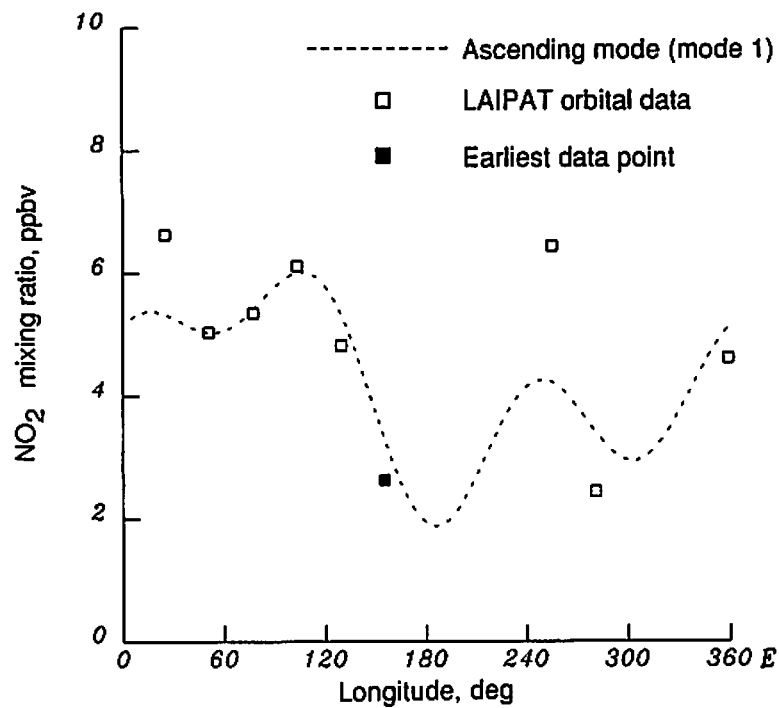
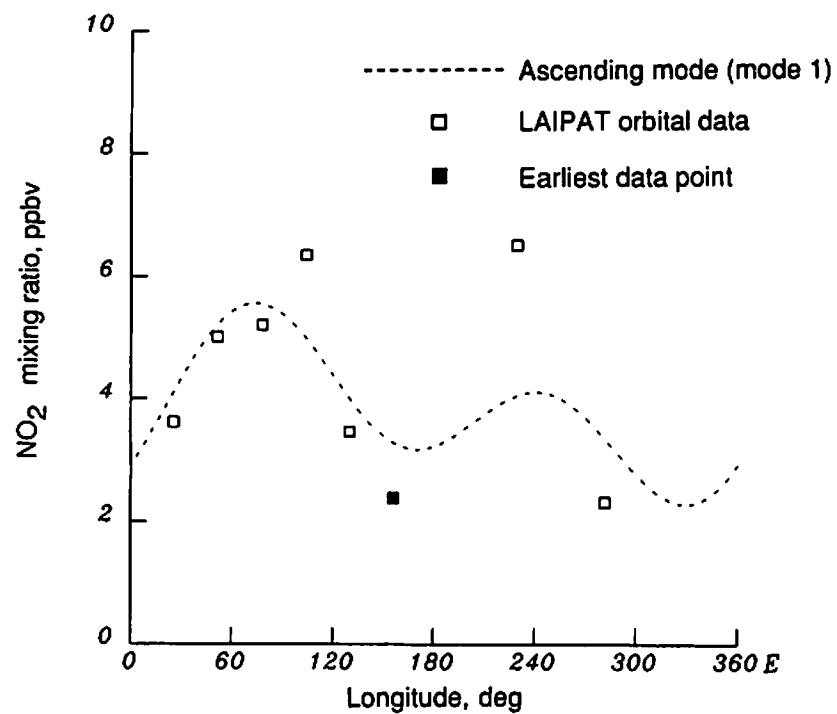


Figure 24. Data and Kalman filter results for ascending and descending modes of NO_2 at 3 mbar for 40°N on January 26, 1979. Square symbols indicate ascending data; diamond symbols, descending data.



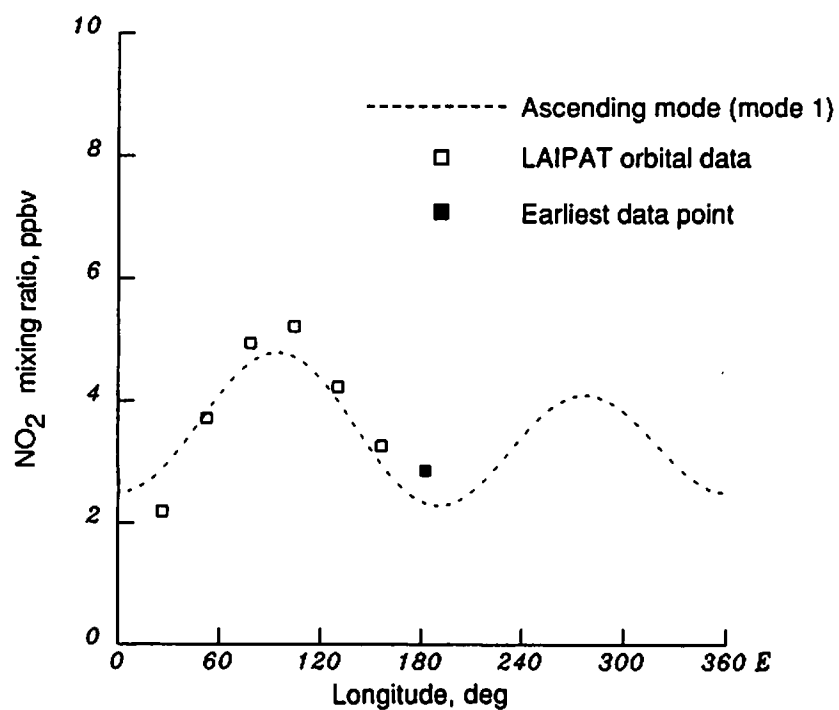
(a) Latitude, 52°N.

Figure 25. Data and Kalman filter results for ascending mode NO₂ at 10 mbar for 52°N, 56°N, and 60°N on January 2, 1979. Square symbols indicate ascending data.



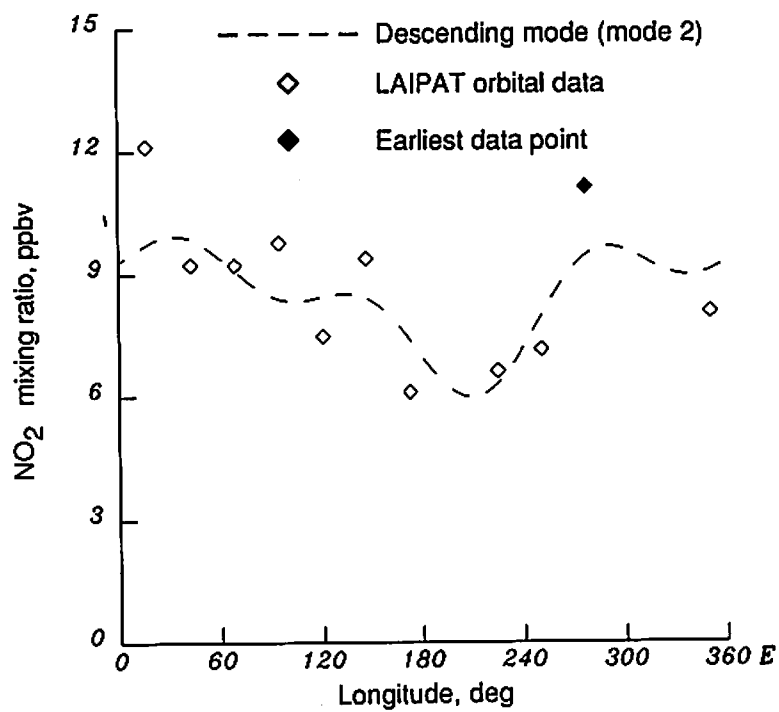
(b) Latitude, 56°N.

Figure 25. Continued.



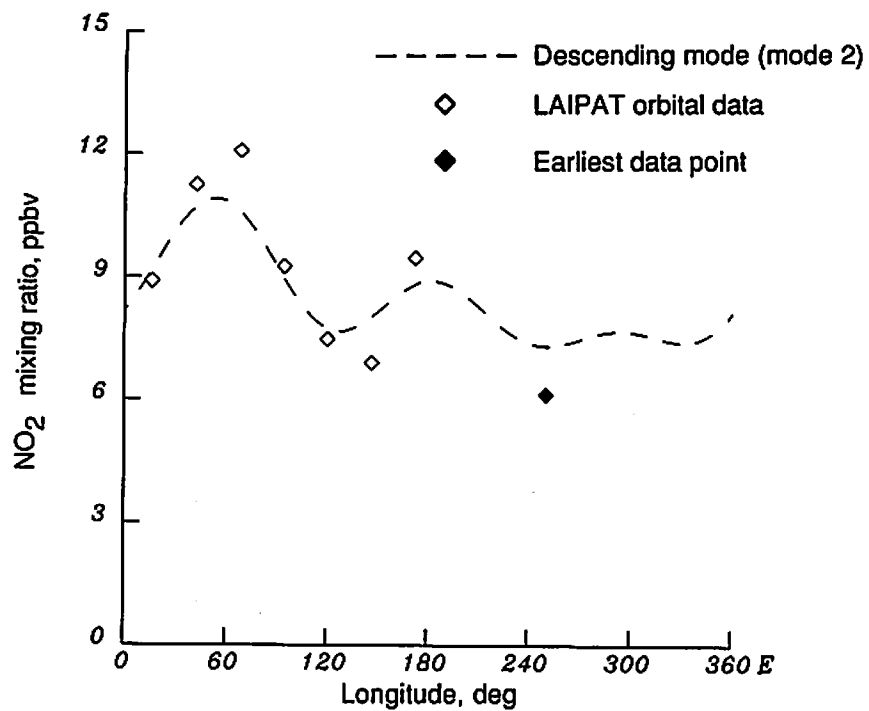
(c) Latitude, 60°N.

Figure 25. Concluded.



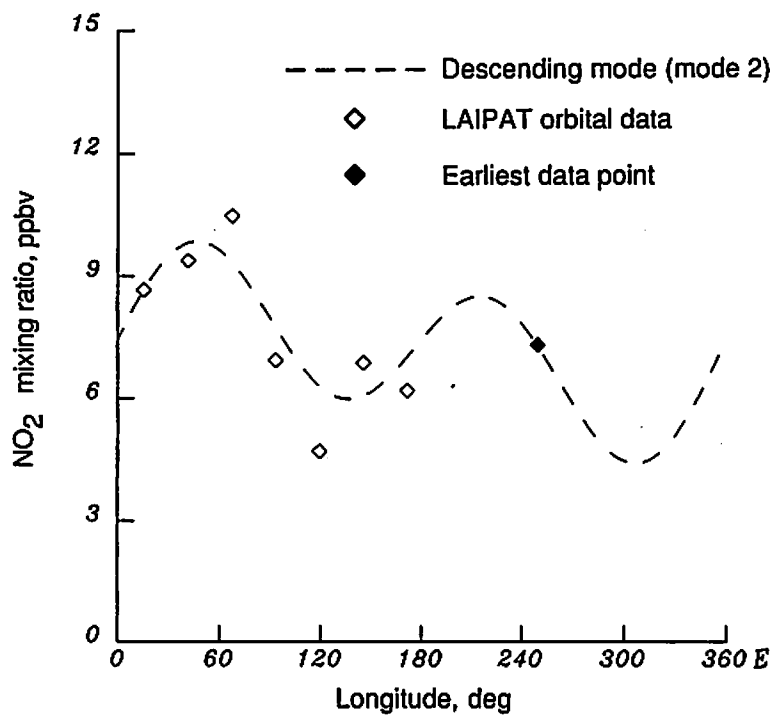
(a) Latitude, 52°N.

Figure 26. Data and Kalman filter results for descending mode NO₂ at 10 mbar for 52°N, 56°N, and 60°N on January 2, 1979. Diamond symbols indicate descending data.



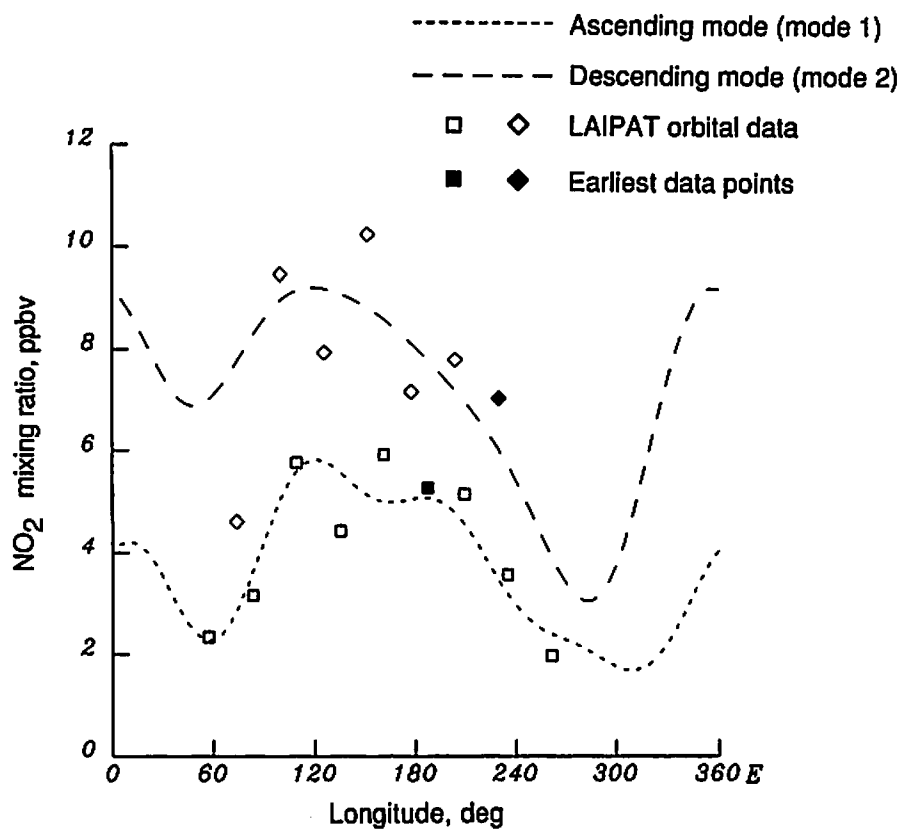
(b) Latitude, 56°N .

Figure 26. Continued.



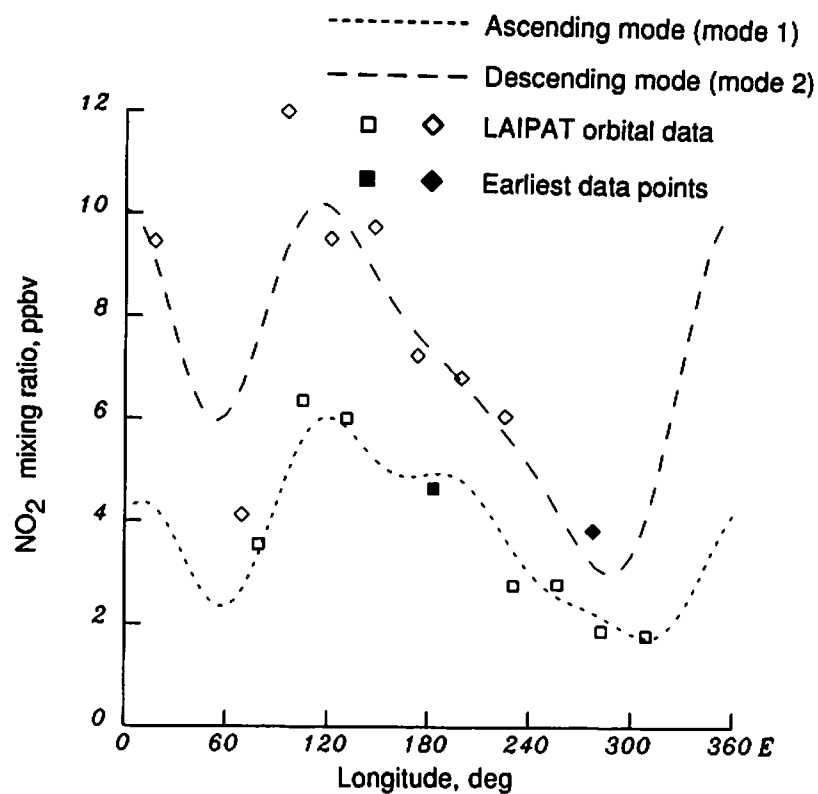
(c) Latitude, 60°N .

Figure 26. Concluded.



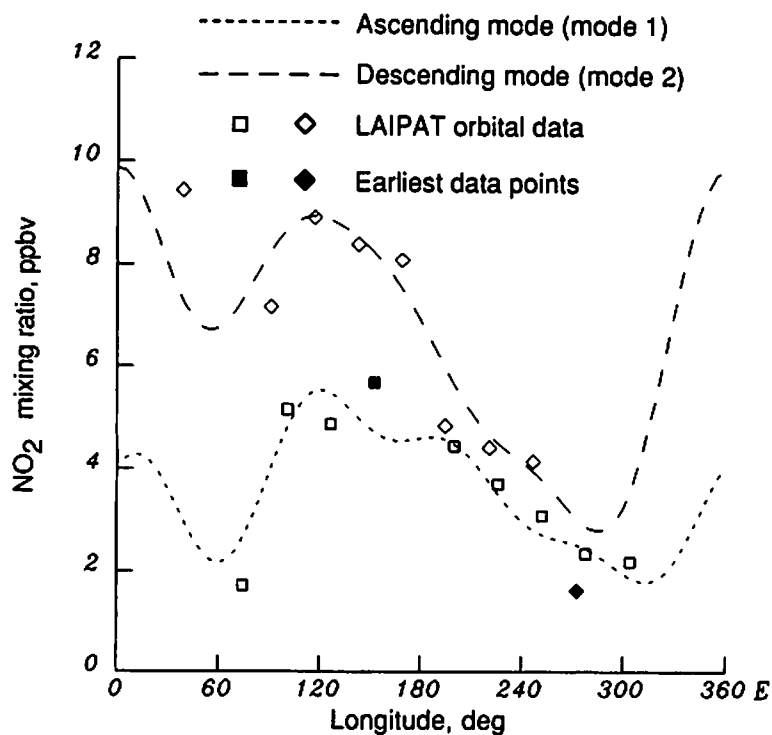
(a) January 24, 1979.

Figure 27. Data and Kalman filter results for ascending and descending modes of NO₂ at 10 mbar for 56°N on January 24, 25, and 26, 1979. Square symbols indicate ascending data; diamond symbols, descending data.



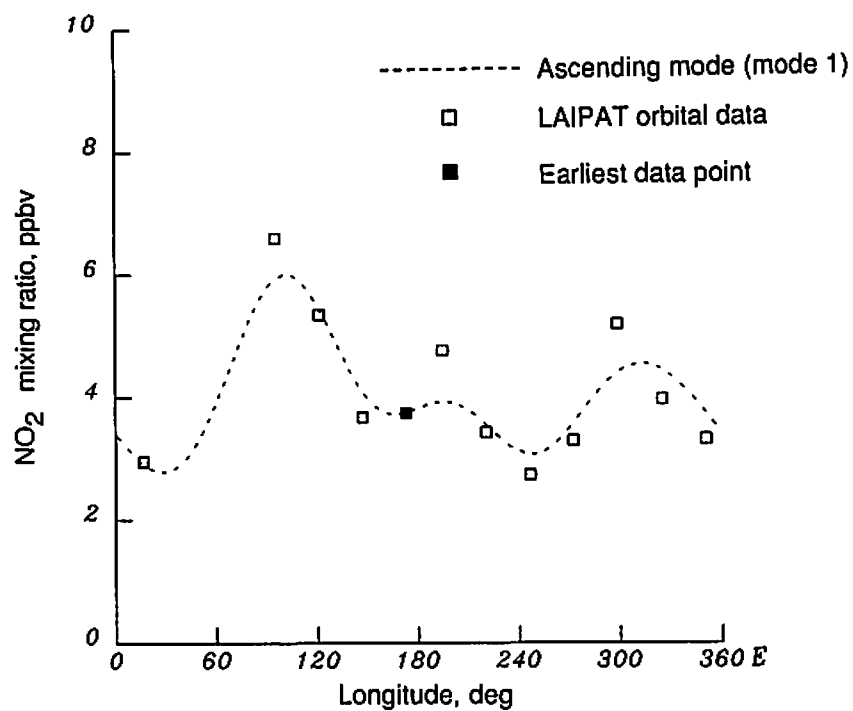
(b) January 25, 1979.

Figure 27. Continued.



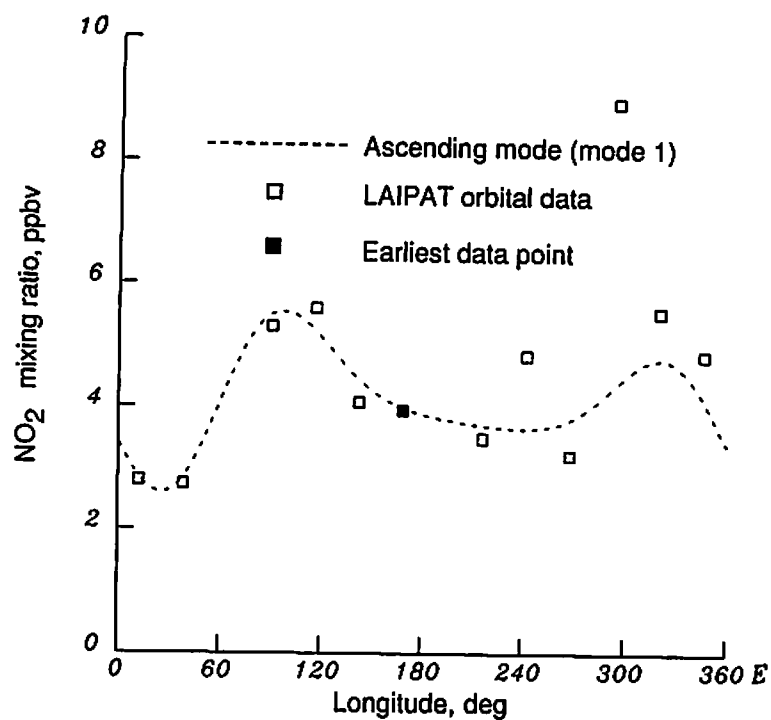
(c) January 26, 1979.

Figure 27. Concluded.



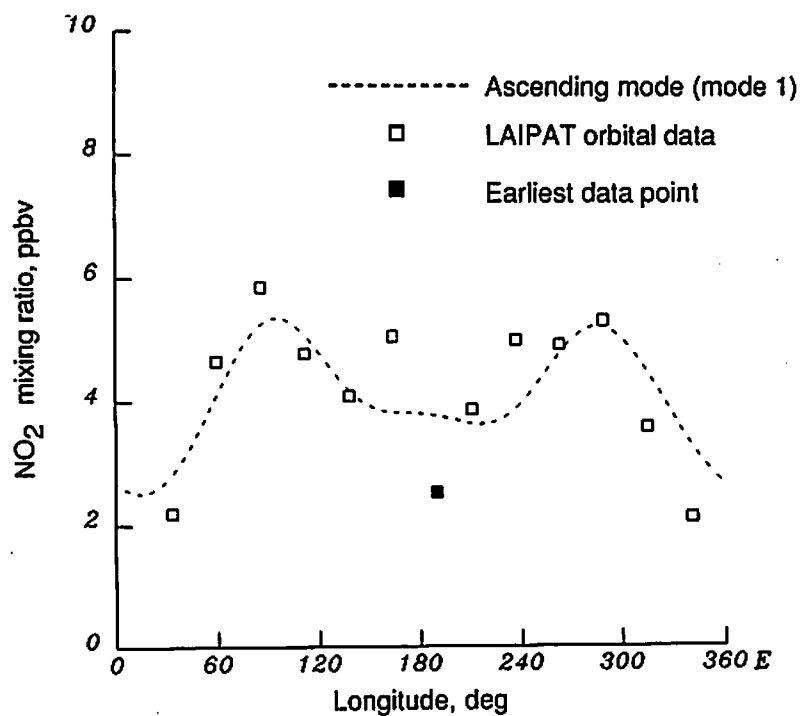
(a) February 25, 1979, at latitude 56°N.

Figure 28. Data and Kalman filter results for ascending mode NO₂ at 10 mbar for latitudes 56°N, 60°N, and 64°N on February 25, 26, and 27, 1979. Square symbols indicate ascending data.



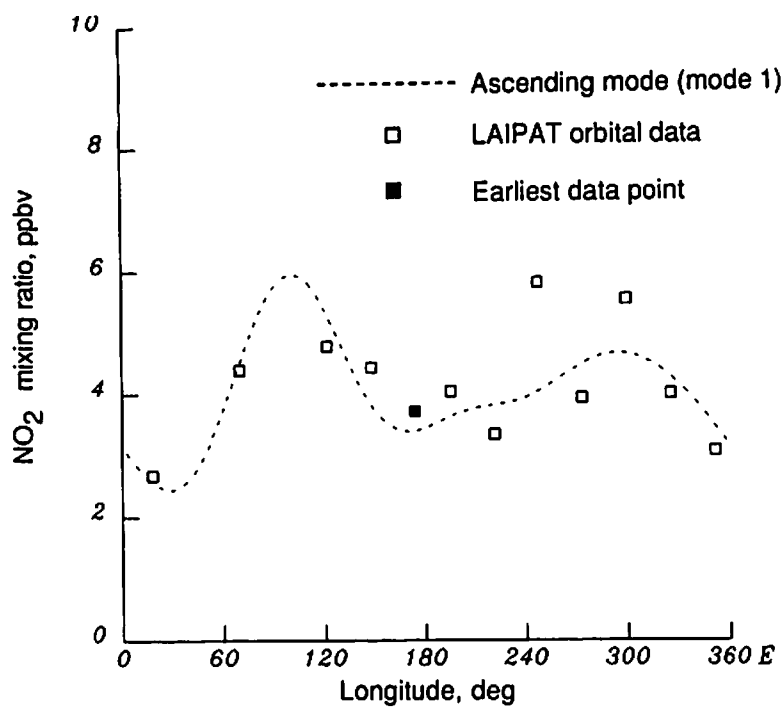
(b) February 26, 1979, at latitude 56°N.

Figure 28. Continued.



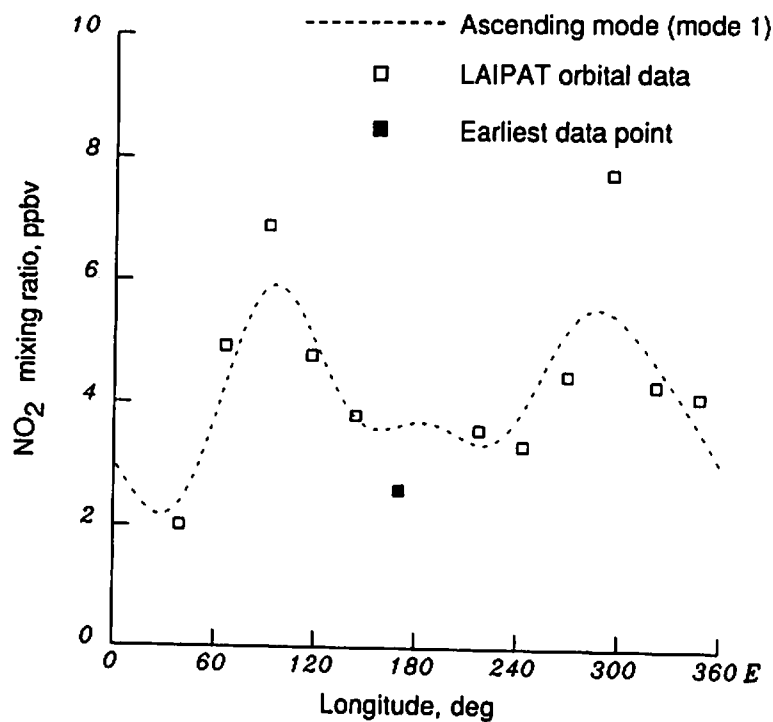
(c) February 27, 1979, at latitude 56°N.

Figure 28. Continued.



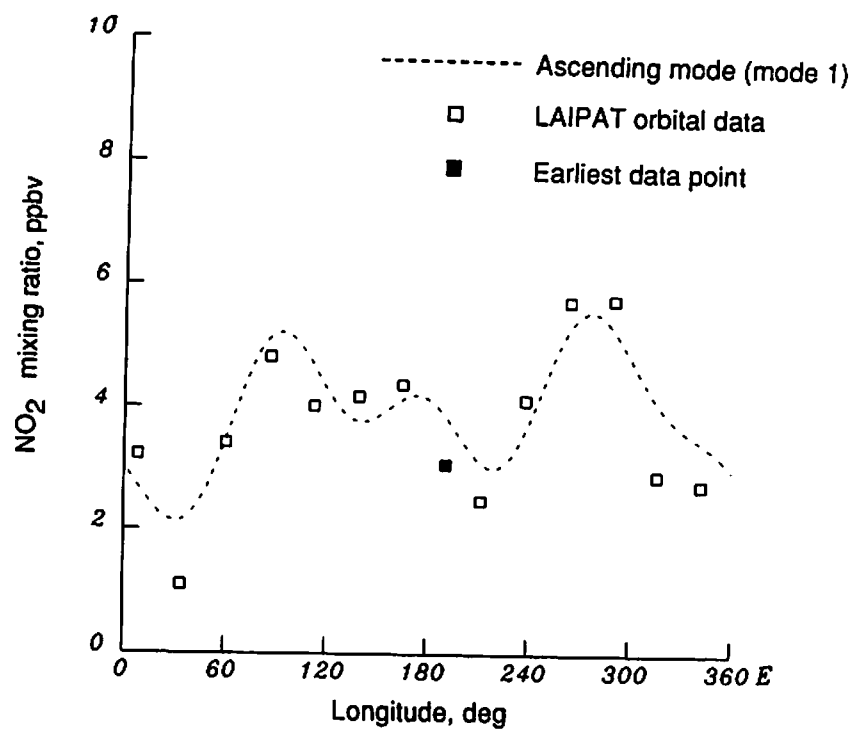
(d) February 25, 1979, at latitude 60°N.

Figure 28. Continued.



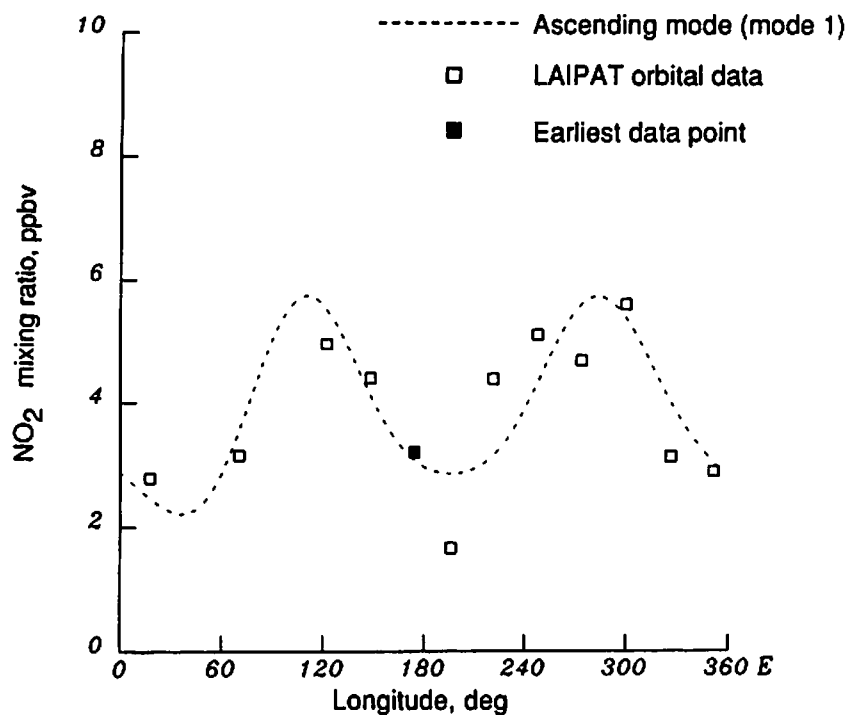
(e) February 26, 1979, at latitude 60°N.

Figure 28. Continued.



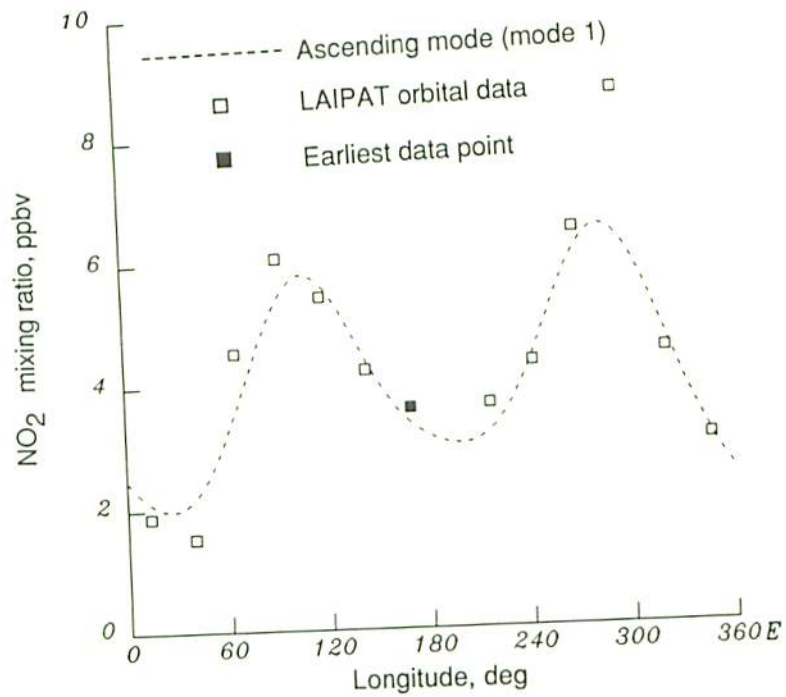
(f) February 27, 1979, at latitude 60°N.

Figure 28. Continued.



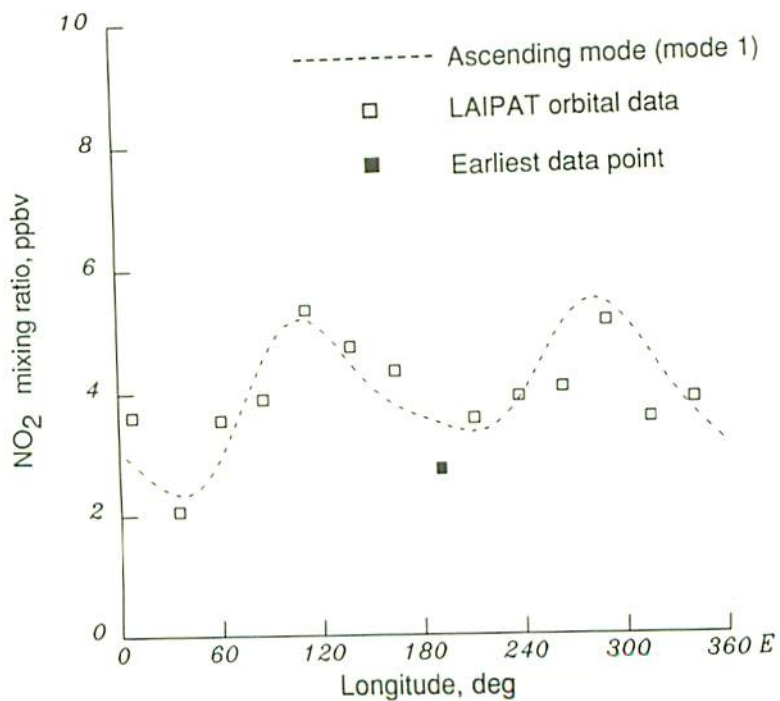
(g) February 25, 1979, at latitude 64°N.

Figure 28. Continued.



(h) February 26, 1979, at latitude 64°N.

Figure 28. Continued.



(i) February 27, 1979, at latitude 64°N.

Figure 28. Concluded.

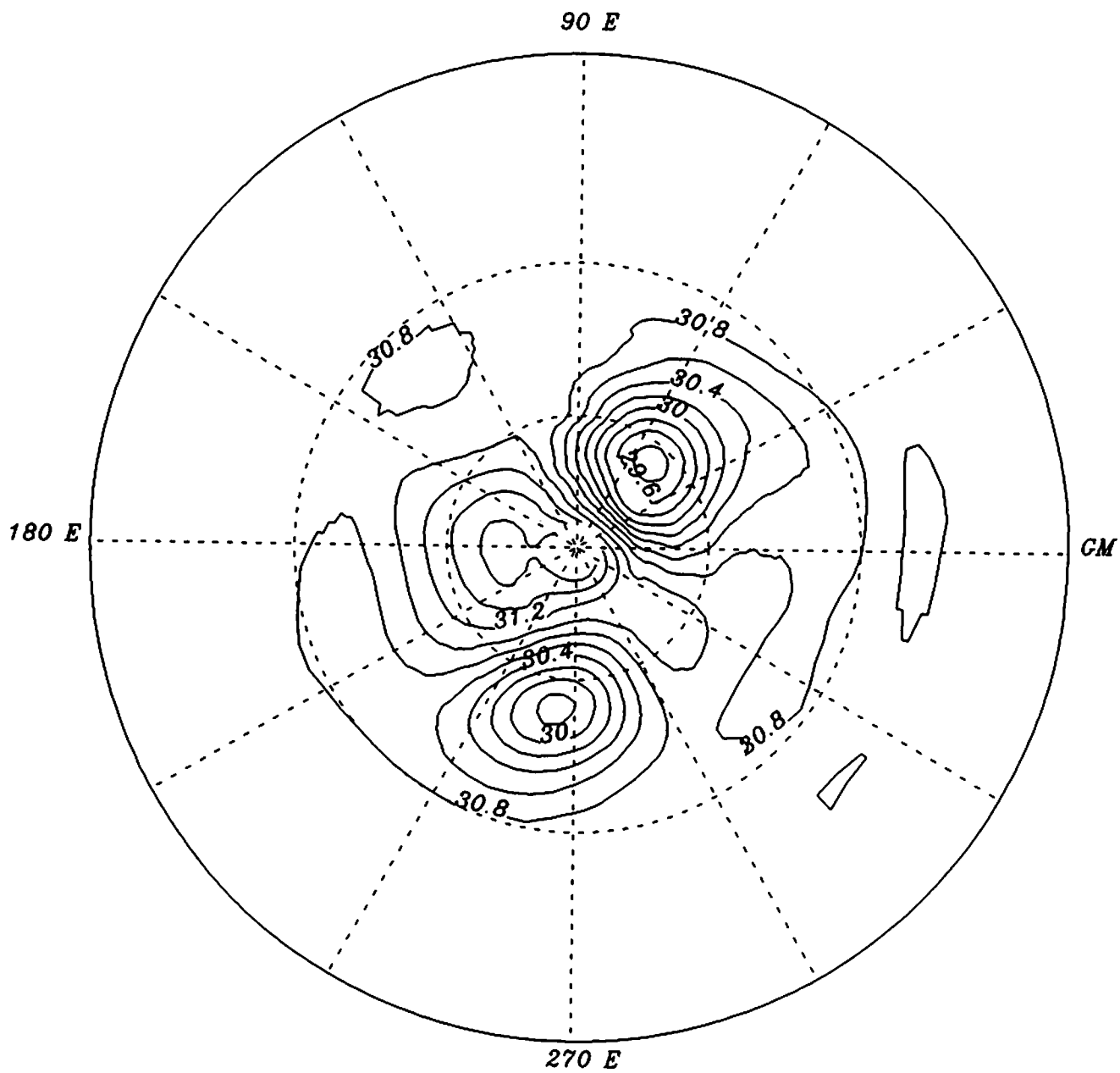


Figure 29. Northern Hemisphere geopotential height field (in gpm) at 10 mbar on February 26, 1979. Dashed circles represent 30°N and 60°N latitudes. Contour interval, 200 gpm.

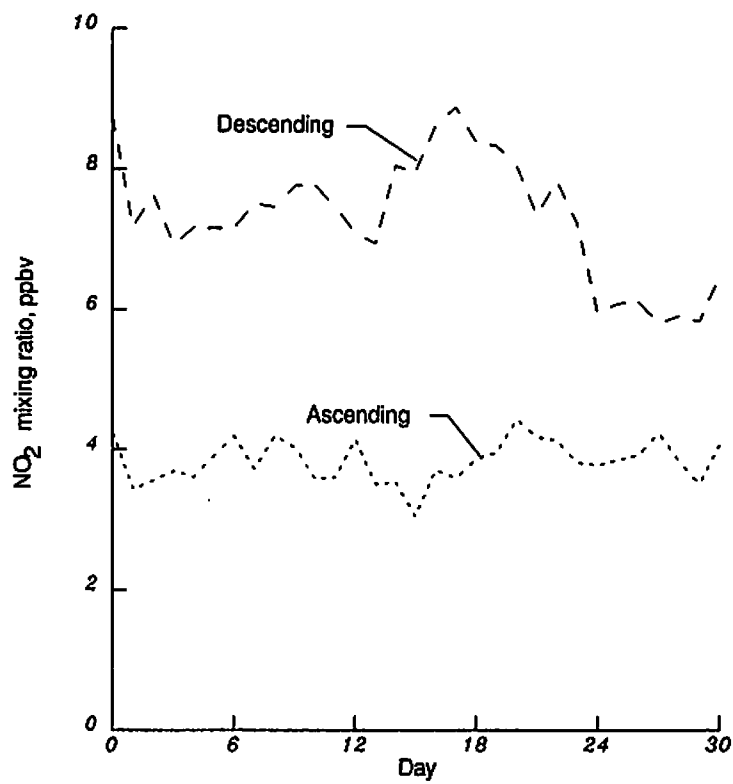
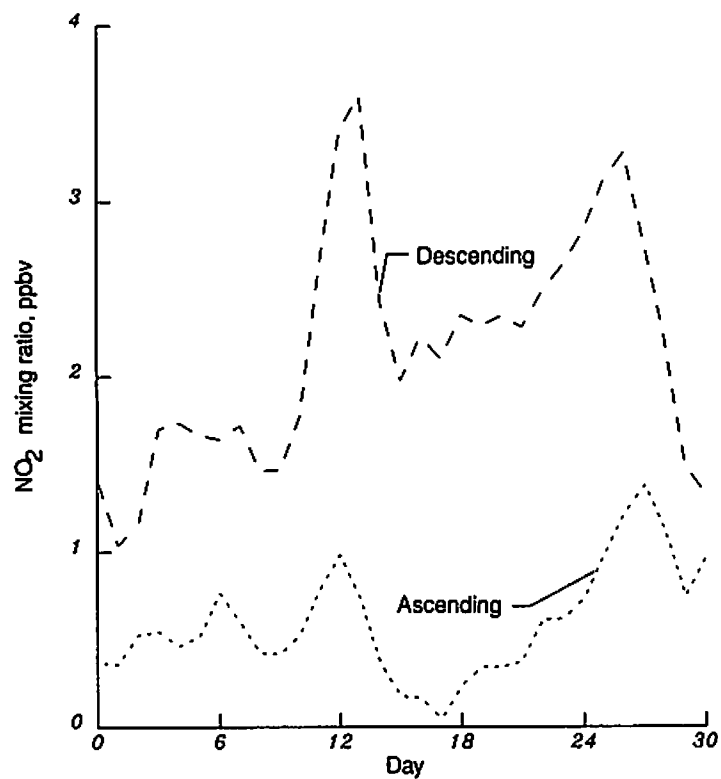
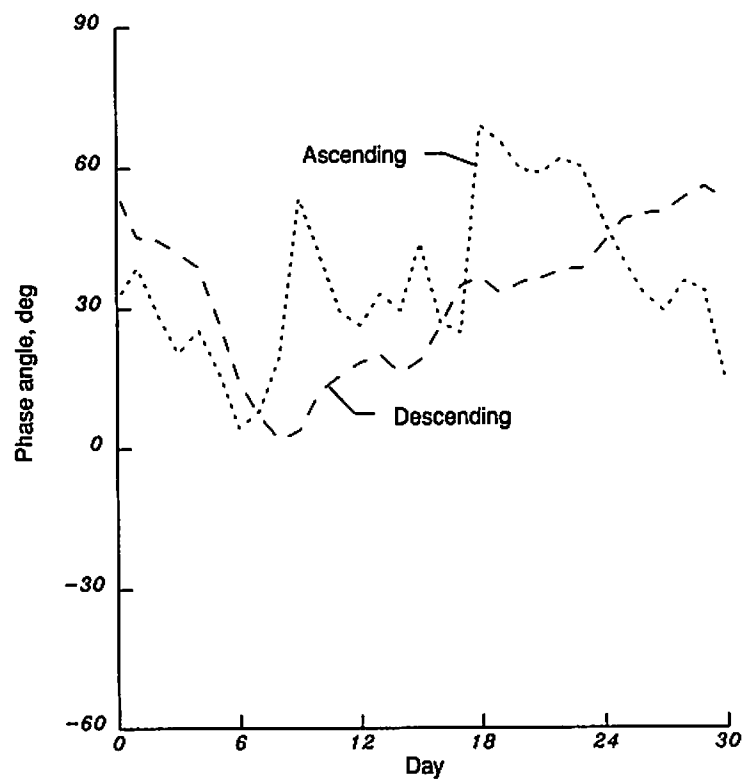


Figure 30. Time series of ascending and descending mode zonal mean coefficient for January 1979 at 10 mbar and 60°N.

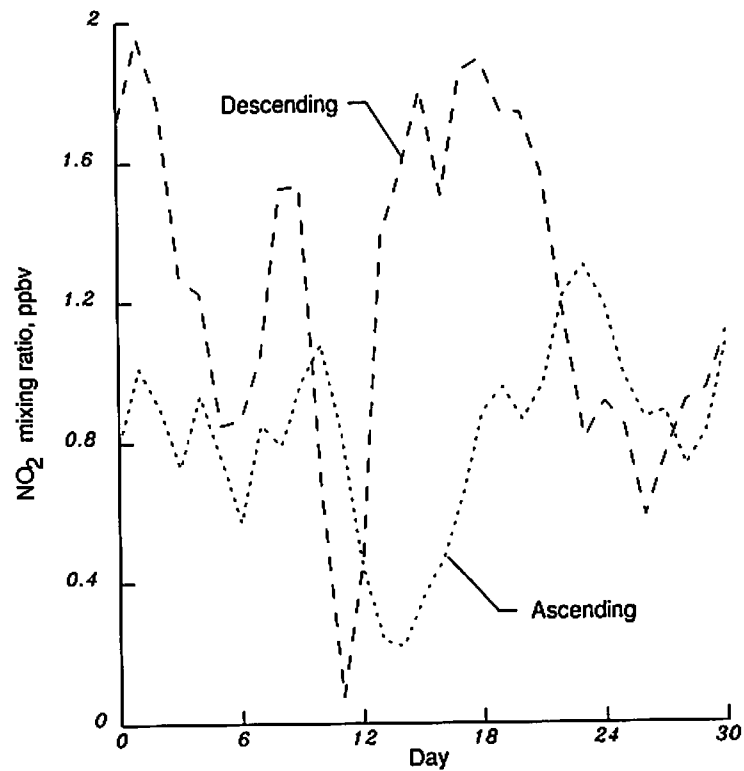


(a) Amplitude of wave 1.

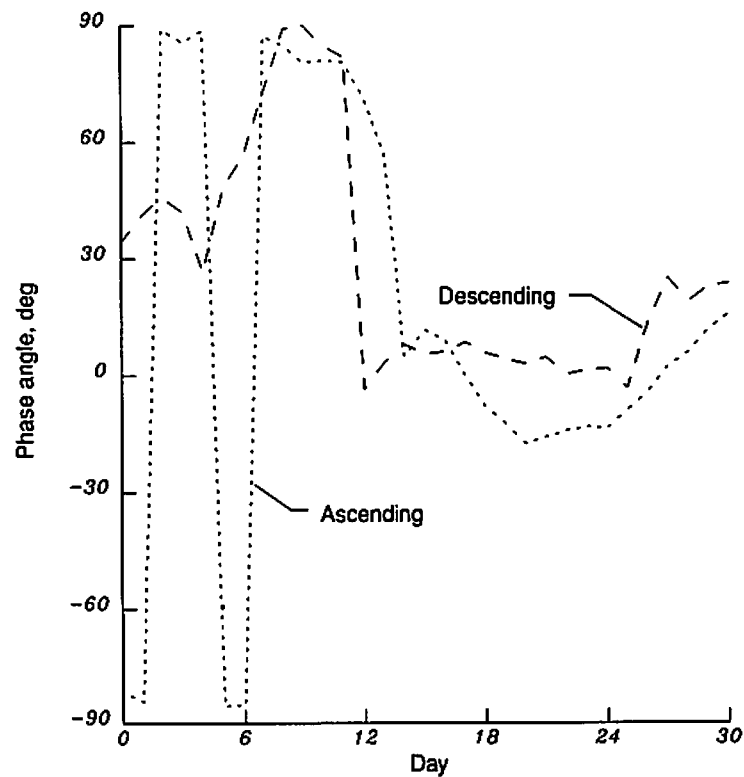


(b) Phase of wave 1.

Figure 31. Time series of ascending and descending mode amplitude and phase of wave 1 for January 1979 at 10 mbar and 60°N .



(a) Amplitude of wave 2.



(b) Phase of wave 2.

Figure 32. Time series of ascending and descending mode amplitude and phase of wave 2 for January 1979 at 10 mbar and 60°N .

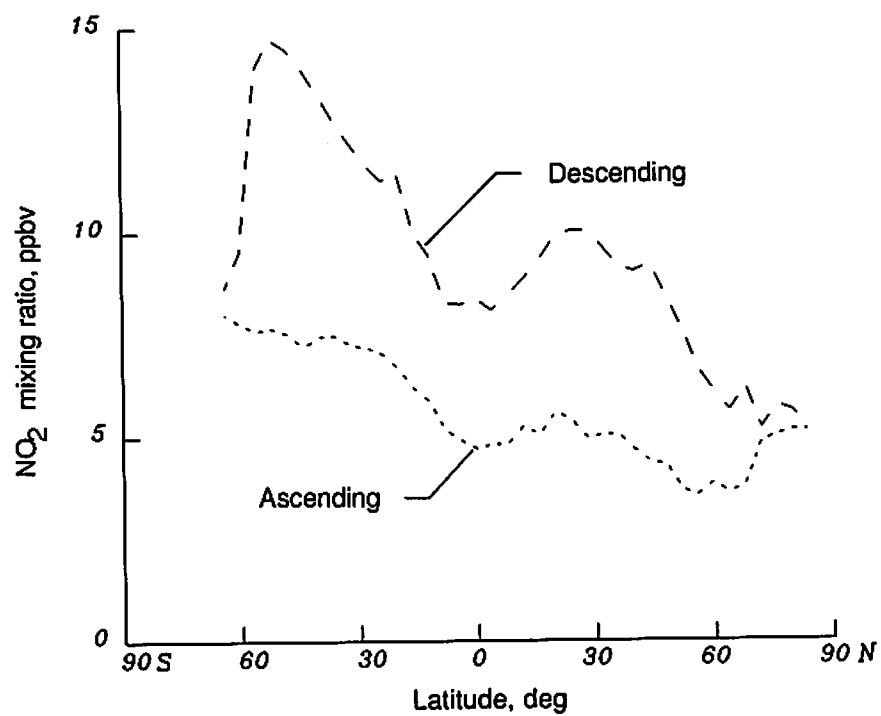
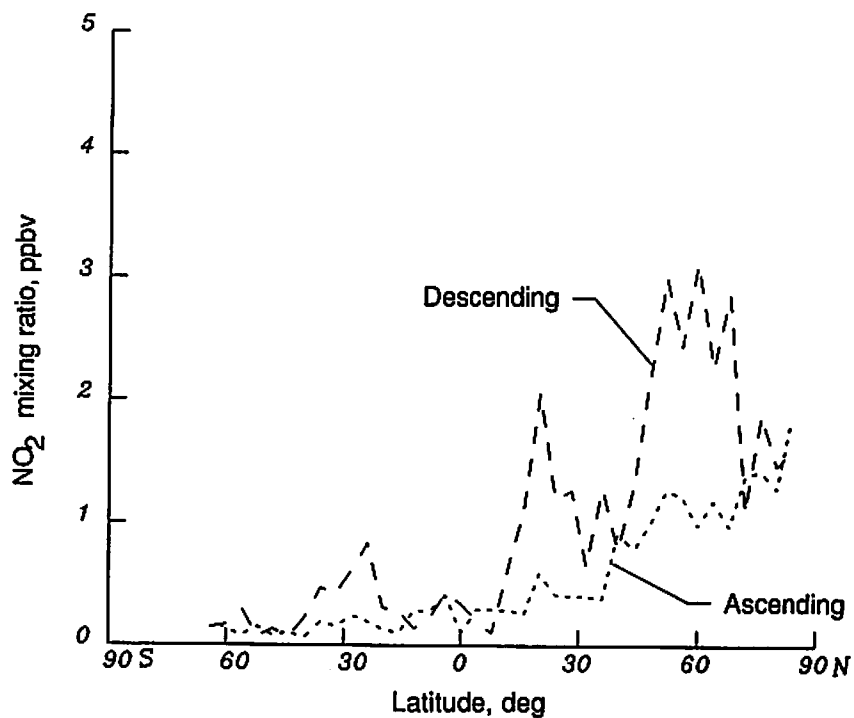
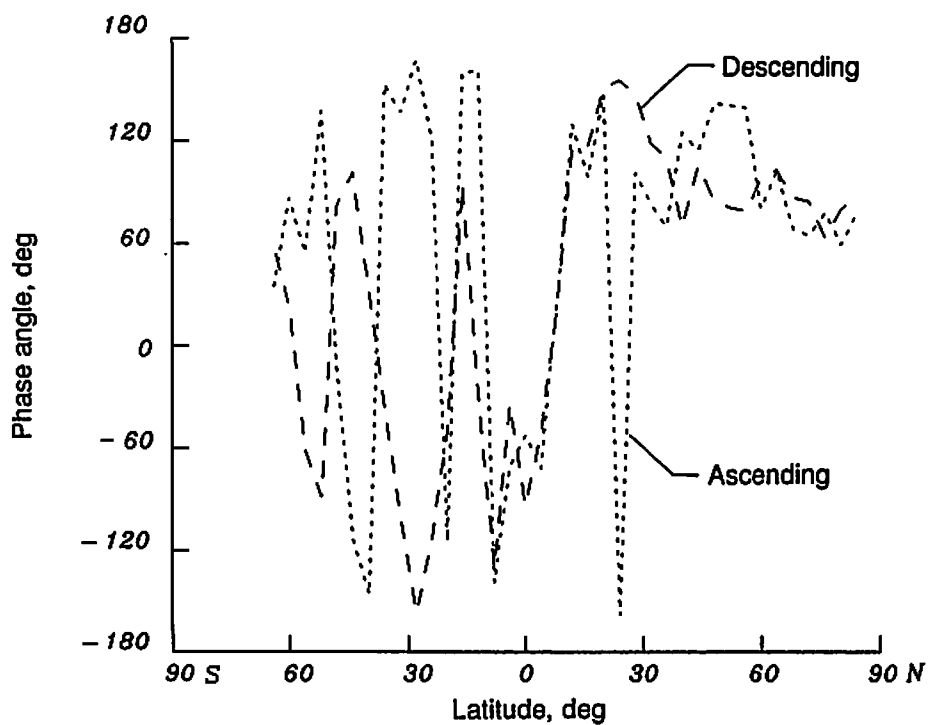


Figure 33. Latitudinal variation of zonal mean coefficient for NO₂ at 10 mbar on January 26, 1979.

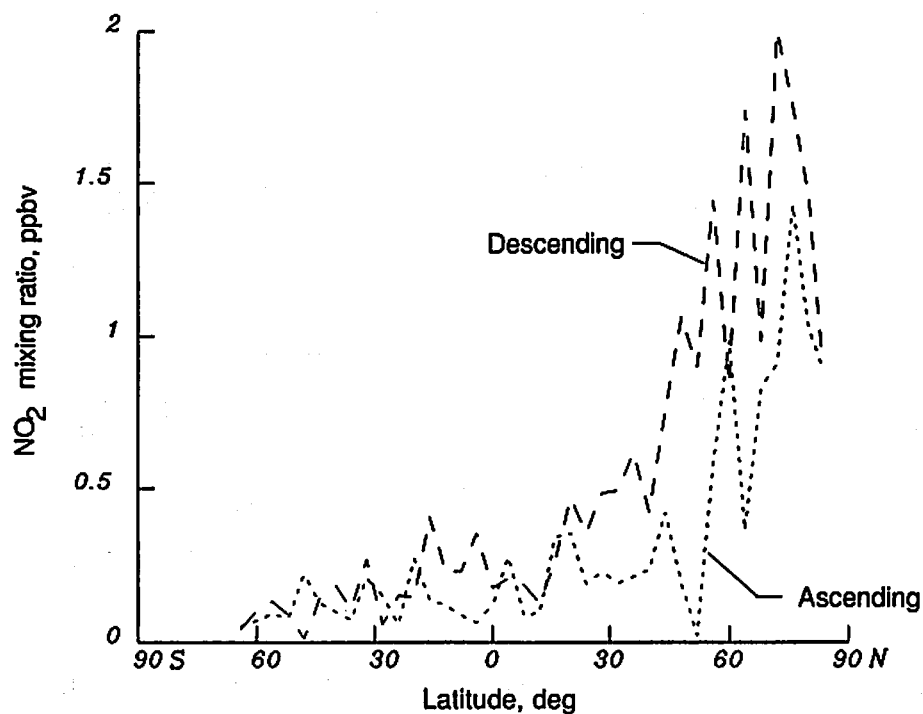


(a) Amplitude of wave 1.

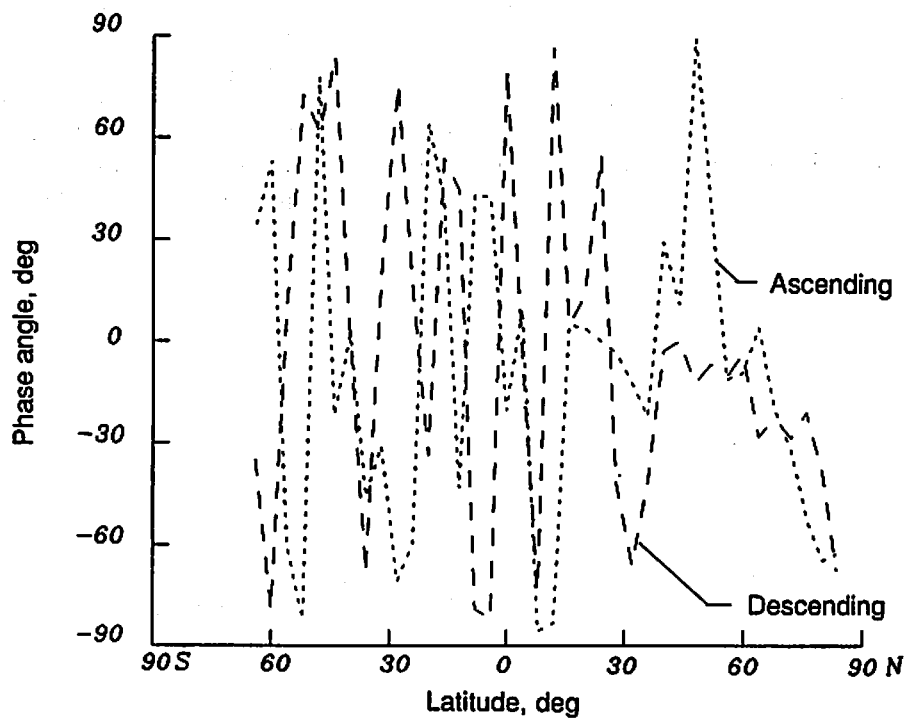


(b) Phase of wave 1.

Figure 34. Amplitude and phase of wave 1 at 10 mbar on January 26, 1979.



(a) Amplitude of wave 2.



(b) Phase of wave 2.

Figure 35. Amplitude and phase of wave 2 at 10 mbar on January 26, 1979.



Report Documentation Page

1. Report No. NASA TP-2761		2. Government Accession No.		3. Recipient's Catalog No.	
4. Title and Subtitle Description of Data on the Nimbus 7 LIMS Map Archive Tape—Water Vapor and Nitrogen Dioxide				5. Report Date February 1988	
				6. Performing Organization Code	
7. Author(s) Kenneth V. Haggard, B. T. Marshall, Robert J. Kurzeja, Ellis E. Remsberg, and James M. Russell III				8. Performing Organization Report No. L-16313	
9. Performing Organization Name and Address NASA Langley Research Center Hampton, VA 23665-5225				10. Work Unit No. 673-41-10-70	
				11. Contract or Grant No.	
				13. Type of Report and Period Covered Technical Paper	
12. Sponsoring Agency Name and Address National Aeronautics and Space Administration Washington, DC 20546-0001				14. Sponsoring Agency Code	
15. Supplementary Notes Kenneth V. Haggard, Ellis E. Remsberg, and James M. Russell III: Langley Research Center, Hampton, Virginia. B. T. Marshall: G and A Technical Software, Hampton, Virginia. Robert J. Kurzeja: Savannah River Laboratory, Aiken, South Carolina. Previous reports in this series: NASA TP-2553 and NASA TP-2625.					
16. Abstract This paper describes the process by which the data and analysis of the Limb Infrared Monitor of the Stratosphere (LIMS) experiment was used to produce estimates of synoptic maps of water vapor and nitrogen dioxide. In addition to a detailed description of the analysis procedure, this paper discusses several interesting features in the data and uses these features to demonstrate how the analysis procedure produced the final maps and how one can estimate the uncertainties in the maps. Also, features in the analysis are noted that would influence how one might use, or interpret, the results. These features include subjects such as smoothing and the interpretation of wave components.					
17. Key Words (Suggested by Authors(s)) LIMS (Limb Infrared Monitor of the Stratosphere) Nimbus 7 Kalman filter Water vapor Nitrogen dioxide				18. Distribution Statement Unclassified—Unlimited Subject Category 47	
19. Security Classif.(of this report) Unclassified		20. Security Classif.(of this page) Unclassified		21. No. of Pages 66	
				22. Price A04	

National Aeronautics and
Space Administration
Code NTT-4

Washington, D.C.
20546-0001

Official Business
Penalty for Private Use, \$300

SPECIAL FOURTH-CLASS RATE
POSTAGE & FEES PAID
NASA
Permit No. G-27



POSTMASTER: If Undeliverable (Section 158
Postal Manual) Do Not Return
